



MOSCOW CENTER
FOR DIAGNOSTICS & TELEMEDICINE

ISSN 2712-8490 (Print)
ISSN 2712-8962 (Online)

DIGITAL DIAGNOSTICS

A peer-reviewed scientific medical journal

4 Volume 1 Issue



2023



ECO • VECTOR

<https://journals.eco-vector.com/DD>

УЧРЕДИТЕЛИ

- ГБУЗ «Научно-практический клинический центр диагностики и телемедицинских технологий ДЗМ»
- ООО «Эко-Вектор»

Свидетельство о регистрации СМИ ПИ
№ ФС 77 - 74099 от 19.10.2018

ИЗДАТЕЛЬ

ООО «Эко-Вектор»
Адрес: 191186, Санкт-Петербург, Аптекарский переулок, д. 3, литера А, помещение 1Н
E-mail: info@eco-vector.com
WEB: <https://eco-vector.com>

РЕКЛАМА

Отдел рекламы
Тел.: +7 (968) 545 78 20
E-mail: adv2@eco-vector.com

РЕДАКЦИЯ

Зав. редакцией
Елена Андреевна Филиппова
E-mail: ddjournal@eco-vector.com
Тел.: +7 (965) 012 70 72
Адрес: 127051, Москва, ул. Петровка,
д. 24, стр. 1

ПОДПИСКА

Подписка на печатную версию через интернет:
www.journals.eco-vector.com/
www.akc.ru
www.ppressa-rf.ru

OPEN ACCESS

В электронном виде журнал распространяется бесплатно — в режиме немедленного открытого доступа

ИНДЕКСАЦИЯ

- SCOPUS
- РИНЦ
- Google Scholar
- Ulrich's International Periodicals Directory
- WorldCat

Оригинал-макет

подготовлен в издательстве «Эко-Вектор».
Литературный редактор: *М.Н. Шошина*
Корректор: *М.Н. Шошина*
Вёрстка: *Ф.А. Игнащенко*
Обложка: *Е.Д. Бугаенко*

Сдано в набор 04.04.2023.
Подписано в печать 13.04.2023. Формат 60 × 88%.
Печать офсетная. Печ. л. 11,25. Усл. печ. л. 10,5.
Уч.-изд. л. 6,1. Тираж 5000 экз. Заказ № 3-3062-1v.
Цена свободная.

Отпечатано в ООО «Типография Фурсова».
196105, Санкт-Петербург, ул. Благодатная, 69.
Тел.: +7 (812) 646-33-77

16+

© ООО «Эко-Вектор», 2023

ISSN 2712-8490 (Print)
ISSN 2712-8962 (Online)

Digital Diagnostics

Том 4 | Выпуск 1 | 2023

ЕЖЕКВАРТАЛЬНЫЙ РЕЦЕНЗИРУЕМЫЙ НАУЧНЫЙ
МЕДИЦИНСКИЙ ЖУРНАЛ

Главный редактор

Синицын Валентин Евгеньевич, д.м.н., профессор (Москва, Россия)
ORCID: 0000-0002-5649-2193

Заместитель главного редактора

Юрий Александрович Васильев, к.м.н., (Москва, Россия)
ORCID: 0000-0002-0208-5218

Научный редактор

Березовская Татьяна Павловна, д.м.н., профессор (Обнинск, Россия)
ORCID: 0000-0002-3549-4499

Ответственный секретарь

Виноградова Ирина Александровна, к.т.н. (Москва, Россия)
ORCID: 0000-0001-6465-4132

Редакционная коллегия

Андрейченко А.Е., к.ф.-м.н. (Москва, Россия)

ORCID: 0000-0001-6359-0763

Berlin L., профессор (Иллинойс, США)

ORCID: 0000-0002-0717-0307

Беляев М.Г., к.ф.-м.н. (Москва, Россия)

ORCID: 0000-0001-9906-6653

Важенни Д.А., д.м.н., доцент (Москва, Россия)

ORCID: 0000-0002-6236-709X

Bisdas S., MBBS, MD, PhD (Лондон, Великобритания)

ORCID: 0000-0001-9930-5549

Гомбелевский В.А., к.м.н. (Москва, Россия)

ORCID: 0000-0003-1816-1315

Доможирова А.С., д.м.н., доцент (Москва, Россия)

ORCID: 0000-0003-0806-3164

Frija B., профессор (Париж, Франция)

ORCID: 0000-0003-0415-0586

Guglielmi G., MD, профессор (Фоджа, Италия)

ORCID: 0000-0002-4325-8330

Holodny A., д.м.н. (Нью-Йорк, США)

ORCID: 0000-0002-1159-2705

Лебедев Г.С., д.т.н., профессор (Москва, Россия)

ORCID: 0000-0002-4289-2102

Li H., MD, профессор (Пекин, КНР)

ORCID: 0000-0002-9102-4176

Mannelli L., MD (Нью-Йорк, США)

ORCID: 0000-0002-9102-4176

Матвеев И.А., д.т.н. (Москва, Россия)

ORCID: 0000-0003-2005-9467

Маццеплишвили С.Т., д.м.н., профессор (Москва, Россия)

ORCID: 0000-0002-5670-167X

Митков В.В., д.м.н., профессор (Санкт-Петербург, Россия)

ORCID: 0000-0003-1959-9618

Морозов С.П., д.м.н., профессор (Москва, Россия)

ORCID: 0000-0001-6545-6170

Neri E., д.м.н. (Пиза, Италия)

ORCID: 0000-0001-7950-4559

Омельяновский В.В., д.м.н., профессор (Москва, Россия)

ORCID: 0000-0003-1581-0703

Омелянская О.В., (Москва, Россия)

ORCID: 0000-0002-0245-4431

Van Ooijen P., к.м.н. (Гронинген, Нидерланды)

ORCID: 0000-0002-8995-1210

Oudkerk M., профессор (Гронинген, Нидерланды)

ORCID: 0000-0003-2800-4110

Ros P.R., MD, MPH, PhD, профессор (Нью-Йорк, США)

ORCID: 0000-0003-3974-0797

Rovira A., профессор (Барселона, Испания)

ORCID: 0000-0002-2132-6750

Решетников Р.В., к.ф.-м.н., (Москва, Россия)

ORCID: 0000-0002-9661-0254

Румянцев П.О., д.м.н. (Москва, Россия)

ORCID: 0000-0002-7721-634X

Аншелес А.А., д.м.н. (Москва, Россия)

ORCID: 0000-0002-2675-3276

Арутюнов Г.П., д.м.н. (Москва, Россия)

ORCID: 0000-0002-6645-2515

Белеский А.С., д.м.н., профессор (Москва, Россия)

ORCID: 0000-0001-6050-724X

Васильева Е.Ю., д.м.н., профессор (Москва, Россия)

ORCID: 0000-0003-4111-0874

Гехт А.Б., д.м.н., профессор (Москва, Россия)

ORCID: 0000-0002-1170-6127

Коблякова О.С., д.м.н., профессор (Москва, Россия)

ORCID: 0000-0003-0098-7403

Кремнева Е.И., к.м.н. (Москва, Россия)

ORCID: 0000-0001-7936-6063

Петриков С.С., д.м.н., профессор (Москва, Россия)

ORCID: 0000-0003-3292-8789

Проценко Д.Н., к.м.н. (Москва, Россия)

ORCID: 0000-0002-5166-3280

Хатьков И.Е., д.м.н., профессор (Москва, Россия)

ORCID: 0000-0002-4088-8118

Редакция не несет ответственности за содержание рекламных материалов. Точка зрения авторов может не совпадать с мнением редакции. К публикации принимаются только статьи, подготовленные в соответствии с правилами для авторов. Направляя статью в редакцию, авторы принимают условия договора публичной оферты. С правилами для авторов и договором публичной оферты можно ознакомиться на сайте: <https://journals.eco-vector.com/DD/>. Полное или частичное воспроизведение материалов, опубликованных в журнале, допускается только с письменного разрешения издателя — издательства «Эко-Вектор».



FOUNDERS

- Moscow Center for Diagnostics and Telemedicine
- Eco-Vector

PUBLISHER

Eco-Vector

Address: 3 liter A, 1H, Aptekarsky pereulok, 191186, Saint Petersburg Russian Federation
E-mail: info@eco-vector.com
WEB: <https://eco-vector.com>

ADVERTISE

Adv. department

Phone: +7 (968) 545 78 20
E-mail: adv2@eco-vector.com

EDITORIAL OFFICE

Executive editor

Elena A. Philippova
E-mail: ddjournal@eco-vector.com
Phone: +7 (965) 012 70 72

SUBSCRIPTION

For print version:
www.journals.eco-vector.com/

PUBLICATION ETHICS

Journal's ethic policies are based on:

- ICMJE
- COPE
- ORE
- CSE
- EASE

OPEN ACCESS

Immediate Open Access is mandatory for all published articles

INDEXATION

- SCOPUS
- Russian Science Citation Index
- Google Scholar
- Ulrich's International Periodicals Directory
- WorldCat

TYPESET

complete in Eco-Vector
Copyeditor: *M.N. Shoshina*
Proofreader: *M.N. Shoshina*
Layout editor: *Ph. Ignashchenko*
Cover: *E. Bugaenko*

ISSN 2712-8490 (Print)
ISSN 2712-8962 (Online)

Digital Diagnostics

Volume 4 | Issue 1 | 2023

QUARTERLY PEER-REVIEW MEDICAL JOURNAL

EDITOR-IN-CHIEF

Valentin E. Sinitsyn, MD, Dr.Sci. (Med), Professor (Moscow, Russia)
ORCID: 0000-0002-5649-2193

DEPUTY EDITOR-IN-CHIEF

Yurii A. Vasilev, MD, Cand.Sci. (Med) (Moscow, Russia)
ORCID: 0000-0002-0208-5218

SCIENTIFIC EDITOR

Tatiana P. Berezovskaya MD, Dr.Sci. (Med.), Professor (Obninsk, Russia)
ORCID: 0000-0002-3549-4499

RESPONSIBLE SECRETARY

Irina A. Vinogradova, Cand.Sci (Tech) (Moscow, Russia)
ORCID: 0000-0001-6465-4132

EDITORIAL BOARD

A.E. Andreychenko, PhD (Moscow, Russia)

ORCID: 0000-0001-6359-0763

L. Berlin, Professor (Illinois, United States)

ORCID: 0000-0002-0717-0307

M.G. Belyaev, Cand.Sci. (Phys-Math), Assistant Professor (Moscow, Russia)

ORCID: 0000-0001-9906-6453

S. Bisdas, MBBS, MD, PhD (London, United Kingdom)

ORCID: 0000-0001-9930-5549

D.A. Vazhenina, MD, Dr.Sci. (Med.), Associate Professor (Moscow, Russia)

ORCID:0000-0002-6236-709X

V.A. Gomboleviskiy, MD, Dr.Sci. (Med) (Moscow, Russia)

ORCID: 0000-0003-1816-1315

A.S. Domozhirova, MD, Dr.Sci. (Med.), Associate Professor (Moscow, Russia)

ORCID: 0000-0003-0806-3164

G. Frija, Professor (Paris, France)

ORCID: 0000-0003-0415-0586

G. Guglielmi, MD, Professor (Foggia, Italy)

ORCID: 0000-0002-4325-8330

A. Holodny, MD (New-York, United States)

ORCID: 0000-0002-1159-2705

H. Li, MD, Professor (Beijing, China)

G.S. Lebedev, Dr.Sci. (Tech.), Professor (Moscow, Russia)

ORCID: 0000-0002-4289-2102

L. Mannelli, MD (New-York, United States)

ORCID: 0000-0002-9102-4176

I.A. Matveev, Dr.Sci. (Tech.) (Moscow, Russia)

ORCID: 0000-0003-2005-9467

V.V. Mit'kov, MD, Dr.Sci. (Med), Professor (St-Petersburg, Russia)

ORCID: 0000-0003-1959-9618

S.T. Matskeplishvili, MD, Dr.Sci. (Med), Professor (Moscow, Russia)

ORCID: 0000-0002-5670-167X

S.P. Morozov, MD, Dr.Sci. (Med), Professor (Moscow, Russia)

ORCID: 0000-0001-6545-6170

E. Neri, MD, Associate Professor (Pisa, Italy)

ORCID: 0000-0001-7950-4559

V.V. Omeļ'yanovskiy, MD, Dr.Sci. (Med), Professor (Moscow, Russia)

ORCID: 0000-0003-1581-0703

D.V. Omelyanskaya, (Moscow, Russia)

ORCID: 0000-0002-0245-4431

P. van Ooijen, PhD, Assoc. Professor (Groningen, Netherlands)

ORCID: 0000-0002-8995-1210

M. Oudkerk, Professor (Groningen, Netherlands)

ORCID: 0000-0003-2800-4110

P.R. Ros, MD, MPH, PhD, Professor (New-York, United States)

ORCID: 0000-0003-3974-0797

A. Rovira, Professor (Barcelona, Spain)

ORCID: 0000-0002-2132-6750

R.V. Reshetnikov, Cand.Sci. (Phys-Math) (Moscow, Russia)

ORCID: 0000-0002-9661-0254

P.O. Rumyantsev, MD, Dr.Sci. (Med) (Moscow, Russia)

ORCID: 0000-0002-7721-634X

A.E. Khramov, Dr.Sci. (Phys-Math), Professor (St-Petersburg, Russia)

ORCID: 0000-0003-2787-2530

A.A. Anshel's, MD, Dr.Sci. (Med)

(Moscow, Russia)

ORCID: 0000-0002-2675-3276

G.P. Arutyunov, MD, Dr.Sci. (Med)

(Moscow, Russia)

ORCID: 0000-0002-6645-2515

A.S. Belevskiy, MD, Dr.Sci. (Med), Professor

(Moscow, Russia)

ORCID: 0000-0001-6050-724X

E.Y. Vasilieva, MD, Dr.Sci. (Med), Professor

(Moscow, Russia)

ORCID: 0000-0003-4111-0874

A.B. Gekht, MD, Dr.Sci. (Med), Professor

(Moscow, Russia)

ORCID: 0000-0002-1170-6127

O.S. Kobayakova, MD, Dr.Sci. (Med), Professor

(Moscow, Russia)

ORCID: 0000-0003-0098-1403

E.I. Kremneva, MD, (Moscow, Russia)

ORCID: 0000-0001-9396-6063

S.S. Petrikov, MD, Dr.Sci. (Med), Professor

(Moscow, Russia)

ORCID: 0000-0003-3292-8789

D.N. Protzenko, MD, Cand.Sci. (Med)

(Moscow, Russia)

ORCID: 0000-0002-5166-3280

I.E. Khatkov, MD, Dr.Sci. (Med), Professor

(Moscow, Russia)

ORCID: 0000-0002-4088-8118

The editors are not responsible for the content of advertising materials. The point of view of the authors may not coincide with the opinion of the editors. Only articles prepared in accordance with the guidelines are accepted for publication. By sending the article to the editor, the authors accept the terms of the public offer agreement. The guidelines for authors and the public offer agreement can be found on the website: <https://journals.eco-vector.com/DD/>. Full or partial reproduction of materials published in the journal is allowed only with the written permission of the publisher — the Eco-Vector publishing house.

16+

© Eco-Vector, 2023



CONTENTS

ORIGINAL STUDY ARTICLES

- Maria M. Suchilova, Ivan A. Blokhin, Olga O. Aleshina, Victor A. Gomboleviskiy, Roman V. Reshetnikov, Viktor Yu. Bosin, Olga V. Omelyanskaya, Anton V. Vladzimirskyy*
Volumetry versus linear diameter lung nodule measurement:
an ultra-low-dose computed tomography lung cancer screening study 5

TECHNICAL REPORTS

- Kirill M. Arzamasov, Viktor A. Drogovoz, Tatiana M. Bobrovskaya, Anton V. Vladzimirskyy*
Tele-ultrasound imaging using smartphones and single-board PCs 15

SYSTEMATIC REVIEWS

- Ivan A. Blokhin, Denis A. Rumyantsev, Maria M. Suchilova, Anna P. Gonchar, Olga V. Omelyanskaya*
Low-dose computed tomography in COVID-19: systematic review 25

REVIEWS

- Egor M. Syrkashev, Faina Z. Kadyrberdieva, Liya R. Abuladze, Dmitriy S. Semenov, Ekaterina G. Privalova*
Basic pulse sequences in the diagnosis of abdominal pathology 39

CASE REPORTS

- Elena N. Karanadze, Valentin E. Sinitsyn, Mariia A. Karanadze*
Diseases and abnormalities of the nipple-areolar complex: a case report series 51
- Sofiya A. Myalina, Ksenia I. Paziuk, Tatiana P. Berezovskaya, Alexey A. Nevolskikh, Aleksandr L. Potapov, Sergey A. Ivanov*
Magnetic resonance imaging in the diagnosis of necrosis of a pulled-through colon segment
after abdomino-anal resection of the rectum for cancer 61
- Yuriy A. Vasilev, Evgeniia A. Grik, Olga Yu. Panina, Anna N. Khoruzhaya, Dmitriy S. Semenov, Alexander V. Bazhin, Yulia N. Vasileva*
Dynamic MRI in a COVID-19 patient: a case series 71

LETTERS TO THE EDITOR

- Dmitry V. Shutov, Dariya E. Sharova, Liya R. Abuladze, Dmitrii V. Drozdov*
Artificial intelligence in clinical physiology: How to improve learning agility 81

СОДЕРЖАНИЕ

ОРИГИНАЛЬНЫЕ ИССЛЕДОВАНИЯ

*М.М. Сучилова, И.А. Блохин, О.О. Алешина, В.А. Гомболевский, Р.В. Решетников,
В.Ю. Босин, О.В. Омелянская, А.В. Владзимирский*

Сравнение измерения линейного размера и объёма лёгочных очагов по данным скрининга
рака лёгких с помощью низкодозной компьютерной томографии 5

ТЕХНИЧЕСКИЕ ОТЧЁТЫ

К.М. Арзамасов, В.А. Дрогозов, Т.М. Бобровская, А.В. Владзимирский

Телеультразвуковые исследования с использованием смартфонов и одноплатных компьютеров 15

СИСТЕМАТИЧЕСКИЕ ОБЗОРЫ

И.А. Блохин, Д.А. Румянцев, М.М. Сучилова, А.П. Гончар, О.В. Омелянская

Низкодозная компьютерная томография органов грудной клетки в диагностике COVID-19:
обзор литературы 25

НАУЧНЫЕ ОБЗОРЫ

Е.М. Сыркашев, Ф.З. Кадырбердиева, Л.Р. Абуладзе, Д.С. Семенов, Е.Г. Привалова

Основные импульсные последовательности в диагностике абдоминальной патологии 39

КЛИНИЧЕСКИЕ СЛУЧАИ

Е.Н. Каранадзе, В.Е. Синицын, М.А. Каранадзе

Диагностика патологии и аномалии сосково-ареолярного комплекса:
серия клинических случаев 51

С.А. Мялина, К.И. Пазюк, Т.П. Березовская, А.А. Невольских, А.Л. Потапов, С.А. Иванов

Магнитно-резонансная томография в диагностике некроза низведённого сегмента
толстой кишки после брюшно-анальной резекции прямой кишки по поводу рака 61

Ю.А. Васильев, Е.А. Грик, О.Ю. Панина, А.Н. Хоружая, Д.С. Семенов, А.В. Бажин, Ю.Н. Васильева

Динамическая магнитно-резонансная томография лёгких у пациентов с COVID-19:
серия клинических случаев 71

ПИСЬМА В РЕДАКЦИЮ

Д.В. Шутов, Д.Е. Шарова, Л.Р. Абуладзе, Д.В. Дроздов

Системы искусственного интеллекта в клинической физиологии:
как сделать их обучение эффективным? 81

DOI: <https://doi.org/10.17816/DD117481>

Сравнение измерения линейного размера и объёма лёгочных очагов по данным скрининга рака лёгких с помощью низкодозной компьютерной томографии

М.М. Сучилова¹, И.А. Блохин¹, О.О. Алешина², В.А. Гомболевский³, Р.В. Решетников¹, В.Ю. Босин¹, О.В. Омелянская¹, А.В. Владзимирский^{1, 4}

¹ Научно-практический клинический центр диагностики и телемедицинских технологий, Москва, Российская Федерация

² Государственная клиническая больница № 13, Москва, Российская Федерация

³ Институт искусственного интеллекта, Москва, Российская Федерация

⁴ Первый Московский государственный медицинский университет имени И.М. Сеченова (Сеченовский Университет), Москва, Российская Федерация

АННОТАЦИЯ

Обоснование. Согласно результатам голландско-бельгийского исследования скрининга рака лёгких NELSON, измерение объёма (волюметрия) очагов позволяет снизить распространённость ложноположительных результатов до 2,1%.

Цель — сравнение диагностической точности и согласованности результатов ручного измерения линейного размера с полуавтоматическим измерением объёма очагов по данным пилотного проекта «Московский скрининг рака лёгкого» с использованием низкодозной компьютерной томографии.

Материалы и методы. В программу скрининга были включены 293 пациента без верифицированного до 2020 года диагноза рака лёгкого, у которых на первичной низкодозной компьютерной томографии, выполненной в период с февраля 2017 по февраль 2018 года, был выявлен очаг в лёгком размером не менее 4 мм. Лучевая нагрузка подбиралась индивидуально и не превышала 1 мЗв. Все изображения низкодозной компьютерной томографии независимо оценивались тремя экспертами для измерения длинной оси очага, а также экстраполированного объёма. В качестве референсного значения размера и объёма брали среднее, полученное по итогам измерений экспертов. Очаг $<6 \text{ мм}/<100 \text{ мм}^3$ признавали ложноположительным результатом, очаг $\geq 6 \text{ мм}/\geq 100 \text{ мм}^3$ — ложноотрицательным.

Результаты. В исследование были включены 293 пациента (166 мужчин; 56%; средний возраст $64,6 \pm 5,3$ года). Лёгочных очагов $<6 \text{ мм}/<100 \text{ мм}^3$ было 199. Экспертами 1, 2 и 3 при измерении объёма зафиксированы отличия от референсного стандарта по 32 [10,9%; 4 ложноположительных, 28 ложноотрицательных], 29 [9,9%; 17 ложноположительных, 12 ложноотрицательных] и 30 [10,2%; 6 ложноположительных, 24 ложноотрицательных] очагам, а также расхождения при измерении линейного размера по 92 [65,5%; 107 ложноположительных, 85 ложноотрицательных], 146 [49,8%; 58 ложноположительных, 88 ложноотрицательных] и 102 [34,8%; 23 ложноположительных, 79 ложноотрицательных] очагам соответственно.

Заключение. Использование волюметрии лёгочных очагов значительно снижает количество ложноположительных и ложноотрицательных результатов в сравнении с измерением линейного размера очагов в программе скрининга рака лёгких методом низкодозной компьютерной томографии.

Ключевые слова: компьютерная томография; скрининг рака лёгкого; лёгочные узлы.

Как цитировать

Сучилова М.М., Блохин И.А., Алешина О.О., Гомболевский В.А., Решетников Р.В., Босин В.Ю., Омелянская О.В., Владзимирский А.В. Сравнение измерения линейного размера и объёма лёгочных очагов по данным скрининга рака лёгких с помощью низкодозной компьютерной томографии // *Digital Diagnostics*. 2023. Т. 4, № 1. С. 5–13. DOI: <https://doi.org/10.17816/DD117481>

DOI: <https://doi.org/10.17816/DD117481>

Volumetry versus linear diameter lung nodule measurement: an ultra-low-dose computed tomography lung cancer screening study

Maria M. Suchilova¹, Ivan A. Blokhin¹, Olga O. Aleshina², Victor A. Gombolevskiy³, Roman V. Reshetnikov¹, Viktor Yu. Bosin¹, Olga V. Omelyanskaya¹, Anton V. Vladzimirskiy^{1, 4}

¹ Moscow Center for Diagnostics and Telemedicine, Moscow, Russian Federation

² City Clinical Hospital No 13, Moscow, Russian Federation

³ Artificial Intelligence Research Institute, Moscow, Russian Federation

⁴ The First Sechenov Moscow State Medical University (Sechenov University), Moscow, Russian Federation

ABSTRACT

BACKGROUND: The Dutch–Belgian Randomized Lung Cancer Screening Trial (NELSON) used a volume-based protocol and significantly reduced the prevalence of false-positive results (2.1%).

AIM: To compare the performance of manual linear diameter and semi-automated volumetric nodule measurement in the pilot project “Moscow Lung Cancer Screening” ultra-low-dose computed tomography pilot study.

MATERIALS AND METHODS: The study included individuals with a lung nodule of at least 4 mm on baseline-computed tomography of the Moscow lung cancer screening between February 2017 and February 2018, without verified lung cancer diagnosis until 2020. The radiation dose was selected individually and did not exceed 1 mSv. All scans were assessed by three blinded readers to measure the maximum and minimum transversal nodule diameter and extrapolated volume. As a reference value of size and volume, the average value from the results of expert measurements was obtained. A false-positive nodule was defined as a nodule <6 mm/ <100 mm³ and a false-negative nodule as a nodule ≥ 6 mm/ ≥ 100 mm³.

RESULTS: Overall, 293 patients were included (166 men; mean age, 64.6 ± 5.3 years); 199 lung nodules were <6 mm/ <100 mm³ and 94 were ≥ 6 mm/ ≥ 100 mm³. Regarding volumetric measurements, 32 [10.9%; 4 false-positive, 28 false-negative], 29 [9.9%; 17 false-positive, 12 false-negative], and 30 [10.2%; 6 false-positive, 24 false-negative] nodule discrepancies were reported by readers 1, 2, and 3 respectively. For linear diameter measurement, 92 [65.5%; 107 false-positive, 85 false-negative], 146 [49.8%; 58 false-positive, 88 false-negative], and 102 [34.8%; 23 false-positive, 79 false-negative] nodule discrepancies were reported by readers 1, 2, and 3 respectively.

CONCLUSIONS: The use of lung nodule volumetry strongly reduces the number of false-positive and false-negative nodules compared with nodule diameter measurements, in an ultra-low-dose computed tomography lung cancer screening program.

Keywords: tomography X-Ray compute, early detection of cancer, lung neoplasms.

To cite this article

Suchilova MM, Blokhin IA, Aleshina OO, Gombolevskiy VA, Reshetnikov RV, Bosin VYu, Omelyanskaya OV, Vladzimirskiy AV. Volumetry versus linear diameter lung nodule measurement: an ultra-low-dose computed tomography lung cancer screening study. *Digital Diagnostics*. 2023;4(1):5–13. DOI: <https://doi.org/10.17816/DD117481>

Received: 13.12.2022

Accepted: 17.01.2023

Published: 03.03.2023

DOI: <https://doi.org/10.17816/DD117481>

根据通过低剂量计算机断层扫描的肺癌筛查数据对肺部病灶线性尺寸和体积进行的测量比较

Maria M. Suchilova¹, Ivan A. Blokhin¹, Olga O. Aleshina², Victor A. Gomboleviskiy³,
Roman V. Reshetnikov¹, Viktor Yu. Bosin¹, Olga V. Omelyanskaya¹, Anton V. Vladzmyrskyy^{1, 4}

¹ Moscow Center for Diagnostics and Telemedicine, Moscow, Russian Federation

² City Clinical Hospital No 13, Moscow, Russian Federation

³ Artificial Intelligence Research Institute, Moscow, Russian Federation

⁴ The First Sechenov Moscow State Medical University (Sechenov University), Moscow, Russian Federation

简评

论证。根据荷兰-比利时NELSON肺癌筛查研究，病灶的体积测量（容量分析法）可以将假阳性结果的发生率降低到2.1%。

目的是根据莫斯科肺癌筛查试点项目的数据通过低剂量计算机断层扫描对人工病灶线性尺寸测量与半自动病灶体积测量的诊断准确性和一致性进行比较。

材料和方法。293名在2020年前没有被核实诊断为肺癌的患者被纳入筛查计划，他们在2017年2月至2018年2月时间内接受了一次低剂量计算机断层扫描，显示肺部结节的大小至少为4毫米。辐射负载是个性化的，不超过1毫西弗。所有低剂量计算机断层扫描图像都由三位专家独立评估，以测量病灶的长轴以及外推体积。从专家测量得到的尺寸和体积的平均值作为参考值。<6毫米/<100毫米³的病灶视为假阳性，≥6毫米/≥100毫米³的病灶视为假阴性。

结果。293名患者（166名男性；56%；平均年龄为64.6±5.3岁）被纳入研究。共有199个<6毫米/<100毫米³的肺部病灶。专家1、2和3分别记录了32个[10.9%；4个假阳性，28个假阴性]、29个[9.9%；17个假阳性，12个假阴性]和30个[10.2%；6个假阳性，24个假阴性]的病灶的体积测量与参考标准的差异，以及分别记录了92个[65.5%；107个假阳性，85个假阴性]、146个[49.8%；58个假阳性，88个假阴性]和102个[34.8%；23个假阳性，79个假阴性]病灶的线性尺寸测量与参考标准的差异。

结论。在低剂量计算机断层扫描肺癌筛查项目中，与病灶的线性大小的测量相比，使用肺部病灶的容积测定法可显著减少假阳性和假阴性结果的数量。

关键词：计算机断层扫描；肺癌筛查；肺部结节。

To cite this article

Suchilova MM, Blokhin IA, Aleshina OO, Gomboleviskiy VA, Reshetnikov RV, Bosin VYu, Omelyanskaya OV, Vladzmyrskyy AV. 根据通过低剂量计算机断层扫描的肺癌筛查数据对肺部病灶线性尺寸和体积进行的测量比较. *Digital Diagnostics*. 2023;4(1):5-13. DOI: <https://doi.org/10.17816/DD117481>

收到: 13.12.2022

接受: 17.01.2023

发布日期: 03.03.2023

BACKGROUND

Lung cancer remains one of the top 10 causes of death worldwide, owing largely to late diagnosis.¹ Low-dose computed tomography (LDCT) screening was found to significantly reduce lung cancer mortality in a high-risk population [1]. LDCT screening is intended to detect lung cancer at an early stage and primarily involves the detection, classification, and subsequent management of lung nodules. Numerous guidelines on pulmonary nodules have been developed to assist with the aforementioned tasks, including the International Early Lung Cancer Action Program [2] and Lung CT Screening Reporting And Data System (Lung-RADS) [4], as well as recommendations of the British Thoracic Society (BTS), [5] European Position Statement on Lung Cancer Screening (EUPS), [6] and National Comprehensive Cancer Network [7].²

According to the results of the Dutch-Belgian NELSON lung cancer screening, the volumetry of nodules can reduce the incidence of false-positive results to 2.1% [1]. Volumetry using semiautomatic volume estimation was thus approved and recommended in the EUPS protocols [6] and later in the NELSON-plus protocols [8]. According to the BTS guidelines for the management of pulmonary nodules identified by LDCT, volumetry should be used instead of measuring linear dimensions whenever possible.

The NELSON study found that lung cancer screening with LDCT was effective [9], although an effective radiation dose of 0.4–1.6 mSv was used for screening, depending on the patient's body weight [10]. Moreover, according to SanPin 2.6.1.2523-09 sanitary standards,³ the annual effective dose during preventive X-ray examinations should not exceed 1 mSv. As a result, the radiation dose in the Moscow Lung Cancer Screening pilot project was limited to 0.7 mSv [12]. To the best of our knowledge, no validation study has compared volumetric data with estimated maximum linear dimensions based on computed tomography with a radiation dose of <1 mSv (ultra-LDCT) performed as part of lung cancer screening. The findings of the Moscow Lung Cancer Screening project provide an invaluable opportunity to conduct such a study [13].

This study aimed to compare the diagnostic accuracy and consistency of the results of manual linear dimension measurement with semiautomatic volumetry in the Moscow Lung Cancer Screening pilot project using LDCT.

MATERIALS AND METHODS

Study design

A cross-sectional retrospective study was performed.

Eligibility criteria

The *inclusion criteria* were as follows: age from 50 to 80 years, smoking index ≥ 30 pack-years, current smoking or quitting <15 years ago, an ultra-LDCT study during the specified time period, and no history of lung cancer.

The *exclusion criteria* were as follows: no pulmonary nodules on LDCT; a history of lung cancer; a history of lung surgeries (except for lung biopsy); severe cardiovascular, immunological, respiratory, or endocrine diseases with a life expectancy of <5 years; acute respiratory diseases; taking antibiotics for at least 12 weeks before LDCT; hemoptysis or weight loss >10 kg in the year before screening.

Study conditions

The study included 293 participants of the Moscow Lung Cancer Screening pilot project. The subject selection flowchart is presented in Fig. 1. The study was conducted in accordance with Order No. 49 dated February 1, 2017, of the Moscow Healthcare Department.

Study duration

The dataset contains the findings of LDCT studies performed between February 2017 and February 2018.

Description of the intervention

Scanning was performed in 10 outpatient clinics, each with one CT scanner. Toshiba Aquilion 64 (Canon Medical Systems, Japan) CT scanners were used with the following scanning parameters: 64-slice CT scanners, tube voltage of 135 kV, intensity of 15–25 mA (depending on the patient's body weight: <69 kg = 15 mA; 70–90 kg = 20 mA; >90 kg = 25 mA), rotation time of 0.50 s, spacing of 1.484, slice thickness of 1 mm, and slice spacing of 1 mm. The matrix size was 512, and the reconstruction filter FC07 was used. Two scanners used a vendor-specific iterative reconstruction algorithm (AIDR 3D), whereas the remaining eight scanners used filtered back projection with quantum noise reduction software (FBP/QDS+) [13]. Only axial slices were retained. After scanning, maximum intensity projections and multiplanar reconstructions were used to analyze the data.

The breath-hold scanning time at maximal inspiration was ≤ 10 s. The field of view was determined on the CT scan from the lung apices to the costophrenic sinuses. The distance from the ribs to the edge of the image reconstruction area was <1 cm. The computed tomography dose index CTDIvol depended on the patient's body weight: <69 kg = 0.8 mGy,

¹ WHO [Internet]. The top 10 causes of death cited 2020 Dec 9]. Available at: <https://www.who.int/news-room/fact-sheets/detail/the-top-10-causes-of-death>.

² American College of Radiology. Lung CT Screening Reporting & Data System (Lung-RADS®), Version 1.1 cited 2021 March 30]. Available at: <https://www.acr.org/Clinical-Resources/Reporting-and-Data-Systems/Lung-Rads>.

³ Resolution of the Russia's Chief Public Health Officer dated July 7, 2009, No. 47 on the approval of SanPiN 2.6.1.2523-09 "Radiation Safety Standards (NRB-99/2009)." Available at: <https://docs.cntd.ru/document/902170553>.

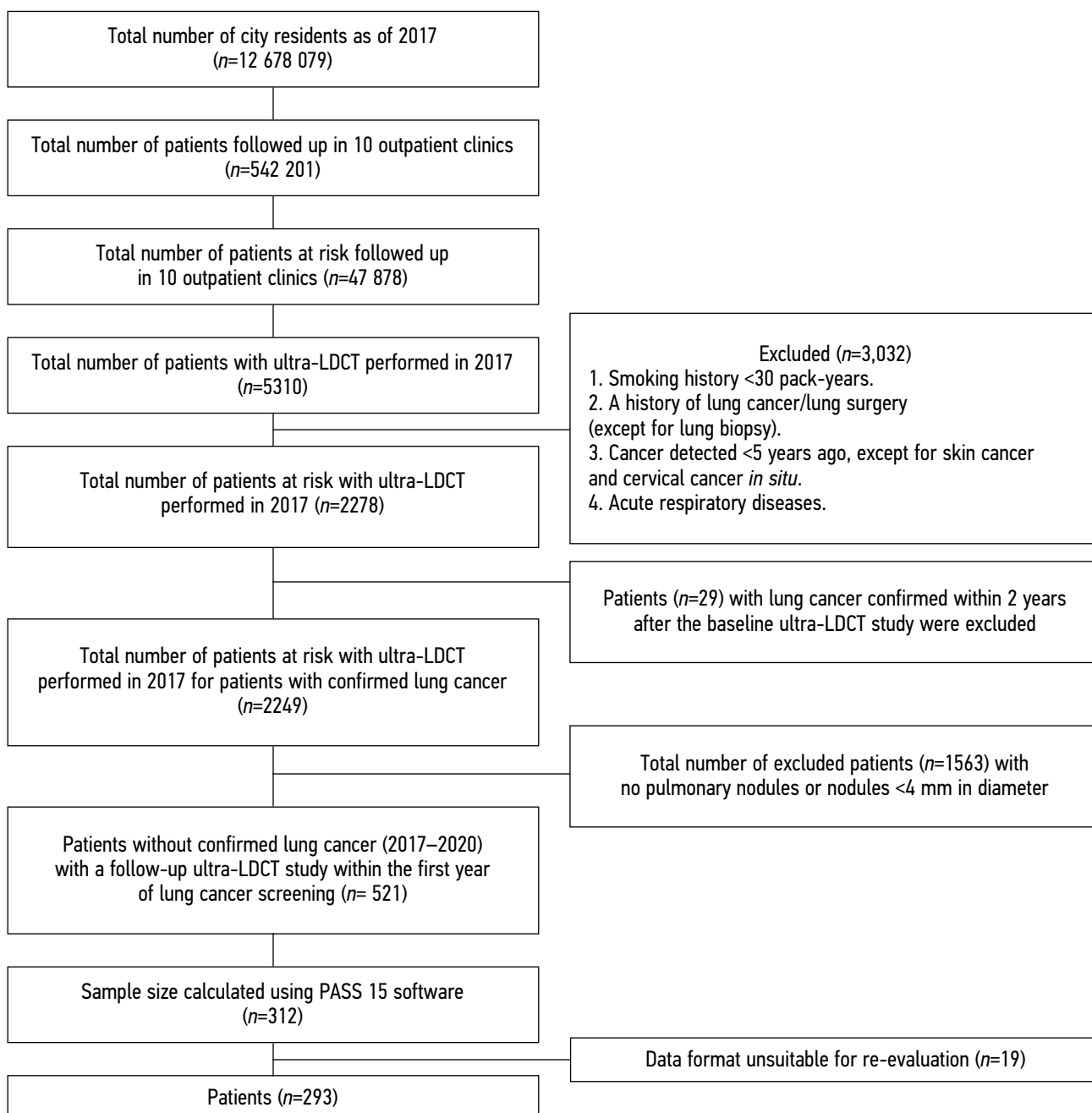


Figure 1. Subject selection flowchart.

70–90 kg = 1.0 mGy, and >90 kg = 1.2 mGy. The radiation dose was selected individually based on the patient's body weight.

Primary study outcome

A total of 1,450 pulmonary nodules were measured, 878 (61%) solid and 572 (39%) subsolid nodules, and the largest nodule was selected for each patient. After selecting the largest nodule, the final analysis included 293 nodules. Table 1 shows the distribution of nodules for each expert based on linear dimensions and volume. Following a consensus decision, 199 pulmonary nodules were classified as benign (<6 mm/<100 mm³) and 94 as requiring further evaluation (≥6 mm/≥100 mm³).

Ethics review

The study was approved by the independent ethics committee of the Central Clinical Hospital and Outpatient Clinic of the Administrative Directorate of the President of the Russian Federation (Moscow) on May 20, 2017. All participants signed an informed consent form.

Statistical analysis

The linear dimensions of pulmonary nodules were rounded to the nearest whole number. Pearson's chi-square test was used to examine differences in discrepancies and false-positive and false-negative results between the pulmonary nodule volume and linear dimensions. Fleiss' kappa was used to determine agreement among three

independent experts. To interpret the magnitude of this parameter, the Landis and Koch (1977) criteria were used: poor agreement, <0; slight agreement, 0.00–0.20; fair agreement, 0.21–0.40; moderate agreement, 0.41–0.60; substantial agreement, 0.61–0.80; and almost perfect agreement, >0.81 [14]. IBM SPSS Statistics version 26 was used for all statistical calculations, and $P < 0.05$ was considered significant.

RESULTS

Study subjects

The study included 293 participants, 166 (57%) of whom were men aged 50–80 (mean age 64.6 ± 5.3) years, with an average smoking history of 34.5 ± 10.7 years.

Main study outcomes

For volumetry, discrepancies with the reference standard were distributed as follows: 32 (10.9%; 4 false-positive results, 28 false-negative results), 29 (9.9%; 17 false-positive results, 12 false-negative results), and 30 (10.2%; 6 false-positive results, 24 false-negative results) nodules for experts 1, 2, and 3, respectively. For linear dimensions, incorrect nodule measurements were identified as 192 (65.5%; 107 false-positive results, 85 false-negative results), 146 (49.8%; 58 false-positive results, 88 false-negative results), and 102 (34.8%; 23 false-positive results, 79 false-negative results) for experts 1, 2, and 3, respectively (Table 2). When the BTS-recommended threshold value of 80 mm^3 was used, the number of incorrect measurements

increased: 35 errors were registered for expert 1, 50 for expert 2, and 41 for expert 3.

When three experts' averages were used, a total of 30 (10.2%) errors were detected for volumetry, compared with 147 (50.2%) for linear dimensions ($P < 0.001$). Volumetry demonstrated significantly fewer false-positive results ($n = 9$; 3.1%) than linear dimensions ($n = 63$; 21.5%; $P < 0.001$) and significantly fewer false-negative results (21; 7.2% vs. 84; 28.7%, respectively; $P < 0.001$).

The expert agreement analysis revealed that measuring volume had higher agreement than measuring linear dimensions. For volumetry, Fleiss' kappa was 0.672 (substantial agreement, 95% confidence interval 0.670–0.674), whereas for linear dimensions, Fleiss' kappa was 0.027 (slight agreement, 95% confidence interval 0.025–0.029).

DISCUSSION

Summary of the main study outcome

According to our findings, the use of volumetry instead of linear dimensions significantly reduced the number of incorrect interpretations while also lowering the number of false-positive and false-negative results. Expert agreement was significantly higher when volumetry was used instead of linear dimensions.

Discussion of the main study outcome

Our findings are consistent with those of the NELSON study and support the use of pulmonary nodule volumetry for

Table 1. Distribution of nodules per expert for linear dimensions and NELSON-plus/EUPS category

Parameters	Expert 1	Expert 2	Expert 3
<i>Linear dimensions</i>			
Nodule $\geq 6 \text{ mm}$	101	147	191
Nodule $< 6 \text{ mm}$	192	146	102
<i>Volume</i>			
$\geq 100 \text{ mm}^3$	223	194	217
$< 100 \text{ mm}^3$	70	99	76

Table 2. Results and discrepancies per expert for volumetry and linear dimensions

Parameters	Expert 1	Expert 2	Expert 3
<i>Volume</i>			
False-positive results	4 (1,4)	17 (5,8)	6 (2,0)
False-negative results	28 (9,6)	12 (4,1)	24 (8,2)
Discrepancies for each expert	32 (10,9)	29 (9,9)	30 (10,2)
<i>Linear dimensions</i>			
False-positive results	107 (36,5)	58 (19,8)	23 (7,8)
False-negative results	85 (29,0)	88 (30,0)	79 (27,0)
Discrepancies for each expert	192 (65,5)	146 (49,8)	102 (34,8)

Note. The percentage of the total number of nodules is shown in parentheses ($n = 293$).

ultra-LDCT results. Oudkerk et al. demonstrated that when using LDCT, the nodule size cannot be accurately interpreted solely by measuring its linear dimensions, especially in contentious cases. When extrapolating the volume from the linear dimensions, nodules measuring 8–10 mm fell into groups with volumes ranging from 50 to 500 mm³, and compared with semiautomatic volumetry, the use of linear dimensions resulted in a significant overestimation of the nodule volume. Previously, Revel et al. [14] also reported a problem in the analysis of small- and medium-sized nodules: the assessment of intra- and inter-expert agreement revealed that the measurement error reached 1.73 mm when assessed by two radiologists. Furthermore, Xie et al. [15] discovered that semiautomated volumetry yielded higher accuracy than manual measurements. Moreover, volumetry, including the use of artificial intelligence algorithms, is recommended by the European Society of Radiology and the European Respiratory Society [16]. In another study with pulmonary nodule marking, several radiologists found that the number of experts affected the correctness and consistency of estimates when measuring the nodule diameter. With an increase in the number of experts performing an independent interpretation of CT findings, the correctness of their assessments increases, whereas consistency decreases [17].

Study limitations

This study has several limitations. Owing to its retrospective design, a sampling bias is possible. Furthermore, this study used a relatively small sample. A larger number of cases may be more representative of a lung cancer screening population. According to Lung-RADS recommendations, the linear dimensions of the nodule along the long and short axes must be measured and the average

value calculated; however, the purpose of this work was to test the findings of the NELSON study.

CONCLUSION

This study shows that the use of semiautomatic volumetry of pulmonary nodules in the interpretation of LDCT findings can significantly reduce the number of false-positive and false-negative results when compared with measuring linear dimensions. This discovery is accompanied by increased agreement among experts and may reduce the unavoidable harms associated with lung cancer screening.

ADDITIONAL INFORMATION

Funding source. This article was prepared by a group of authors as part of the research work (USIS No. 123031400009-1) in accordance with the Order issued by the Moscow Health Care Department No. 1196 dated December 21, 2022.

Competing interests. The authors declare that they have no competing interests.

Authors' contribution. All authors made a substantial contribution to the conception of the work, acquisition, analysis, interpretation of data for the work, drafting and revising the work, final approval of the version to be published and agree to be accountable for all aspects of the work. M.M. Suchilova, I.A. Blokhin, V.Yu. Bosin — writing the original draft; O.O. Aleshina — data curation, investigation; V.A. Gombolevskiy, O.V. Omelyanskaya — conceptualization, study design; R.V. Reshetnikov, A.V. Vladzimirskyy — data curation.

Acknowledgments. The authors are grateful to V. Chernina, H. Lancaster, S. Zheng, M. Silva, M. Dorrius, J. Gratama, and M. Oudkerk for their help with the article.

REFERENCES

1. De Koning HJ, van der Aalst CM, de Jong PA, et al. Reduced lung-cancer mortality with volume CT screening in a randomized trial. *N Engl J Med*. 2020;382(6):503–513. doi: 10.1056/NEJMoa1911793
2. Henschke CI, Boffetta P, Yankelevitz DF, Altorki N. Computed tomography screening: The International Early Lung Cancer Action Program Experience. *Thoracic Sur Clin*. 2015;25(2):129–143. doi: 10.1016/j.thorsurg.2014.12.001
3. Callister ME, Baldwin DR, Akram AR, et al. Correction: British Thoracic Society guidelines for the investigation and management of pulmonary nodules: Accredited by NICE. *Thorax*. 2015;70(Suppl 2):ii1–ii54. doi: 10.1136/thoraxjnl-2015-207168
4. Oudkerk M, Devaraj A, Vliegthart R, et al. European Position Statement on Lung Cancer Screening. *Lancet Oncology*. 2017;18(12):e754–766. doi: 10.1016/S1470-2045(17)30861-6
5. Wood DE, Kazerooni EA, Baum SL, et al. Lung cancer screening, version 3.2018, NCCN clinical practice guidelines in oncology. *J Natl Compr Canc Netw*. 2018;16(4):412–441. doi: 10.6004/jnccn.2018.0020
6. Horeweg N, Scholten ET, de Jong PA, et al. Detection of lung cancer through low-dose CT screening (NELSON): A prespecified analysis of screening test performance and interval cancers. *Lancet Oncology*. 2014;15(3):1342–1350. doi: 10.1016/S1470-2045(14)70387-0
7. Oudkerk M, Liu S, Heuvelmans MA, et al. Lung cancer LDCT screening and mortality reduction: Evidence, pitfalls and future perspectives. *Nat Rev Clin Oncol*. 2021;18(3):135–151. doi: 10.1038/s41571-020-00432-6
8. Duffy SW, Field JK. Mortality reduction with low-dose CT screening for lung cancer. *N Engl J Med*. 2020;382(6):572–573. doi: 10.1056/NEJMe1916361
9. Morozov SP, Kuzmina ES, Vetsheva NN, et al. Moscow screening: Screening of lung cancer using low-dose computed tomography. *Problems Social Hygiene Healthcare History Med*. 2019;27(S):630–636. (In Russ). doi: 10.32687/0869-866X-2019-27-si1-630-636
10. Gombolevsky VA, Barchuk AA, Laipan AS, et al. Lung cancer screening with low-dose computed tomography: Management and efficiency. *Radiology Practice*. 2018;(1):28–36. (In Russ).
11. Landis JR, Koch GG. The measurement of observer agreement for categorical data. *Biometrics*. 1977;33(1):159–174.
12. Revel MP, Bissery A, Bienvenu M, et al. Are two-dimensional ct measurements of small noncalcified pulmonary nodules reliable?

Radiology. 2004;231(2):453–458. doi: 10.1148/radiol.2312030167

13. Xie X, Willeminck MJ, Zhao Y, et al. Inter- and intrascanner variability of pulmonary nodule volumetry on low-dose 64-row CT: an anthropomorphic phantom study. *BJR*. 2013;86(1029):20130160. doi: 10.1259/bjr.20130160

СПИСОК ЛИТЕРАТУРЫ

1. De Koning H.J., van der Aalst C.M., de Jong P.A., et al. Reduced lung-cancer mortality with volume CT screening in a randomized trial // *New Eng J Med*. 2020. Vol. 382, N 6. P. 503–513. doi: 10.1056/NEJMoa1911793

2. Henschke C.I., Boffetta P., Yankelevitz D.F., Altorki N. Computed tomography screening: The International Early Lung Cancer Action Program Experience // *Thoracic Sur Clin*. 2015. Vol. 25, N 2. P. 129–143. doi: 10.1016/j.thorsurg.2014.12.001

3. Callister M.E., Baldwin D.R., Akram A.R., et al. Correction: British Thoracic Society guidelines for the investigation and management of pulmonary nodules: Accredited by NICE // *Thorax*. 2015. Vol. 70, Suppl 2. P. ii1–ii54. doi: 10.1136/thoraxjnl-2015-207168

4. Oudkerk M., Devaraj A., Vliegenthart R., et al. European Position Statement on Lung Cancer Screening // *Lancet Oncology*. 2017. Vol. 18, N 12. P. e754–e766. doi: 10.1016/S1470-2045(17)30861-6

5. Wood D.E., Kazerooni E.A., Baum S.L., et al. Lung cancer screening, version 3.2018, NCCN clinical practice guidelines in oncology // *J Nation Compr Can Netw*. 2018. Vol. 16, N 4. P. 412–441. doi: 10.6004/jnccn.2018.0020

6. Horeweg N., Scholten E.T., de Jong P.A., et al. Detection of lung cancer through low-dose CT screening (NELSON): A prespecified analysis of screening test performance and interval cancers // *Lancet Oncology*. 2014. Vol. 15, N 12. P. 1342–1350. doi: 10.1016/S1470-2045(14)70387-0

7. Oudkerk M., Liu S., Heuvelmans M.A., et al. Lung cancer LDCT screening and mortality reduction: Evidence, pitfalls and future perspectives // *Nat Rev Clin Oncol*. 2021. Vol. 18, N 3. P. 135–151. doi: 10.1038/s41571-020-00432-6

14. Kulberg NS, Reshetnikov RV, Novik VP, et al. Inter-observer variability between readers of CT images: all for one and one for all. *Digital Diagnostics*. (In Russ). 2021;2(2):105–118 doi: 10.17816/DD60622

8. Duffy S.W., Field J.K. Mortality reduction with low-dose CT screening for lung cancer // *New Eng J Med*. 2020. Vol. 382, N 6. P. 572–573. doi: 10.1056/NEJMe1916361

9. Морозов С.П., Кузьмина Е.С., Ветшева Н.Н., и др. Московский скрининг: скрининг рака лёгкого с помощью низкодозовой компьютерной томографии // *Проблемы социальной гигиены, здравоохранения и истории медицины*. 2019. Т. 27, № 5. С. 630–636. doi: 10.32687/0869-866X-2019-27-si1-630-636

10. Гомболевский В.А., Барчук А.А., Лайпан А.Ш., и др. Организация и эффективность скрининга злокачественных новообразований легких методом низкодозной компьютерной томографии // *Радиология-практика*. 2018. № 1. С. 28–36.

11. Landis J.R., Koch G.G. The measurement of observer agreement for categorical data // *Biometrics*. 1977. Vol. 33, N 1. P. 159–174.

12. Revel M.P., Bissery A., Bienvenu M., et al. Are two-dimensional CT measurements of small noncalcified pulmonary nodules reliable? // *Radiology*. 2004. Vol. 231, N 2. P. 453–458. doi: 10.1148/radiol.2312030167

13. Xie X, Willeminck M.J., Zhao Y., et al. Inter-and intrascanner variability of pulmonary nodule volumetry on low-dose 64-row CT: An anthropomorphic phantom study // *Brit J Radiol*. 2013. Vol. 86, N 1029. P. 20130160. doi: 10.1259/bjr.20130160

14. Кульберг Н.С., Решетников Р.В., Новик В.П., и др. Вариабельность заключений при интерпретации КТ-снимков: один за всех и все за одного // *Digital Diagnostics*. 2021. Т. 2, № 2. С. 105–118. doi: 10.17816/DD60622

AUTHORS' INFO

* **Maria M. Suchilova**, MD;

address: 24/1 Petrovka street, 127051 Moscow, Russia;
ORCID: <https://orcid.org/0000-0003-1117-0294>;
eLibrary SPIN: 4922-1894; e-mail: m.suchilova@npcmr.ru

Ivan A. Blokhin, MD;

ORCID: <https://orcid.org/0000-0002-2681-9378>;
eLibrary SPIN: 3306-1387; e-mail: i.blokhin@npcmr.ru

Olga O. Aleshina, MD;

ORCID: <https://orcid.org/0000-0001-9924-0204>;
eLibrary SPIN: 6004-2422; e-mail: olya.aleshina.tula@gmail.com

Victor A. Gombolevskiy, MD, Cand. Sci. (Med);

ORCID: <https://orcid.org/0000-0003-1816-1315>;
eLibrary SPIN: 6810-3279; e-mail: gombolevskiy@npcmr.ru

Roman V. Reshetnikov, Cand. Sci. (Phys.-Math.);

ORCID: <https://orcid.org/0000-0002-9661-0254>;
eLibrary SPIN: 8592-0558; e-mail: reshetnikov@fbb.msu.ru

ОБ АВТОРАХ

* **Сучилова Мария Максимовна**;

адрес: Россия, 127051, Москва, ул. Петровка, д. 24, стр. 1;
ORCID: <https://orcid.org/0000-0003-1117-0294>;
eLibrary SPIN: 4922-1894; e-mail: m.suchilova@npcmr.ru

Блохин Иван Андреевич;

ORCID: <https://orcid.org/0000-0002-2681-9378>;
eLibrary SPIN: 3306-1387; e-mail: i.blokhin@npcmr.ru

Алёшина Ольга Олеговна;

ORCID: <https://orcid.org/0000-0001-9924-0204>;
eLibrary SPIN: 6004-2422; e-mail: olya.aleshina.tula@gmail.com

Гомболевский Виктор Александрович, к.м.н.;

ORCID: <https://orcid.org/0000-0003-1816-1315>;
eLibrary SPIN: 6810-3279; e-mail: gombolevskiy@npcmr.ru

Решетников Роман Владимирович, к.ф.-м.н.;

ORCID: <https://orcid.org/0000-0002-9661-0254>;
eLibrary SPIN: 8592-0558; e-mail: reshetnikov@fbb.msu.ru

* Corresponding author / Автор, ответственный за переписку

Viktor Yu. Bosin, MD, Dr. Sci. (Med.);

ORCID: <https://orcid.org/0000-0002-4619-2744>;

eLibrary SPIN: 3380-7889; e-mail: bosin@npcmr.ru

Olga V. Omelyanskaya;

ORCID: <https://orcid.org/0000-0002-0245-4431>;

eLibrary SPIN: 8948-6152; e-mail: o.omelyanskaya@npcmr.ru

Anton V. Vladzimirskyy, MD, Dr. Sci (Med.);

ORCID: <https://orcid.org/0000-0002-2990-7736>;

eLibrary SPIN: 3602-7120; e-mail: a.vladzimirskiy@npcmr.ru

Босин Виктор Юрьевич, д.м.н.;

ORCID: <https://orcid.org/0000-0002-4619-2744>;

eLibrary SPIN: 3380-7889; e-mail: bosin@npcmr.ru

Омелянская Ольга Васильевна;

ORCID: <https://orcid.org/0000-0002-0245-4431>;

eLibrary SPIN: 8948-6152; e-mail: o.omelyanskaya@npcmr.ru

Владзimirский Антон Вячеславович, д.м.н.;

ORCID: <https://orcid.org/0000-0002-2990-7736>;

eLibrary SPIN: 3602-7120; e-mail: a.vladzimirskiy@npcmr.ru

DOI: <https://doi.org/10.17816/DD111816>

Телеультразвуковые исследования с использованием смартфонов и одноплатных компьютеров

К.М. Арзамасов¹, В.А. Дроговоз², Т.М. Бобровская¹, А.В. Владзимирский^{1, 3}

¹ Научно-практический клинический центр диагностики и телемедицинских технологий, Москва, Российская Федерация

² Научно-производственное объединение «Русские базовые информационные технологии», Москва, Российская Федерация

³ Первый Московский государственный медицинский университет имени И.М. Сеченова (Сеченовский Университет), Москва, Российская Федерация

АННОТАЦИЯ

Обоснование. Рост доступности и вычислительной мощности мобильных устройств приводит к расширению их области применения. Медицина не стала исключением: одноплатные компьютеры и смартфоны активно применяются в телемедицине.

Цель — изучить техническую возможность реализации телеультразвуковых исследований при помощи одноплатных компьютеров и смартфонов.

Материалы и методы. В данном исследовании проводили захват ультразвукового видеоизображения при помощи внешних USB-устройств видеозахвата. В качестве платформы для сервера телеультразвуковых исследований использовали одноплатные компьютеры Raspberry Pi, а также смартфон на базе Android. В качестве программного обеспечения использовали VLC, Motion, USB Camera. Дистанционная оценка экспертом проводилась также на мобильных устройствах: посредством VLC при работе на сервере программного обеспечения VLC, в остальных случаях — Google Chrome на Windows 7 и Android, Chromium на Raspberry Pi.

Результаты. Устройство видеозахвата на базе чипсета UTV007 позволяет получить более качественное изображение по сравнению с устройством на базе чипсета AMT630A. Оптимальное разрешение видеоизображения 720×576 при 25 кадрах в секунду. Оптимальным программным обеспечением для организации телеУЗИ на Raspberry Pi является VLC из-за низких требований к пропускной способности каналов связи ($0,64 \pm 0,17$ Мбит/с). Для Android-смартфонов телеультразвуковое исследование может быть реализовано на программном обеспечении USB Camera, но требует большей пропускной способности каналов связи ($5,2 \pm 0,3$ Мбит/с).

Заключение. Использование устройств на базе одноплатных компьютеров и смартфонов позволяет реализовать бюджетную телеультразвуковую систему, что потенциально способствует повышению качества выполняемых исследований за счёт дистанционного обучения и консультирования врачей. Данные решения могут применяться в том числе в удалённых регионах, для задач «полевой» медицины и других возможных направлений мобильного здравоохранения.

Ключевые слова: ультразвуковое исследование; УЗИ; телеУЗИ; телемедицина; видеозахват.

Как цитировать

Арзамасов К.М., Дроговоз В.А., Бобровская Т.М., Владзимирский А.В. Телеультразвуковые исследования с использованием смартфонов и одноплатных компьютеров // *Digital Diagnostics*. 2023. Т. 4, № 1. С. 15–23. DOI: <https://doi.org/10.17816/DD111816>

DOI: <https://doi.org/10.17816/DD111816>

Tele-ultrasound imaging using smartphones and single-board PCs

Kirill M. Arzamasov¹, Viktor A. Drogovoz², Tatiana M. Bobrovskaya¹, Anton V. Vladzimirskyy^{1, 3}

¹ Moscow Center for Diagnostics and Telemedicine, Moscow, Russian Federation

² Scientific and Production Association "Russian Basic Information Technologies", Moscow, Russian Federation

³ The First Sechenov Moscow State Medical University, Moscow, Russian Federation

ABSTRACT

BACKGROUND: Mobile devices are widely available and their computational performance increases. Nonetheless, medicine should not be an exception: single-board computers and mobile phones are crucial aides in telehealth.

AIM: To explore tele-ultrasound scope using smartphones and single-board computers

MATERIALS AND METHODS: This study focused on capturing ultrasound videos using external video recording devices connected via USB. Raspberry Pi single-board computers and Android smartphones have been used as platforms to host a tele-ultrasound server. Used software: VLC, Motion, and USB camera. A remote expert assessment was performed with mobile devices using the following software: VLC acted as a VLC server, Google Chrome for OS Windows 7 and OS Android was used in the remaining scenarios, and Chromium browser was installed on the Raspberry Pi computer.

OUTCOMES: The UTV007 chip-based video capture device produces better images than the AMT630A-based device. The optimum video resolution was 720×576 and 25 frames per second. VLC and OBS studios are considered the most suitable for a raspberry-based ultrasound system owing to low equipment and bandwidth requirements (0.64±0.17 Mbps for VLC; 0.5 Mbps for OBS studio). For Android phone OS, the ultrasound system was set with the USB camera software, although it required a faster network connection speed (5.2±0.3 Mbps).

CONCLUSION: The use of devices based on single-board computers and smartphones implements a low-cost tele-ultrasound system, which potentially improves the quality of studies performed through distance learning and consulting doctors. These solutions can be used in remote regions for "field" medicine tasks and other possible areas of m-health.

Keywords: Tele-ultrasound, telehealth, ultrasound, video capturing.

To cite this article

Arzamasov KM, Drogovoz VA, Bobrovskaya TM, Vladzimirskyy AV. Tele-ultrasound imaging using smartphones and single-board PCs. *Digital Diagnostics*. 2023;4(1):15–23. DOI: <https://doi.org/10.17816/DD111816>

Received: 11.10.2022

Accepted: 10.03.2023

Published: 04.04.2023

DOI: <https://doi.org/10.17816/DD111816>

使用智能手机和单板电脑进行远程超声检查

Kirill M. Arzamasov¹, Viktor A. Drogovoz², Tatiana M. Bobrovskaya¹,
Anton V. Vladzimirskyy^{1,3}

¹ Moscow Center for Diagnostics and Telemedicine, Moscow, Russian Federation

² Scientific and Production Association "Russian Basic Information Technologies", Moscow, Russian Federation

³ The First Sechenov Moscow State Medical University, Moscow, Russian Federation

简评

论证。移动设备的可用性和计算能力不断提高，导致其应用不断扩大。医学也不例外：单板电脑和智能手机被积极用于远程医疗。

目的是研究使用单板计算机和智能手机进行远程超声检查的技术可行性。

材料和方法。在这项研究中，超声视频图像采集是使用USB外置视频采集设备进行的。一台树莓派（Raspberry Pi）单板电脑和一台安卓（Android）智能手机被用作远程超声检查服务器的平台。VLC、Motion和USB摄像头被用作软件。专家也在移动设备上进行了远程评估，使用的是：VLC——当在VLC软件服务器上运行时；在其他情况下，在Windows 7和安卓上使用谷歌浏览器（Google Chrome）；在树莓派上使用Chromium。

结果。与基于AMT630A芯片组的设备相比，基于UTV007芯片组的视频采集设备提供更好的图像质量。最佳视频分辨率为720x576，每秒25帧。由于通信信道带宽要求低（ 0.64 ± 0.17 Mbps），树莓派上的进行远程超声检查的最佳软件是VLC。对于安卓智能手机，远程超声检查是可以在USB摄像头软件上进行的，但需要更高的通信信道带宽（ 5.2 ± 0.3 Mbps）。

结论。使用基于单板电脑和智能手机的设备使实现不贵的远程超声系统有可能，这潜在地有助于通过远程培训和咨询医生提高所做检查的质量。这些解决方案也可用于偏远地区、野外医疗和其他可能的移动医疗领域。

关键词：远程超声检查，远程医疗，超声检查，视频采集。

To cite this article

Arzamasov KM, Drogovoz VA, Bobrovskaya TM, Vladzimirskyy AV. 使用智能手机和单板电脑进行远程超声检查. *Digital Diagnostics*. 2023;4(1):15–23. DOI: <https://doi.org/10.17816/DD111816>

收到: 11.10.2022

接受: 10.03.2023

发布日期: 04.04.2023

BACKGROUND

At present, mobile devices show higher performance with lower costs. These factors expand the scope of mobile device applications, including medicine and telemedicine. [1–3]

Teleultrasonography (or teleultrasound) is a unique example of telemedicine. [4] In this diagnostic technique, a functional diagnostics specialist or an ultrasound specialist receives and analyzes data from a remote ultrasonogram and sends back a medical report or recommendations. This process requires a special software and hardware complex.

Some cases of teleultrasound using a smartphone have been reported, [5–8] i.e., when an image from the screen of an ultrasound scanner was captured by a smartphone camera and transmitted using communication programs. No additional equipment is required, and this is the great advantage of this technique. However, some technical difficulties were reported, such as the need for additional staff or special devices for holding a smartphone when recording an examination and the lower quality of ultrasound images delivered to an expert compared with the original.

At present, there are mobile video capture devices that can be connected not only to a personal computer but also to mobile devices such as single-board computers (SBCs) and smartphones.

This study aimed to evaluate technical opportunities for implementing teleultrasound techniques using SBCs and smartphones.

MATERIALS AND METHODS

Software

The study used Sequoya 512 Acuson and SonoAce-8000 ultrasound scanners. One of the study authors volunteered to undergo a standard ultrasound examination of brachiocephalic arteries performed by a functional diagnostics specialist. Based on an expert review (three specialists with >10 years of experience), the image quality and possibility of interpretation were subjectively assessed. Thus, fragments of the examination provided were stored in an ultrasound scanner in the form of 5-s cine loops, which were then cyclically reproduced on the ultrasound scanner. A total of nine cine loops were recorded, three for each mode: B-mode only, B-mode + color Doppler mapping, and B-mode + spectral Doppler. The expert could evaluate the image on the monitor screen of the ultrasound scanner and screen of the client device in real time. Moreover, the above technique allowed experts to evaluate results obtained with different software and hardware systems during the same examination (on the same cine loop).

We used a Defender C-090 USB camera and low-cost video capture systems from an ultrasound scanner. Since low-cost systems use two types of microcircuits (chipsets) as an analog-to-digital converter, i.e., UTV007 and AMT630A, both options were tested:

- 1) Gembird UVG-002, a video capture device based on the UTV007 chipset with a resolution of 720 × 576 at 25 frames per second,
- 2) Espada USB 2.0 –RCA/S–video EUsbRca63 (hereinafter referred to as EUsbRca63) is a video capture device based on the AMT630A chipset with a resolution of 720 × 576 at 25 frames per second.

The following software was used for the on-server study:

- VLC version 3.0.8 is a free video transmitting and playing software with the option to stream video from external devices. It runs under different operating systems, including Linux and Android. The study used this software simultaneously on the server and client of the telemedicine system.
- Motion Release 4.3.0, free software designed for CCTV cameras, focused on motion detection in a frame. This software runs under the Linux operating system and was installed on SBCs. It has the option of running as a background process. However, this software can only broadcast images without sound. Access required user identification and a password.
- USB Camera version 9.7.9. is freely distributed software designed to transfer images from USB cameras, and a non-commercial version was used to operate as a server on Android devices.

The main criterion for software selection was the ability to use various operating platforms. Then, these software and hardware solutions were assessed for suitability for use as a telemedicine system. Data transfer speed was evaluated (expressed as mean ± standard deviation). Microsoft Excel software was used for statistical processing of the results.

Telemedicine System

A telemedicine system consists of a server and a client. In this paper, a server is a software and hardware complex that transmits a video image from an ultrasound scanner. A client is a device that receives and plays video. The client and the server were connected through a local network using a Wi-Fi router with a bandwidth of 72 Mbps. During testing, the highest video signal quality (maximum resolution and maximum frame rate) was selected. The client was connected to the server using protocols supported by the installed software, such as HTTP and RTSP. The following client programs were required for video playback: VLC for RTSP, Google Chrome on Windows 7 and Android, and Chromium on Raspberry Pi for HTTP. Each software installed on the server supported its codec: JPEG (Motion), VideoH.264 (VLC), and H.264 (USB Camera).

Two connection options are available (Fig. 1).

1. The server is a smartphone (Android 7.0, 2 GHz 8-core processor, 3 GB RAM, or Onyx Max3 Android 9.0, 2 GHz 8-core processor, 4 GB RAM) connected to a video capture device via an OTG-USB cable. The video capture device is connected to the video output of the

ultrasound scanner. The client is a laptop based on AMD E-450 APU, 8 GB RAM, 64-bit OS Windows 7, or a smartphone.

- The server is a single-board microcomputer (Raspberry Pi 1 Model B, CPU 700 MHz, 512 MB or Raspberry Pi 4, CPU Quad Core Cortex 1.5 GHz, 4 GB with Linux version 4.19.118-v7+ installed) connected to the video capture device via a USB cable with a USB webcam. Raspberry Pi 1 did not have a Wi-Fi module and was connected to the router via a LAN cable. The client is a laptop based on AMD E-450 APU, 8 GB RAM, 64-bit OS Windows 7, or a smartphone.

RESULTS

Ultrasound scanners. Two video outputs were tested on the Sequoya 512 ultrasound scanner, including a coaxial output for connecting a video printer and an S-Video output for connecting a VCR. When the image was analyzed at the output of the video printer, a black-and-white image was obtained, partially going beyond the fields of video capture devices. Conversely, when connected to the S-Video output, a color image was obtained, corresponding to the original on the monitor screen of the ultrasound scanner. Sequoya 512 was used with Raspberry Pi-based systems. SonoAce-8000 was used to implement teleultrasound based on Android devices. As in the previous case, S-Video was selected for the video output.

UVG-002. This device was successfully detected on all mobile devices and ran normally with all tested programs. It provided the declared maximum resolution on all devices.

The maximum frame rate was reached on all devices, except for Raspberry Pi 1.

EUsbRca63. This device was successfully identified on all mobile devices and operated normally with all tested programs, except for VLC on Raspberry. The declared maximum resolution was not achieved on any of the devices. The maximum resolution was 640 × 480.

USB camera. The USB camera was successfully detected on all mobile devices and ran normally with all tested programs. The maximum resolution was 640 × 480, and the frame rate was 30 per second.

Motion software. It has been configured to run as a server: continuous recording and transmission of images from video devices with maximum resolution. Owing to the low performance, Raspberry Pi 1 was able to produce 1–1.5 frames per second. Raspberry Pi 4 had none of these problems; thus, it was possible to run several processes simultaneously with the same quality of the broadcast video.

VLC software. The successful installation on Raspberry Pi 4 allowed streaming from external video capture devices. We also successfully implemented two VLC applications simultaneously with video capture from a video capture device and a webcam, whereas the image quality and frame rate corresponded to the maximum. In addition, we tested the ability to run VLC and Motion simultaneously on a Raspberry Pi 4. VLC was installed on Android devices; however, in this version, it did not allow the operation of a server but only functioned in client mode. In the client mode, it was also used on a Windows laptop.

USB-Cam software. The implementation of a telemedicine server based on this software was extremely sensitive to the

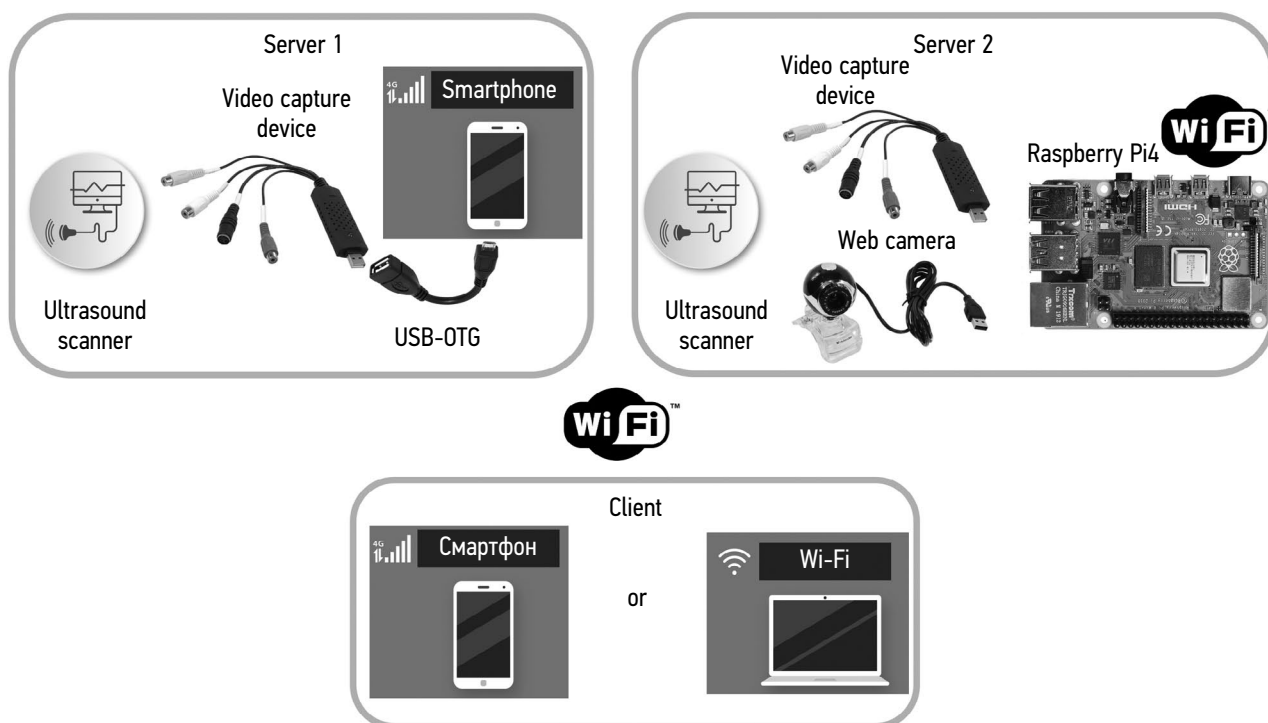


Figure 1. Connection diagram.

quality of the communication channel. Therefore, at a signal level below 80 dB, it was disconnected, and there was no difference in which side the low quality of the connection was from, the server or the client side.

DISCUSSION

Based on the study results, we prepared a list of devices and software solutions for the implementation of mobile teleultrasound systems. The test results are presented in Table 1: a video capture device based on the UTV007 chipset allows us to obtain a subjectively better image than a device based on the AMT630A chipset. The UVG-002 device can operate on all platforms and with all the used software. This demonstrated a high-quality picture.

The EUsbRca63 video capture module showed satisfactory performance on mobile devices. We were unable to set this module for operating with VLC, even though Motion EUsbRca63 smoothly ran with the same driver. The quality of the resulting ultrasound image was extremely low on all platforms: the inscriptions on the image were illegible, and adequate assessment of the ultrasound image of such quality was impossible.

For optimal software selection, the platform planned to be used with the teleultrasound server was determined. Therefore, in the case of an Android-based smartphone, USB-Cam is the only software considered; however, in this variant, teleultrasound will require a special bandwidth of the communication channel. In our case, the channel capacity for transmitting ultrasound data was 4.4–5.2 Mbit/s, which is practically difficult to achieve using cellular networks. Conversely, when connecting to Wi-Fi, this requirement for the bandwidth of the communication channel becomes less important. During the testing, this software and hardware complex was highly sensitive to the quality of the Wi-Fi signal (i.e., distance from the access point). Given these facts, opportunities for the implementation of teleultrasound in mobile networks are seriously limited.

At present, SBCs are increasingly and actively used in telemedicine. [9, 10] We consider recent SBCs to be the optimal platform for the implementation of teleultrasound. The tested Raspberry Pi models showed a significant increase in computing power, with the first generation of Pi 1 being only able to transmit video at a speed of ≥ 1.5

frames per second (in our study, the minimum frame rate on the ultrasound scanner was 16 frames per second), which is thought to be insufficient to implement a teleultrasound server. However, this device may act as a client in this system. Raspberry Pi 4 demonstrated high performance by simultaneously broadcasting two video streams.

The increased computing power of SBCs allows the implementation of machine-learning technologies, [11, 12] including in healthcare. [13] The available computing power of an SBC may be sufficient for use with a medical decision support system in parallel with the teleultrasound server for evaluating ultrasound images for abnormalities.

The choice between Motion or VLC must be guided by the bandwidth of the communication channel. Therefore, our data show that one video stream for VLC required 0.5–0.6 Mbps, and for Motion, the bandwidth should be at least 10 times greater. The literature review demonstrates that a connection speed from 0.6 [14] to 1.5 Mbps [15] is the minimum allowable for comfortable work of a remote expert, provided that the frame rate is 15 per second and the original video resolution is preserved. If it is necessary to transfer only the image from the screen of the ultrasound scanner and there is no limitation on the bandwidth of the communication channel, the Motion software is the best solution because it allows autonomously starting and deploying the teleultrasound server without human intervention. In other cases, VLC may be selected. Our study also revealed the possibility of simultaneously using two different systems.

In a previous paper [16], we showed the possibility of using streaming technologies in a PC-based teleultrasound system. However, the use of smartphones and SBCs makes teleultrasound an even more mobile technique. A device for a teleultrasound server with the necessary cables fits easily into a doctor's pocket, allowing him/her to keep the connection kit ready and, if necessary, organize broadcasting the examination within seconds.

Study Limitations

In this study, only two models of ultrasound scanners were analyzed. However, this technical solution can be also suitable for other ultrasound scanners that have similar or different supported video outputs. This study included only a small number of modern mobile devices, video capture devices, and software for working with video

Table 1. Test results for software and video signal devices

Parameters		Motion	VLC	USB-Cam
Codec		JPEG	VideoH.264	H.264
Connection protocol		HTTP	HTTP, RTSP	HTTP
Transfer rate, Mbps	UVG-002	18,7±2,8	0,64±0,17	5,2±0,3
	EUsbRca63	8,6±1,4	-	4,4±0,2
	Webcam	15,3±5	0,49±0,19	2,0±0,1

capture devices and webcams; however, we created several functioning low-cost systems for mobile teleultrasound. We focused on searching for the most affordable way to perform teleultrasound. During the study, the cost of a mobile device (Raspberry Pi4) and a video capture module did not exceed 6,000 rubles. At present, a similar package costs from 12,000 rubles. The software used (Motion, VLC, and USB-Cam) had a free license or was distributed with an open-source code. It is assumed that the operating system (Windows, Linux, and Android) is installed on the devices as part of the telemedicine system.

For such testing, the bandwidth [17] and security of communication channels used for healthcare data transmission must be considered. [3] The organization of VPN tunnels is one of the possible ways to ensure the security of transmitted data. However, the study of information security during teleultrasound is not the goal of this paper. This study is unique in that it proposes a new technical solution for teleultrasound.

Portable ultrasound systems are now available, including those with the function of image transmission (teleultrasound), such as Butterfly iQ + Butterfly Network Inc., Kosmos EchoNous, Vscan Air General Electric, and Lumif Philips Healthcare. However, these systems are expensive (>500,000 rubles) and do not have all the options necessary for a complete examination using a stationary ultrasound scanner. [18] The advantage of our approach is the use of ultrasound equipment, which is part of the standard ultrasound equipment.

REFERENCES

- Shi J, Wang F, Qin M, et al. New ECG compression method for portable ECG monitoring system merged with binary convolutional auto-encoder and residual error compensation. *Biosensors (Basel)*. 2022;12(7):524. doi: 10.3390/bios12070524
- Palacios DR, Shen K, Baig S, et al. Wide field of view handheld smart fundus camera for telemedicine applications. *J Med Imaging (Bellingham)*. 2021;8(2):026001. doi: 10.1117/1.JMI.8.2.026001
- Shewale AD, Patil SA, Patil SR. Raspberry-pi based automatic health care modelling: An IoT approach. *Compliance Engineering J*. 2021;12(3):99–104.
- Recker F, Höhne E, Damjanovic D, Schäfer VS. Ultrasound in telemedicine: A brief overview. *Appl Sci*. 2022;12:958. doi: 10.3390/app12030958
- Lim TH, Choi HJ, Kang BS. Feasibility of dynamic cardiac ultrasound transmission via mobile phone for basic emergency teleconsultation. *J Telemed Telecare*. 2010;5(16):281–285. doi: 10.1258/jtt.2010.091109
- Miyashita T, Iketani Y, Nagamine Y, Goto T. FaceTime® for teaching ultrasound-guided anesthetic procedures in remote place. *J Clin Monit Comput*. 2014;2(28):211–215. doi: 10.1007/s10877-013-9514-x
- Kim C, Cha H, Kang BS, et al. A feasibility study of smartphone-based teleultrasonography for evaluating cardiac dynamic function and diagnosing acute appendicitis with control of the image quality of the transmitted videos. *J Digit Imaging*. 2016;3(29):347–356. doi: 10.1007/s10278-015-9849-6
- Boissin C, Blom L, Wallis L, et al. Image-based teleconsultation using smartphones or tablets: qualitative assessment of medical experts. *Emergency Med J*. 2017;34(2):95–99. doi: 10.1136/emmermed-2015-205258
- Beckhauser E, Petrolini VA, Savaris A, et al. Are single-board computers an option for a low-cost multimodal telemedicine platform? First tests in the context of Santa Catarina state integrated telemedicine and telehealth system. In: Conference: 2016 IEEE 29th International Symposium on Computer-Based Medical Systems (CBMS). 2016. P. 163–168. doi: 10.1109/CBMS.2016.57
- Bhojwani H, Sain GK, Sharma GP. A hybrid connectivity oriented telemedicine system for Indian landscape using Raspberry Pi SBC & IOT. In: Conference: 2018 3rd Technology Innovation Management and Engineering Science International Conference (TIMES-iCON). 2018. P. 1–5. doi: 10.1109/TIMES-iCON.2018.8621799
- De Oliveira DC, Wehrmeister MA. Using deep learning and low-cost rgb and thermal cameras to detect pedestrians in aerial images captured by multirotor UAV. *Sensors (Basel)*. 2018;7(18):2244. doi: 10.3390/s18072244
- Kim W, Jung WS, Choi HK. Lightweight driver monitoring system based on multi-task mobilenets. *Sensors (Basel)*. 2019;14(19):3200. doi: 10.3390/s19143200
- Peine A, Hallawa A, Schöffski O, et al. A deep learning approach for managing medical consumable materials in intensive care units via convolutional neural networks: technical proof-of-concept study. *JMIR Med Informatics*. 2019;4(7):e14806–e14806. doi: 10.2196/14806

CONCLUSION

The use of devices based on SBCs and smartphones allows the creation of a low-cost teleultrasound system, which potentially contributes to improving the quality of examinations performed for distance learning and consulting HCPs. These solutions can be also used in remote regions as a part of the “field” of medicine and other possible areas of mobile healthcare.

ADDITIONAL INFORMATION

Funding source. This study was not supported by any external sources of funding.

Competing interests. The authors declare that they have no competing interests.

Authors' contribution. All authors made a substantial contribution to the conception of the work, acquisition, analysis, interpretation of data for the work, drafting and revising the work, final approval of the version to be published and agree to be accountable for all aspects of the work. K.M. Arzamasov — research design development, research volunteer; K.M. Arzamasov, T.M. Bobrovskaya — data analysis; K.M. Arzamasov, T.M. Bobrovskaya, V.A. Drogovoz — data interpretation; K.M. Arzamasov, V.A. Drogovoz — writing the text of the manuscript.

Acknowledgments. The authors are grateful to collaborators of Moscow Center for Diagnostics and Telemedicine: doctor of functional diagnostics, MD PhD D.V. Shutov and the leading researcher, MD PhD A.E. Demkina for their help in this study.

14. Yoo SK, Kim DK, Jung SM, et al. Performance of a web-based, realtime, tele-ultrasound consultation system over high-speed commercial telecommunication lines. *J Telemed Telecare*. 2004;10(3):175–179. doi: 10.1258/135763304323070841
15. Panayides A, Antoniou ZC, Mylonas Y, et al. High-resolution, low-delay, and error-resilient medical ultrasound video communication using H.264/AVC over mobile WiMAX networks. *IEEE J Biomed Health Inform*. 2013;17(3):619–628. doi: 10.1109/TITB.2012.2232675
16. Arzamasov KM, Bobrovskaya TM, Drogovoz VA. Streaming technology: From games to tele-ultrasound. *Digital Diagnostics*. 2022;2(3):131–140. (In Russ). doi: 10.17816/DD100779
17. Arzamasov KM, Drogovoz VA. Systematic review of technologies and methods of tele-ultrasound. *Medical Technologies Assessment Choice*. 2020;(3):44–54. (In Russ). doi: 10.17116/medtech20204103144
18. Le MT, Voigt L, Nathanson R, et al. Comparison of four handheld point-of-care ultrasound devices by expert users. *Ultrasound J*. 2022;14(1):27. doi: 10.1186/s13089-022-00274-6

СПИСОК ЛИТЕРАТУРЫ

1. Shi J., Wang F., Qin M., et al. New ECG compression method for portable ECG monitoring system merged with binary convolutional auto-encoder and residual error compensation // *Biosensors (Basel)*. 2022. Vol. 12, N 7. P. 524. doi: 10.3390/bios12070524
2. Palacios D.R., Shen K., Baig S., et al. Wide field of view handheld smart fundus camera for telemedicine applications // *J Med Imaging (Bellingham)*. 2021. Vol. 8, N 2. P. 026001. doi: 10.1117/1.JMI.8.2.026001
3. Shewale A.D., Patil S.A., Patil S.R. Raspberry-pi based automatic health care modelling: An IoT approach // *Compliance Engineering J*. 2021. Vol. 12, N 3. P. 99–104.
4. Recker F., Höhne E., Damjanovic D., Schäfer V.S. Ultrasound in telemedicine: A brief overview // *Appl Sci*. 2022. Vol. 12, N 3. P. 958. doi: 10.3390/app12030958
5. Lim T.H., Choi H.J., Kang B.S. Feasibility of dynamic cardiac ultrasound transmission via mobile phone for basic emergency teleconsultation // *J Telemed Telecare*. 2010. Vol. 16, N 5. P. 281–285. doi: 10.1258/jtt.2010.091109
6. Miyashita T., Iketani Y., Nagamine Y., Goto T. FaceTime® for teaching ultrasound-guided anesthetic procedures in remote place // *J Clin Monit Comput*. 2014. Vol. 28, N 2. P. 211–215. doi: 10.1007/s10877-013-9514-x
7. Kim C., Cha H., Kang B.S., et al. A feasibility study of smartphone-based telephonography for evaluating cardiac dynamic function and diagnosing acute appendicitis with control of the image quality of the transmitted videos // *J Digit Imaging*. 2016. Vol. 29, N 3. P. 347–356. doi: 10.1007/s10278-015-9849-6
8. Boissin C., Blom L., Wallis L., et al. Image-based teleconsultation using smartphones or tablets: Qualitative assessment of medical experts // *Emergency Med J*. 2017. Vol. 34, N 2. P. 95–99. doi: 10.1136/emered-2015-205258
9. Beckhauser E., Petrolini V.A., Savaris A., et al. Are single-board computers an option for a low-cost multimodal telemedicine platform: First tests in the context of santa catarina state integrated telemedicine and telehealth system // 2016 IEEE 29th International Symposium on Computer-Based Medical Systems (CBMS). 2016. P. 163–168.
10. Bhojwani H., Sain G.K., Sharma G.P. A hybrid connectivity oriented telemedicine system for Indian landscape using raspberry Pi SBC & IOT // 2018 3rd Technology Innovation Management and Engineering Science International Conference (TIMES-iCON). 2018. P. 1–5. doi: 10.1109/TIMES-iCON.2018.8621799
11. De Oliveira D.C., Wehrmeister M.A. Using deep learning and low-cost rgb and thermal cameras to detect pedestrians in aerial images captured by multirotor UAV // *Sensors (Basel)*. 2018. Vol. 18, N 7. P. 2244. doi: 10.3390/s18072244
12. Kim W., Jung W.S., Choi H.K. Lightweight driver monitoring system based on multi-task mobilenets // *Sensors (Basel)*. 2019. Vol. 19, N 14. P. 3200. doi: 10.3390/s19143200
13. Peine A., Hallawa A., Schöffski O., et al. A deep learning approach for managing medical consumable materials in intensive care units via convolutional neural networks: Technical proof-of-concept study // *JMIR Med Informatics*. 2019. Vol. 7, N 4. P. e14806–e14806. doi: 10.2196/14806
14. Yoo S.K., Kim D.K., Jung S.M., et al. Performance of a web-based, realtime, tele-ultrasound consultation system over high-speed commercial telecommunication lines // *J Telemed Telecare England*. 2004. Vol. 10, N 3. P. 175–179. doi: 10.1258/135763304323070841
15. Panayides A, Antoniou Z.C., Mylonas Y., et al. High-resolution, low-delay, and error-resilient medical ultrasound video communication using H.264/AVC over mobile WiMAX networks // *IEEE J Biomed Health Inform*. 2013. Vol. 17, N 3. P. 619–628. doi: 10.1109/TITB.2012.2232675
16. Арзамасов К.М., Бобровская Т.М., Дроговоз В.А. Стриминговые технологии: из игровой индустрии в телеультразвуковые исследования // *Digital Diagnostics*. 2022. Т. 3, № 2. С. 131–140. doi: 10.17816/DD100779
17. Арзамасов К.М., Дроговоз В.А. Систематический обзор технологий и методов телеультразвуковых исследований // *Медицинские технологии. Оценка и выбор*. 2020. № 3. С. 44–54. doi: 10.17116/medtech20204103144
18. Le M.T., Voigt L., Nathanson R., et al. Comparison of four handheld point-of-care ultrasound devices by expert users // *Ultrasound J*. 2022. Vol. 14, N 1. P. 27. doi: 10.1186/s13089-022-00274-6

AUTHORS' INFO

* Kirill M. Arzamasov, MD, Cand. Sci. (Med.);
address: 24/1 Petrovka street, 127051 Moscow, Russia;
ORCID: <http://orcid.org/0000-0001-7786-0349>;
eLibrary SPIN: 3160-8062; e-mail: ArzamasovKM@zdrav.mos.ru

ОБ АВТОРАХ

* Арзамасов Кирилл Михайлович, к.м.н.;
адрес: Россия, 127051, Москва, ул. Петровка, д. 24, стр. 1;
ORCID: <http://orcid.org/0000-0001-7786-0349>;
eLibrary SPIN: 3160-8062; e-mail: k.arzamasov@npcmr.ru

* Corresponding author / Автор, ответственный за переписку

Viktor A. Drogovoz, Cand. Sci. (Tech.);
ORCID: <https://orcid.org/0000-0001-9582-7147>;
eLibrary SPIN: 1804-2636; e-mail: Vdrog@mail.ru

Tatiana M. Bobrovskaya, MD;
ORCID: <http://orcid.org/0000-0002-2746-7554>;
eLibrary SPIN: 3400-8575; e-mail: BobrovskayaTM@zdrav.mos.ru

Anton V. Vladzimirskyy, MD, Dr. Sci. (Med.);
ORCID: <https://orcid.org/0000-0002-2990-7736>;
eLibrary SPIN: 3602-7120; e-mail: VladzimirskijAV@zdrav.mos.ru

Дроговоз Виктор Анатольевич, к.т.н.;
ORCID: <https://orcid.org/0000-0001-9582-7147>;
eLibrary SPIN: 1804-2636; e-mail: Vdrog@mail.ru

Бобровская Татьяна Михайловна;
ORCID: <http://orcid.org/0000-0002-2746-7554>;
eLibrary SPIN: 3400-8575; e-mail: t.bobrovskaya@npcmr.ru

Владзимирский Антон Вячеславович, д.м.н.;
ORCID: <https://orcid.org/0000-0002-2990-7736>;
eLibrary SPIN: 3602-7120; e-mail: a.vladzimirsky@npcmr.ru

DOI: <https://doi.org/10.17816/DD119870>

Низкодозная компьютерная томография органов грудной клетки в диагностике COVID-19: обзор литературы

И.А. Блохин, Д.А. Румянцев, М.М. Сучилова, А.П. Гончар, О.В. Омелянская

Научно-практический клинический центр диагностики и телемедицинских технологий, Москва, Российская Федерация

АННОТАЦИЯ

Обоснование. Повышение числа исследований компьютерной томографии во время пандемии COVID-19 актуализировало задачу снижения лучевой нагрузки на пациента, так как воздействие радиационного излучения достоверно связано с повышением риска развития онкологических заболеваний. В работе отделений лучевой диагностики даже в условиях пандемии должен соблюдаться принцип минимальной дозы облучения при максимальном уровне качества диагностики — ALARA (as low as reasonably achievable), предложенный Международной комиссией по радиационной защите.

Цель — систематизация данных о возможностях снижения лучевой нагрузки при диагностике поражения лёгких при COVID-19 методом компьютерной томографии.

Материалы и методы. Проведён анализ релевантных отечественных и зарубежных источников литературы в научных библиотеках PubMed и eLIBRARY по запросам «low dose computed tomography COVID-19» и «низкодозная компьютерная томография COVID-19», опубликованных в период с 2020 по 2022 год. Публикации включались в обзор после оценки их соответствия теме обзора путём анализа названия и абстракта. Списки литературы также были проанализированы на предмет выявления пропущенных при поиске статей, попадающих под критерии включения.

Результаты. Изучение опубликованных результатов исследований позволило обобщить современные данные о лучевой диагностике поражения лёгких при COVID-19 и использовании компьютерной томографии, а также определить возможные варианты снижения дозы лучевой нагрузки.

Заключение. Представлены способы уменьшения лучевой нагрузки при компьютерной томографии органов грудной клетки и сохранения высокого качества диагностического изображения, потенциально достаточного для надёжного выявления признаков COVID-19. Снижение дозы облучения является оправданным подходом к получению актуальной диагностической информации, сохраняющим возможности внедрения технологий продвинутого компьютерного анализа в клиническую практику.

Ключевые слова: компьютерная томография; низкодозная компьютерная томография; обзор литературы; COVID-19; диагностика COVID-19.

Как цитировать

Блохин И.А., Румянцев Д.А., Сучилова М.М., Гончар А.П., Омелянская О.В. Низкодозная компьютерная томография органов грудной клетки в диагностике COVID-19: обзор литературы // *Digital Diagnostics*. 2023. Т. 4 № 1. С. 25–37. DOI: <https://doi.org/10.17816/DD119870>

DOI: <https://doi.org/10.17816/DD119870>

Low-dose computed tomography in COVID-19: systematic review

Ivan A. Blokhin, Denis A. Rumyantsev, Maria M. Suchilova, Anna P. Gonchar, Olga V. Omelyanskaya

Moscow Center for Diagnostics and Telemedicine, Moscow, Russian Federation

ABSTRACT

BACKGROUND: The increased number of computed tomography scans during the COVID-19 pandemic has emphasized the task of decreasing radiation exposure of patients, since it is known to be associated with an elevated risk of cancer development. The ALARA (as low as reasonably achievable) principle, proposed by the International Commission on Radiation Protection, should be adhered to in the operation of radiation diagnostics departments, even during the pandemic.

AIM: To systematize data on the appropriateness and effectiveness of low-dose computed tomography in the diagnosis of lung lesions in COVID-19.

MATERIALS AND METHODS: Relevant national and foreign literature in scientific libraries PubMed and eLIBRARY, using English and Russian queries “low-dose computed tomography” and “COVID-19,” published between 2020 and 2022 were analyzed. Publications were evaluated after assessing the relevance to the review topic by title and abstract analysis. The references were further analyzed to identify articles omitted during the search that may meet the inclusion criteria.

RESULTS: Published studies summarized the current data on the imaging of COVID-19 lung lesions and the use of computed tomography scans and identified possible options for reducing the effective dose.

CONCLUSION: We present techniques to reduce radiation exposure during chest computed tomography and preserve high-quality diagnostic images potentially sufficient for reliable detection of COVID-19 signs. Reducing radiation dose is a valid approach to obtain relevant diagnostic information, preserving opportunities for the introduction of advanced computational analysis technologies in clinical practice.

Keywords: computed tomography; low-dose computed tomography; literature review; COVID-19; COVID-19 diagnosis.

To cite this article

Blokhin IA, Rumyantsev DA, Suchilova MM, Gonchar AP, Omelyanskaya OV. Low-dose computed tomography in COVID-19: systematic review. *Digital Diagnostics*. 2023;4(1):25–37. DOI: <https://doi.org/10.17816/DD119870>

Received: 22.12.2022

Accepted: 06.02.2023

Published: 31.03.2023

DOI: <https://doi.org/10.17816/DD119870>

胸部低剂量计算机断层扫描在COVID-19诊断中的应用：系统综述

Ivan A. Blokhin, Denis A. Rumyantsev, Maria M. Suchilova, Anna P. Gonchar, Olga V. Omelyanskaya

Moscow Center for Diagnostics and Telemedicine, Moscow, Russian Federation

简评

论证。在COVID-19大流行期间，计算机断层扫描检查数量的增加使减少病人的辐射量的任务成为现实，因为暴露于辐射与增加癌症风险有着可靠的联系。国际放射防护委员会提出的在最高诊断质量下的最小辐射剂量原则——ALARA (as low as reasonably achievable)，在辐射诊断部门的工作中应该得到遵守，即使在大流行的情况下。

目的是整理关于通过计算机断层扫描诊断COVID-19肺部病变时减少辐射暴露的潜力的数据。

材料和方法。对PubMed和eLIBRARY科学图书馆中2020年至2022年期间发表的国内国外相关文献进行了分析，搜索查询包括“low dose computed tomography COVID-19”和“низкодозная компьютерная томография COVID-19”（低剂量计算机断层扫描COVID-19）。通过分析标题和摘要评估其与综述主题的相关性后，将出版物纳入综述。还对参考文献列表进行了分析，以确定搜索中遗漏的符合纳入标准的文章。

结果。对已发表的研究进行了，研究已发表的科学著作允许总结关于目前COVID-19肺部病变的辐射诊断和计算机断层扫描的使用的数据，并确定减少辐射剂量的可能方法。

结论。介绍了在胸部计算机断层扫描过程中减少辐射量并保留高质量诊断图像的方法，这些图像可能足以可靠地检测COVID-19征候。减少辐射剂量是获得现实诊断信息的一种有道理的方法，保留将先进计算机化分析技术引入临床实践的可能性。

关键词：计算机断层扫描，低剂量计算机断层扫描，文献综述，COVID-19，COVID-19诊断。

To cite this article

Blokhin IA, Rumyantsev DA, Suchilova MM, Gonchar AP, Omelyanskaya OV. 胸部低剂量计算机断层扫描在COVID-19诊断中的应用：系统综述. *Digital Diagnostics*. 2023;4(1):25–37. DOI: <https://doi.org/10.17816/DD119870>

收到: 22.12.2022

接受: 06.02.2023

发布日期: 31.03.2023

BACKGROUND

At the time of writing this paper (December 22, 2022), the number of coronavirus disease 2019 (COVID-19) cases reaches 650 million.¹ Spread of the disease and consequent mortality can be prevented and reduced with a combination of measures, including early diagnosis.²

The main method of laboratory diagnostics is reverse-transcription polymerase chain reaction (RT PCR). At the first peak of the coronavirus pandemic, disadvantages of this technique were revealed, such as a high rate of false-positive results, limited test availability, and long waiting time for results. [1] Moreover, computed tomography (CT) of the chest can also provide false-negative results in patients with signs of COVID-19. [2]

According to Russian [3] and international³ guidelines, diagnostic radiology for COVID-19-associated pneumonia includes radiography and CT. Chest X-ray imaging has low sensitivity to viral pneumonia [4], so CT plays an important role in the diagnosis of COVID-19-associated pneumonia and its complications. [5]

The active use of CT during the pandemic leads to high radiation exposure to the population. [6, 7] To assess changes in patient condition during the hospital stay, 2–6 CTs are usually performed within a short period since a clear trend toward CT regression of abnormal changes is one of the criteria for patient discharge.[3] Patients with suspected COVID-19 may undergo 1–2 outpatient CT scans to detect signs of the disease. [8, 9]

Radiation exposure is significantly associated with the increased risk of developing cancer. [10] In radiology departments, even in a pandemic, the “as low as reasonably achievable” principle proposed by the International Commission of Radiological Protection [11] should be observed. In March 2020, Kang et al. proposed the use of low-dose CT (LDCT) as the first stage of radiation diagnosis in patients with COVID-19-associated pneumonia. [6] The important role of LDCT in COVID-19 was also highlighted by the webinar “*COVID-19 and Chest CT: Protocol and Dose Optimization*,” which was held in April 2020 and attended by 1633 people from 100 countries. During the video conference, it was found that 55%, 43%, and 2% of healthcare institutions use standard (CTDIvol 5–10 mGy), low-dose (CTDIvol <5 mGy), and high-dose protocols (CTDIvol >10 mGy). [12] However, even a superficial assessment of an X-ray workstation reveals a significant number of scan parameters that affect radiation exposure, [13], and the relationship between different protocol settings and radiation dose may not be obvious, especially considering the pathology examined.

This literature review aimed to systematize data on opportunities for reducing radiation exposure during lung CT in patients with COVID-19.

MATERIALS AND METHODS

Relevant Russian and foreign literature sources were reviewed in PubMed and eLIBRARY scientific libraries for search queries “low dose computed tomography COVID-19” and “низкодозная компьютерная томография COVID-19” for the period from 2020 to 2022.

Publications were included in the review after assessing their relevance according to their titles and abstracts. The review included original studies and meta-analyses, and literature reviews, case reports, and congress abstracts were excluded. References were also reviewed for relevant studies on general principles of CT dose reduction that might have been published before 2020. When such articles were found, the most recent study was included in the review.

RESULTS AND DISCUSSION

In total, 45 foreign papers and five Russian papers were reviewed. The latest search date was December 22, 2022.

Methods for Reducing Radiation Exposure

Methods for reducing radiation exposure can be divided into hardware and software ones. Hardware methods are related to tube potential, tube current, pitch factor, and X-ray beam filter. Software methods are related to the reconstruction filter, slice thickness, and iterative reconstructions.

Hardware Methods. Tube potential (kVp) is nonlinearly related to radiation exposure. [14] Zarb et al. [15] showed that a decrease in tube potential by 14%–17% provides a radiation dose decrease by 32%–38%. In this case, reducing the tube potential increases the noise level while performing non-contrast-enhanced examinations. A phantom study showed that these parameters are interrelated via an exponent of -1.3 . [16] Moreover, reducing the tube potential in contrast-enhanced examinations improves the quality of images by significantly reducing radiation exposure. [17]

Tube current (mAs) is linearly related to radiation exposure. [18] For example, a 50% decrease in tube current leads to a 50% decrease in the effective dose [17], while the signal-to-noise ratio is inversely proportional to the square root of the current. [19]

A pitch factor for multislice CT has almost no effect on radiation exposure. [20] As the pitch factor increases,

¹ World Health Organization. Novel Coronavirus (COVID-19) situation. Available at <https://who.sprinklr.com>.

² Centers for Disease Control and Prevention. Coronavirus 2019 disease (COVID-19). Available at <https://www.cdc.gov/coronavirus/2019-ncov/index.html>.

³ World Health Organization. Use of chest imaging in COVID-19: A rapid advice guide [11 June 2020]. Available at <https://apps.who.int/iris/handle/10665/332336>.

the signal-to-noise ratio decreases, and the tomograph automatically increases the tube current to prevent deterioration of image quality. [21]

An X-ray beam filter is used to absorb low-energy photons that cannot pass through the patient tissues and do not reach the detectors. Therefore, the use of an additional tin filter can significantly reduce radiation exposure during CT [22] but requires additional costs for scanner modification.

Software Methods. The choice of the reconstruction filter (convolution kernel) does not affect radiation exposure but affects the signal-to-noise ratio, amplifying or smoothing out the difference between pixels of different organs or structures. [23]

A low slice thickness is associated with lower image quality but decreases the risk of missing small abnormal changes. Thus, slice thickness can be optimized. For example, for the examination of pulmonary nodes, this parameter may be 2 mm. [24]

The main way to reduce “noise” is iterative reconstructions, which allow CTs with lower radiation doses and a similar signal-to-noise ratio to the standard data reconstruction technique. [25] The use of artificial neural networks for image reconstruction is one of the promising methods. [26, 27]

Based on the literature review, reducing the tube current reduces radiation exposure, and the signal-to-noise ratio can be optimized using a reconstruction filter that smoothens the difference between adjacent pixels (soft tissue) and iterative reconstruction.

Low-dose CT in the diagnosis of COVID-19

In the literature review, a single, well-defined low-dose protocol is warranted for COVID-19 (Table 1 [28–54]). The reduced radiation exposure dose is achieved mainly by changing the tube potential, tube current, use of iterative reconstructions, and a tin filter. Some studies reviewed had shortcomings related to data presentation: dosimetric parameters (CTDI, DLP, SSDE, and effective dose) were not mentioned, and small sample sizes were used.

Interestingly, a parameter to be changed when optimizing the scanning protocol can be universal for various clinical tasks. Therefore, in LDCT for lung cancer screening, different groups of authors also changed the tube current [55, 56]. However, the development of a specialized LDCT protocol should be initiated with a study on a model object (phantom) to select the optimal method for reducing the exposure. For example, Gombolevsky et al. [57] developed the LDCT protocol for the diagnosis of COVID-19 using a phantom with thickening plates, while setting the automatic tube current control system (Sure Exposure 3D) to a sufficient level to detect ground-glass lesions with a maximum reduction in radiation exposure (SD = 36). A comparison of the protocol selected according to the results of the phantom study with standard CT and LDCT for lung cancer screening is shown in Fig. 1.

Any special low-dose protocols require clinical validation and comparison with the gold standard. Therefore, clinical trials of the developed LDCT protocol for COVID-19 used

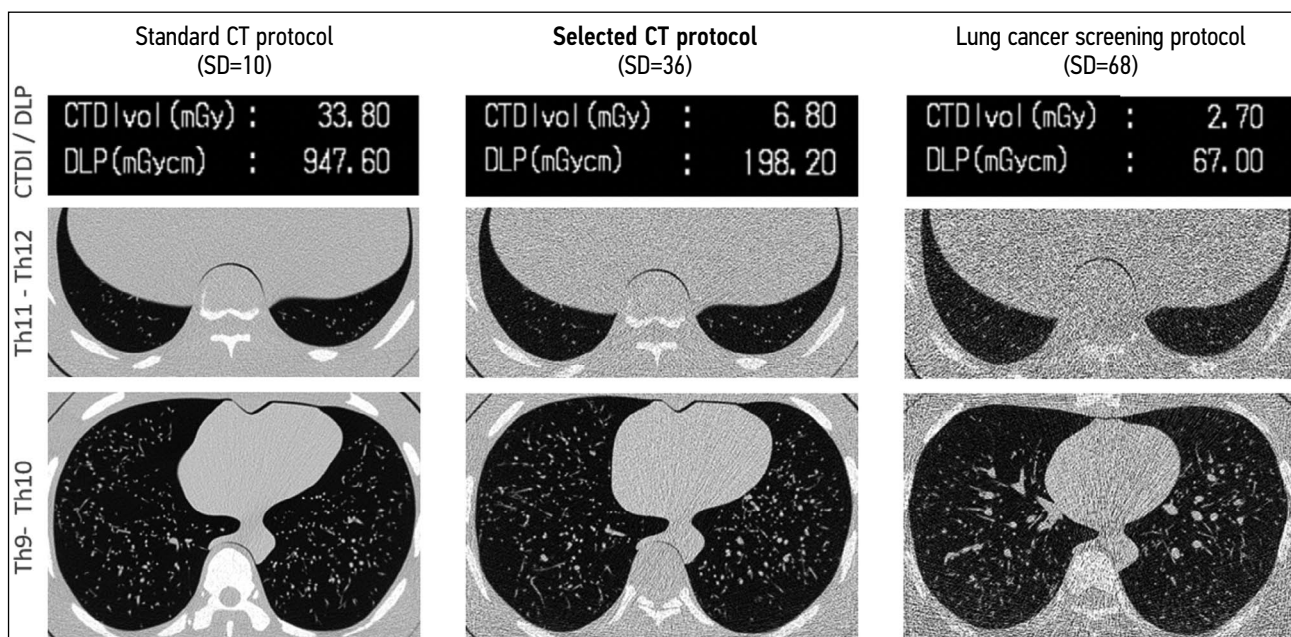


Figure 1. Comparison of a dedicated low-dose computed tomography protocol for COVID-19 (SD = 36) with standard and low-dose computed tomography for lung cancer screening. Data on radiation exposure and axial tomograms of the phantom at the level of the lower and middle zones of the lungs. Low-dose computed tomography for lung cancer screening was developed considering the need for radiation exposure limitation as preventive measures according to SanPin (disease control and prevention standards) and has the lowest signal-to-noise ratio. The proposed protocol for low-dose computed tomography for COVID-19 considers the densitometric characteristics of ground-glass lesions with a significant reduction in radiation exposure.

Table 1. Parameters of low-dose computed tomography for diagnosis of COVID-19 based on the literature review

Author, year, link	Tube potential (kV)	Tube current, mA	Average radiation dose (mSv)	Slice thickness (mm)	Reconstruction filter	Use of Iterative Reconstruction
Blokhin et al. (2022) [28]	120	10–500, noise level 36 (SD)	3	1	FC51, FC07	No
Filatova et al. (2020) [29]	100/110	40–120	1,27	1	-	Yes
Afshar et al. (2022) [30]	110	20	1–1,5	2	D40s	-
Fukumoto et al. (2022) [31]	120	20–25	CTDI 1.3 mGy	5	Lung and soft tissue	-
Bieba et al. (2022) [32]	Depending on weight	Depending on weight	-	1 and 3	-	-
Barrio et al. (2022) [33]	100/150	Anthropomorphic current modulation system	-	1	Br32 Bl60	-
Thieß et al. (2022) [34]	100	10–100	0,53	0,5 b 0,625	Fc01 Fc85	Yes
Greffier et al. (2021) [35]	100/120	10	0,2	1	I30f, mediastinal, I50f, lung images	Yes
Karakaş et al. (2021), [36]	80	40	0,18	5	lung	Yes
Julie et al. (2021) [37]	120	45	-	1,2	-	-
Desmet et al. (2021) [38]	80–140	20–30	0,64	0,6	-	-
Aslan et al. (2021) [39]	80	35–50	0,2856	3	lung	Yes
Stoleriu et al. (2021) [40]	120	40–113	35–100 mGy×cm 0.78–2.91 mGy	1,25	Medium Soft	Yes
Bai et al. (2021) [41]	120	120–380	1,21±0,10	1,25	Standard	Yes
Agostini et al. (2021) [42]	100	95	0,39	1,5	Sharp	Yes
Zali et al. (2021) [43]	100–120	50–100	-	1–3	-	-
Argentieri et al. (2021) [44]	80	20	0,219	2	Sharp	-
Leger et al. (2020) [45]	120	45	0,49	1,2	-	-
Hamper et al. (2020) [46]	100	20–120	0,5	0,625–1	Lung	Yes
Li et al. (2020) [47]	120	30	1,22±0,14	1	-	Yes
Dangis et al. (2020) [48]	100	20	0,56	1	Lung (150f)	Yes
Radpour et al. (2020) [49]	100–120	50–100	-	1–3	-	-
Kang et al. (2020) [6]	80–100	10–25	0,203	0,6	-	Yes
Tofighi et al. (2020) [50]	100	40	2,03	-	-	No
Tabatabaei et al. (2020) [51]	120	30	1,8	3	-	-
Schulze-Hagen et al. (2020) [52]	80	35	1,7	1 and 3	170f 130f	-
Zhao Yue et al. (2020) [53]	100	50	1,5	1	-	-
Castelli et al. (2020) [54]	120	45	0,47	1,2	-	-

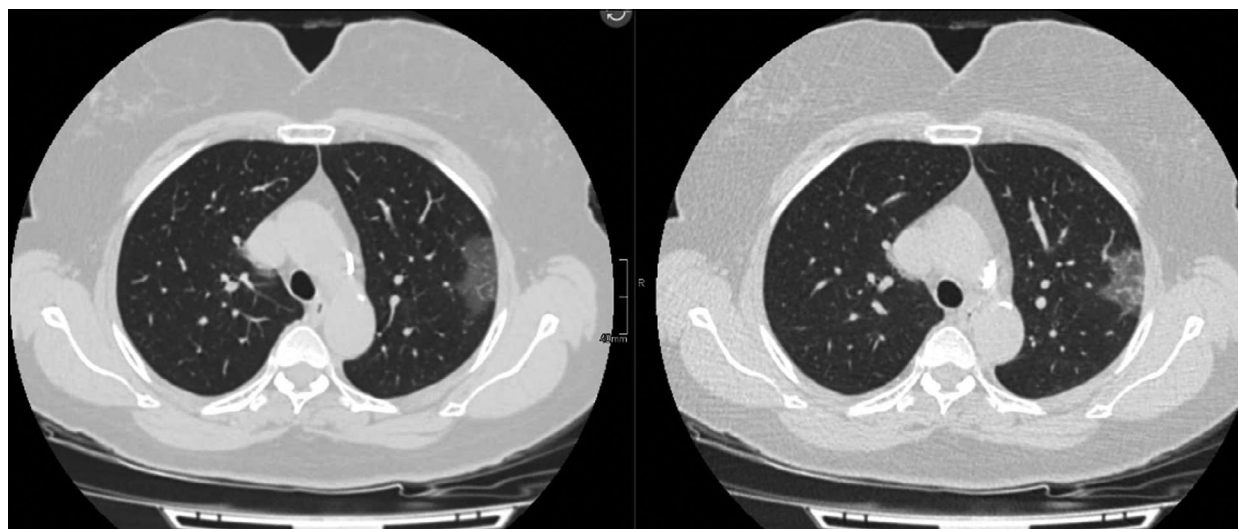


Figure 2. Radiation exposure is reduced by 5 times. Patient, 59 y. o., BMI 29 kg/m². Computed tomography with a soft tissue filter (effective dose: 9.7 mSv), low-dose computed tomography with a soft tissue filter (effective dose: 2.1 mSv). In the upper lobe of the left lung, there was a peripheral ground-glass lesion.

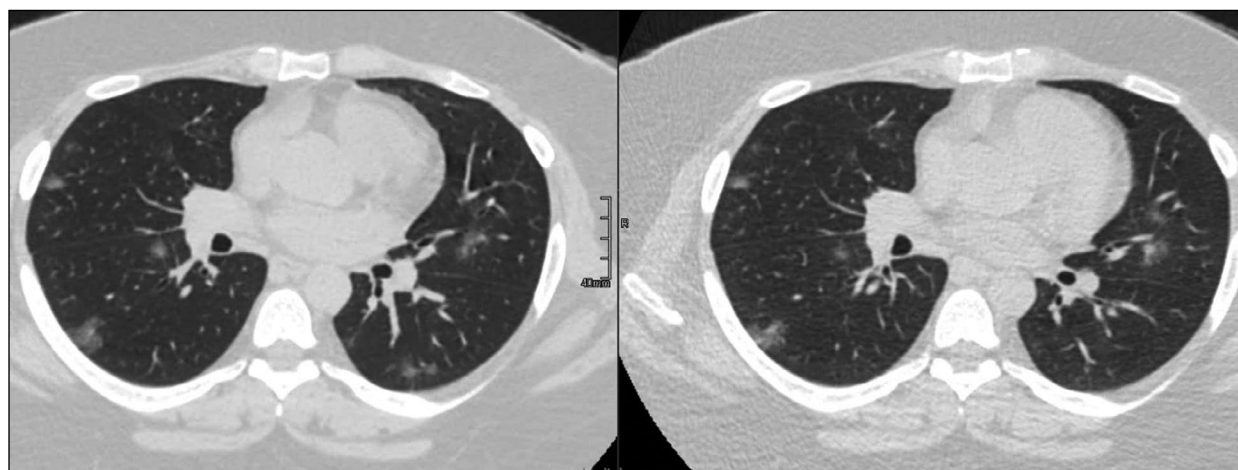


Figure 3. Radiation exposure is reduced by 1.5 times. Patient, 44 y. o., BMI 46 kg/m². Computed tomography with a soft tissue filter (effective dose: 15.3 mSv), low-dose computed tomography with a soft tissue filter (effective dose: 10.5 mSv). Bilateral peripheral ground-glass lesions.

standard CT as a reference technique. [28] Some of the clinical images obtained using the developed protocol are shown in Figs. 2 and 3.

Limitations of LDCT

Kim et al. [58] showed that obesity (body mass index > 25) appears to limit the use of chest LDCT in routine practice due to X-ray absorption by adipose tissue. However, studies on the inter-expert agreement of COVID-19 examinations indicate the opposite. [59]

In addition, LDCT empirically appears to be related to the negative effect of increased image noise on the operation of AI systems, including the calculation of an emphysema index in densitometric analysis, [60] and the radiomic analysis of subsolid pulmonary nodules. [61] Effect of a scanning protocol on the results of a quantitative analysis can be reduced using relative parameters, for example, the percentage of affected

lung tissue in COVID-19, [62] or by normalizing the obtained data with special algorithms. [63]

CONCLUSION

Methods are presented to reduce radiation exposure during chest CT and maintain high-quality diagnostic images that are hypothetically sufficient to reliably detect signs of COVID-19. Although there is no single way to optimize scan protocols, dose reduction provides relevant diagnostic information and retains the ability to incorporate advanced computer-assisted technologies into clinical pathways.

ADDITIONAL INFORMATION

Funding source. This article was prepared by a team of authors as part of the research work (EGISU number: AAAA-A20-120071090058-7) in

accordance with the Program of the Moscow Department of Health "Scientific support of metropolitan health" for 2020–2022.

Competing interests. The authors declare that they have no competing interests.

Authors' contribution. All authors made a substantial contribution to the conception of the work, acquisition, analysis, interpretation of data for the work, drafting and revising the work, final approval

of the version to be published and agree to be accountable for all aspects of the work. The largest contributions were distributed as follows: I.A. Blokhin — editing and approval of the final manuscript text, advisory support; D.A. Romyantsev — data analysis, article text writing; M.M. Suchilova, A.P. Gonchar — editing and approval of the final manuscript text; O.V. Omelyanskaya — study concept and design.

REFERENCES

1. Yang Y, Yang M, Shen C, et al. Evaluating the accuracy of different respiratory specimens in the laboratory diagnosis and monitoring the viral shedding of 2019-nCoV infections. *medRxiv*. 2020. doi: 10.1101/2020.02.11.20021493
2. Rubin GD, Ryerson CJ, Haramati LB, et al. The role of chest imaging in patient management during the COVID-19 pandemic: A multinational consensus statement from the Fleischner society. *Radiology*. 2020;296(1):172–180. doi: 10.1148/radiol.2020201365
3. Temporary methodological recommendations prevention, diagnosis and treatment of new coronavirus infection (COVID-19). Version 12 (09/21/2021). Moscow; 2021. 232 p.
4. Ng M, Lee EY, Yang J, et al. Imaging profile of the COVID-19 infection: Radiologic findings and literature review. *Radiology: Cardiothoracic Imaging*. 2020;2(1):e200034. doi: 10.1148/ryct.2020200034
5. Ai T, Yang Z, Hou H, et al. Correlation of chest CT and RT-PCR testing for coronavirus disease 2019 (COVID-19) in China: A report of 1014 cases. *Radiology*. 2020;296(2):E32–E40. doi: 10.1148/radiol.2020200642
6. Kang Z, Li X, Zhou S. Recommendation of low-dose CT in the detection and management of COVID-2019. *Eur Radiology*. 2020;30(8):4356–4357. doi: 10.1007/s00330-020-06809-6
7. Morozov SP, Kuzmina ES, Ledekhova NV, et al. Mobilization of the scientific and practical potential of the radiation diagnostics service of Moscow in the COVID-19 pandemic. *Digital Diagnostics*. 2020;1(1):5–12. (In Russ). doi: 10.17816/DD51043
8. Pan F, Ye T, Sun P, et al. Time course of lung changes on chest CT during recovery from 2019 novel coronavirus (COVID-19) pneumonia. *Radiology*. 2020;295(3):715–721. doi: 10.1148/radiol.2020200370
9. Lei DP, Fan B, Mao J, et al. The progression of computed tomographic (CT) images in patients with coronavirus disease (COVID-19) pneumonia: Running title: the CT progression of COVID-19 pneumonia. *J Infect*. 2020;80(6):e30–e31. doi: 10.1016/j.jinf.2020.03.020
10. Power SP, Moloney F, Twomey M, et al. Computed tomography and patient risk: Facts, perceptions and uncertainties. *World J Radiol*. 2016;8(12):902–915. doi: 10.4329/wjr.v8.i12.902
11. Yeung AW. The "As low as reasonably achievable" (ALARA) principle: A brief historical overview and a bibliometric analysis of the most cited publications. *Radioprotection*. 2019;54(2):103–109. doi: 10.1051/radiopro/2019016
12. Kalra MK, Homayounieh F, Arru C, et al. Chest CT practice and protocols for COVID-19 from radiation dose management perspective. *Eur Radiol*. 2020;30(12):6554–6560. doi: 10.1007/s00330-020-07034-x
13. Krasnov AS, Kabanov DO, Tereshchenko GV. Fundamentals of dosimetry and dose load optimization during multispiral computed tomography. *Issues Hematology Oncology Immunopathology Pediatrics*. 2018;17(3):127–132. (In Russ).
14. Singh S, Kalra MK, Thrall JH, Mahesh M. CT radiation dose reduction by modifying primary factors. *J Am Coll Radiol*. 2011;8(5):369–372. doi: 10.1016/j.jacr.2011.02.001
15. Zarb F, Rainford L, McEntee MF. Developing optimized CT scan protocols: Phantom measurements of image quality. *Radiography*. 2011;17(2):109–114. doi: 10.1016/j.radi.2010.10.004
16. Hilts M, Duzenli C. Image noise in X-ray CT polymer gel dosimetry. *J Physics: Conference Series*. 2004;3(1):252. doi: 10.1088/1742-6596/3/1/040
17. Lira D, Padole A, Kalra MK, Singh S. Tube potential and CT radiation dose optimization. *Am J Roentgenol*. 2015;204(1):W4–W10. doi: 10.2214/AJR.14.13281
18. Reid J, Gamberoni J, Dong F, Davros W. Optimization of kVp and mAs for pediatric low-dose simulated abdominal CT: Is it best to base parameter selection on object circumference? *AJR Am J Roentgenol*. 2010;195(4):1015–1020. doi: 10.2214/AJR.09.3862
19. Khoramian D, Sistani S, Firouzjah RA. Assessment and comparison of radiation dose and image quality in multi-detector CT scanners in non-contrast head and neck examinations. *Paul J Radiol*. 2019;84:61–67. doi: 10.5114/pjr.2019.82743
20. Mahesh M, Scatarige JC, Cooper J, Fishman EK. Dose and pitch relationship for a particular multislice CT scanner. *AJR Am J Roentgenol*. 2001;77(6):1273–1275. doi: 10.2214/ajr.177.6.1771273
21. Tack D, Gevenois PA, Abada H. Radiation dose from adult and pediatric multidetector computed tomography. *Springer*. 2007. doi: 10.1007/978-3-540-68575-3
22. Greffier J, Pereira F, Hamard A, et al. Effect of tin filter-based spectral shaping CT on image quality and radiation dose for routine use on ultralow-dose CT protocols: A phantom study. *Diagnostic Interventional Imaging*. 2020;101(6):373–381. doi: 10.1016/j.diii.2020.01.002
23. Paul J, Krauss B, Banckwitz R, et al. Relationships of clinical protocols and reconstruction kernels with image quality and radiation dose in a 128-slice CT scanner: Study with an anthropomorphic and water phantom // *Eur J Radiology*. 2012;81(5):e699–e703. doi: 10.1016/j.ejrad.2011.01.078
24. Hashemi S, Mehrez H, Cobbold RS, Paul NS. Optimal image reconstruction for detection and characterization of small pulmonary nodules during low-dose CT. *Eur Radiol*. 2014;24(6):1239–1250. doi: 10.1007/s00330-014-3142-9
25. Beister M, Kolditz D, Kalender WA. Iterative reconstruction methods in X-ray CT. *Physica Medica*. 2012;28(2):94–108. doi: 10.1016/j.ejmp.2012.01.003
26. Shiri I, Akhavanallaf A, Sanaat A, et al. Ultra-low-dose chest CT imaging of COVID-19 patients using a deep residual neural network. *Eur Radiology*. 2021;31(3):1420–1431. doi: 10.1007/s00330-020-07225-6
27. Shan H, Padole A, Homayounieh F, et al. Competitive performance of a modularized deep neural network compared to commercial algorithms for low-dose CT image reconstruction. *Nat Machine Intelligence*. 2019;1(6):269–276. doi: 10.1038/s42256-019-0057-9
28. Blokhin I, Gombolevskiy V, Chernina V, et al. Inter-observer agreement between low-dose and standard-dose CT with soft and

- sharp convolution kernels in COVID-19 pneumonia. *J Clin Med*. 2022;11:669. doi: 10.3390/jcm11030669
29. Filatova DA, Sinitsyn VE, Mershina EA. The possibilities of reducing radiation exposure during computed tomography to assess changes in the lungs characteristic of COVID-19: The use of adaptive statistical iterative reconstruction. *Digital Diagnostics*. 2021;2(2):94–104. (In Russ). doi: 10.17816/DD62477
30. Afshar P, Rafiee MJ, Naderkhani F, et al. Human-level COVID-19 diagnosis from low-dose CT scans using a two-stage time-distributed capsule network. *Sci Rep*. 2022;12(1):4827. doi: 10.1038/s41598-022-08796-8
31. Fukumoto W, Nakamura Y, Yoshimura K, et al. Triaging of COVID-19 patients using low dose chest CT: Incidence and factor analysis of lung involvement on CT images. *J Infect Chemother*. 2022;28(6):797–801. doi: 10.1016/j.jiac.2022.02.025
32. Bieba CM, Desmet JN, Dubbeldam A, et al. Radiological findings in low-dose CT for COVID-19 pneumonia in 182 patients: Correlation of signs and severity with patient outcome. *Medicine (Baltimore)*. 2022;101(9):e28950. doi: 10.1097/MD.00000000000028950
33. Piqueras BM, Casajús EA, Iriarte UC, et al. Low-dose chest CT for preoperative screening for SARS-CoV-2 infection. *Radiologia (Engl Ed)*. 2022;64(4):317–323. doi: 10.1016/j.rxeng.2021.11.004
34. Thieß HM, Bressemer KK, Adams L, et al. Do submillisievert-chest CT protocols impact diagnostic quality in suspected COVID-19 patients? *Acta Radiol Open*. 2022;11(1):20584601211073864. doi: 10.1177/20584601211073864
35. Greffier J, Hoballah A, Sadate A, et al. Ultra-low-dose chest CT performance for the detection of viral pneumonia patterns during the COVID-19 outbreak period: A monocentric experience. *Quant Imaging Med Surg*. 2021;11(7):3190–3199. doi: 10.21037/qims-20-1176
36. Karakaş HM, Yıldırım G, Çiçek ED. The reliability of low-dose chest CT for the initial imaging of COVID-19: Comparison of structured findings, categorical diagnoses and dose levels. *Diagn Interv Radiol*. 2021;27(5):607–614. doi: 10.5152/dir.2021.20802
37. Finance J, Zieleskewicz L, Habert P, et al. Low dose chest CT and lung ultrasound for the diagnosis and management of COVID-19. *J Clin Med*. 2021;10(10):2196. doi: 10.3390/jcm10102196
38. Desmet J, Bieba C, De Wever W, et al. Performance of low-dose chest CT as a triage tool for suspected COVID-19 patients. *J Belgian Society Radiology*. 2021;105(1):9. doi: 10.5334/jbsr.2319
39. Aslan S, Bekçi T, Çakır İM, et al. Diagnostic performance of low-dose chest CT to detect COVID-19: A Turkish population study. *Diagn Interv Radiol*. 2021;27(2):181–187. doi: 10.5152/dir.2020.20350
40. Stoleriu MG, Gerckens M, Obereisenbuchner F, et al. Automated quantitative thin slice volumetric low dose CT analysis predicts disease severity in COVID-19 patients. *Clin Imaging*. 2021;79:96–101. doi: 10.1016/j.clinimag.2021.04.008
41. Bai L, Zhou J, Shen C, et al. Assessment of radiation doses and image quality of multiple low-dose CT exams in COVID-19 clinical management. *Chin J Acad Radiol*. 2021;4(4):257–261. doi: 10.1007/s42058-021-00083-1
42. Agostini A, Borgheresi A, Carotti M, et al. Third-generation iterative reconstruction on a dual-source, high-pitch, low-dose chest CT protocol with tin filter for spectral shaping at 100 kV: A study on a small series of COVID-19 patients. *Radiol Med*. 2021;126(3):388–398. doi: 10.1007/s11547-020-01298-5
43. Zali A, Sohrabi MR, Mahdavi A, et al. Correlation between low-dose chest computed tomography and RT-PCR results for the diagnosis of COVID-19: A report of 27,824 cases in Tehran, Iran. *Acad Radiol*. 2021;28(12):1654–1661. doi: 10.1016/j.acra.2020.09.003
44. Argentieri G, Bellesi L, Pagnamenta A, et al. Diagnostic yield, safety, and advantages of ultra-low dose chest CT compared to chest radiography in early stage suspected SARS-CoV-2 pneumonia: A retrospective observational study. *Medicine (Baltimore)*. 2021;100(21):e26034. doi: 10.1097/MD.00000000000026034
45. Leger T, Jacquier A, Barral PA, et al. Low-dose chest CT for diagnosing and assessing the extent of lung involvement of SARS-CoV-2 pneumonia using a semi quantitative score. *PLoS One*. 2020;15(11):e0241407. doi: 10.1371/journal.pone.0241407
46. Hamper CM, Fleckenstein FN, Büttner L, et al. Submillisievert chest CT in patients with COVID-19: experiences of a German Level-I center. *Eur J Radiol Open*. 2020;7:100283. doi: 10.1016/j.ejro.2020.100283
47. Li J, Wang X, Huang X, et al. Application of Care Dose 4D combined with Karl 3D technology in the low dose computed tomography for the follow-up of COVID-19. *BMC Med Imaging*. 2020;20(1):56. doi: 10.1186/s12880-020-00456-5
48. Dangis A, Gieraerts C, De Bruecker Y, et al. Accuracy and reproducibility of low-dose submillisievert chest CT for the diagnosis of COVID-19. *Radiol Cardiothorac Imaging*. 2020;2(2):e200196. doi: 10.1148/ryct.2020200196
49. Radpour A, Bahrami-Motlagh H, Taaghi MT, et al. COVID-19 evaluation by low-dose high resolution CT scans protocol. *Acad Radiol*. 2020;27(6):901. doi: 10.1016/j.acra.2020.04.016
50. Tofighi S, Najafi S, Johnston SK, Gholamrezaezhad A. Low-dose CT in COVID-19 outbreak: Radiation safety, image wisely, and image gently pledge. *Emerg Radiol*. 2020;27(6):601–605. doi: 10.1007/s10140-020-01784-3
51. Tabatabaei SM, Talari H, Gholamrezaezhad A, et al. A low-dose chest CT protocol for the diagnosis of COVID-19 pneumonia: A prospective study. *Emerg Radiol*. 2020;27(6):607–615. doi: 10.1007/s10140-020-01838-6
52. Schulze-Hagen M, Hübel C, Meier-Schroers M, et al. Low-dose chest CT for the diagnosis of COVID-19: A systematic, prospective comparison with PCR. *Dtsch Arztebl Int*. 2020;117(22-23):389–395. doi: 10.3238/arztebl.2020.0389
53. Zhao Y, Wang Y, Duan W, et al. Low-dose chest CT presentation and dynamic changes in patients with novel coronavirus disease 2019. *Radiol Infect Dis*. 2020;7(4):186–194. doi: 10.1016/j.jrid.2020.08.001
54. Castelli M, Maurin A, Bartoli A, et al. Prevalence and risk factors for lung involvement on low-dose chest CT (LDCT) in a paucisymptomatic population of 247 patients affected by COVID-19. *Insights Imaging*. 2020;11(1):117. doi: 10.1186/s13244-020-00939-7
55. Morozov SP, Kuzmina ES, Vetsheva NN, et al. Moscow screening: screening of lung cancer using low-dose computed tomography. *Problems Social Hygiene Healthcare History Med*. 2019;27(S):630–636. (In Russ). doi: 10.32687/0869-866X-2019-27-si1-630-636
56. Patent RUS No. 2701922 C1. Gombolevsky VA, Morozov SP, Chernina VYu, et al. A method for screening lung cancer using ultra-low-dose computed tomography in patients with a body weight of up to 69 kg. mode: Available from: <https://patents.google.com/patent/RU2701922C1/ru>. Accessed: 15.01.2023.
57. Gombolevskiy V, Morozov S, Chernina V, et al. A phantom study to optimise the automatic tube current modulation

for chest CT in COVID-19. *Eur Radiol Exp.* 2021;5(1):21. doi: 10.1186/s41747-021-00218-0

58. Kim YK, Lee BE, Lee SJ, et al. Ultra-low-dose CT of the thorax using iterative reconstruction: Evaluation of image quality and radiation dose reduction. *Am J Roentgenol.* 2015;204(6):1197–1202. doi: 10.2214/AJR.14.13629

59. Blokhin IA, Gonchar AP, Kotenko MR, et al. The influence of body mass index on the reliability of the 0–4 CT scale: Comparison of computed tomography protocols. *Digital Diagnostics.* 2022;3(2):108–118. (In Russ). doi: 10.17816/DD104358

60. Gierada DS, Bierhals AJ, Choong CK, et al. Effects of CT section thickness and reconstruction kernel on emphysema quantification. *Academic Radiology.* 2010;17(2):146–156. doi: 10.1016/j.acra.2009.08.007

СПИСОК ЛИТЕРАТУРЫ

1. Yang Y., Yang M., Shen C., et al. Evaluating the accuracy of different respiratory specimens in the laboratory diagnosis and monitoring the viral shedding of 2019-nCoV infections // medRxiv. 2020. doi: 10.1101/2020.02.11.20021493
2. Rubin G.D., Ryerson C.J., Haramati L.B., et al. The role of chest imaging in patient management during the COVID-19 Pandemic: A multinational consensus statement from the fleischner society // *Radiology.* 2020. Vol. 296, N 1. P. 172–180. doi: 10.1148/radiol.2020201365
3. Временные методические рекомендации. Профилактика, диагностика и лечение новой коронавирусной инфекции (COVID-19). Версия 12 (21.09.2021). Москва, 2021. 232 с.
4. Ng M., Lee E.Y., Yang J., et al. Imaging profile of the COVID-19 infection: Radiologic findings and literature review // *Radiology: Cardiothoracic Imaging.* 2020. Vol. 2, N 1. P. e200034. doi: 10.1148/ryct.2020200034
5. Ai T., Yang Z., Hou H., et al. Correlation of chest CT and RT-PCR testing for coronavirus disease 2019 (COVID-19) in China: A report of 1014 cases // *Radiology.* 2020. Vol. 296, N 2. P. E32–E40. doi: 10.1148/radiol.2020200642
6. Kang Z., Li X., Zhou S. Recommendation of low-dose CT in the detection and management of COVID-2019 // *European Radiology.* 2020. Vol. 30, N 8. P. 4356–4357. doi: 10.1007/s00330-020-06809-6
7. Морозов С.П., Кузьмина Е.С., Ледихова Н.В., и др. Мобилизация научно-практического потенциала службы лучевой диагностики г. Москвы в пандемию COVID-19 // *Digital Diagnostics.* 2020. Т. 1, № 1. С. 5–12. doi: 10.17816/DD51043
8. Pan F., Ye T., Sun P., et al. Time course of lung changes on chest CT during recovery from 2019 novel coronavirus (COVID-19) pneumonia // *Radiology.* 2020. Vol. 295, N 3. P. 715–721. doi: 10.1148/radiol.2020200370
9. Lei D.P., Fan B., Mao J., et al. The progression of computed tomographic (CT) images in patients with coronavirus disease (COVID-19) pneumonia. Running title: The CT progression of COVID-19 pneumonia // *J Infect.* 2020. Vol. 80, N 6. P. e30–e31. doi: 10.1016/j.jinf.2020.03.020
10. Power S.P., Moloney F., Twomey M., et al. Computed tomography and patient risk: Facts, perceptions and uncertainties // *World J Radiol.* 2016. Vol. 8, N 12. P. 902–915. doi: 10.4329/wjr.v8.i12.902
11. Yeung A.W. The “As low as reasonably achievable” (ALARA) principle: A brief historical overview and a bibliometric analysis of the most cited publications // *Radioprotection.* 2019. Vol. 54, N 2. P. 103–109. doi: 10.1051/radiopro/2019016
12. Kalra M.K., Hodayounieh F., Arru C., et al. Chest CT practice and protocols for COVID-19 from radiation dose management perspective // *Eur Radiol.* 2020. Vol. 30, N 12. P. 6554–6560. doi: 10.1007/s00330-020-07034-x
13. Краснов А.С., Кабанов Д.О., Терещенко Г.В. Основы дозиметрии и оптимизации дозовой нагрузки при проведении мульти-спиральной компьютерной томографии // *Вопросы гематологии, онкологии и иммунопатологии в педиатрии.* 2018. Т. 17, № 3. С. 127–132.
14. Singh S., Kalra M.K., Thrall J.H., Mahesh M. CT radiation dose reduction by modifying primary factors // *J Am Coll Radiol.* 2011. Vol. 8, N 5. P. 369–372. doi: 10.1016/j.jacr.2011.02.001
15. Zarb F., Rainford L., McEntee M.F. Developing optimized CT scan protocols: Phantom measurements of image quality // *Radiography.* 2011. Vol. 17, N 2. P. 109–114. doi: 10.1016/j.radi.2010.10.004
16. Hilts M., Duzenli C. Image noise in X-ray CT polymer gel dosimetry // *J Physics: Conference Series.* 2004. Vol. 3, N 1. P. 252. doi: 10.1088/1742-6596/3/1/040
17. Lira D., Padole A., Kalra M.K., Singh S. Tube potential and CT radiation dose optimization // *Am J Roentgenol.* 2015. Vol. 204, N 1. P. W4–W10. doi: 10.2214/AJR.14.13281
18. Reid J., Gamberoni J., Dong F., Davros W. Optimization of kVp and mAs for pediatric low-dose simulated abdominal CT: Is it best to base parameter selection on object circumference? // *AJR Am J Roentgenol.* 2010. Vol. 195, N 4. P. 1015–1020. doi: 10.2214/AJR.09.3862
19. Khoramian D., Sistani S., Firouzjah R.A. Assessment and comparison of radiation dose and image quality in multi-detector CT scanners in non-contrast head and neck examinations // *Paul J Radiol.* 2019. Vol. 84. P. 61–67. doi: 10.5114/pjr.2019.82743
20. Mahesh M., Scatarige J.C., Cooper J., Fishman E.K. Dose and pitch relationship for a particular multislice CT scanner // *AJR Am J Roentgenol.* 2001. Vol. 177, N 6. P. 1273–1275. doi: 10.2214/ajr.177.6.1771273
21. Tack D., Gevenois P.A., Abada H. Radiation dose from adult and pediatric multidetector computed tomography // *Springer.* 2007. doi: 10.1007/978-3-540-68575-3
22. Greffier J., Pereira F., Hamard A., et al. Effect of tin filter-based spectral shaping CT on image quality and radiation dose for routine use on ultralow-dose CT protocols: A phantom study // *Diagnostic and Interventional Imaging.* 2020. Vol. 101, N 6. P. 373–381. doi: 10.1016/j.diii.2020.01.002

23. Paul J., Krauss B., Banckwitz R., et al. Relationships of clinical protocols and reconstruction kernels with image quality and radiation dose in a 128-slice CT scanner: Study with an anthropomorphic and water phantom // *Eur J Radiology*. 2012. Vol. 81, N 5. P. e699–e703. doi: 10.1016/j.ejrad.2011.01.078
24. Hashemi S., Mehrez H., Cobbold R.S., Paul N.S. Optimal image reconstruction for detection and characterization of small pulmonary nodules during low-dose CT // *Eur Radiol*. 2014. Vol. 24, N 6. P. 1239–1250. doi: 10.1007/s00330-014-3142-9
25. Beister M., Kolditz D., Kalender W.A. Iterative reconstruction methods in X-ray CT // *Physica Medica*. 2012. Vol. 28, N 2. P. 94–108. doi: 10.1016/j.ejmp.2012.01.003
26. Shiri I., Akhavanallah A., Sanaat A., et al. Ultra-low-dose chest CT imaging of COVID-19 patients using a deep residual neural network // *Eur Radiology*. 2021. Vol. 31, N 3. P. 1420–1431. doi: 10.1007/s00330-020-07225-6
27. Shan H., Padole A., Homayounieh F., et al. Competitive performance of a modularized deep neural network compared to commercial algorithms for low-dose CT image reconstruction // *Nat Machine Intelligence*. 2019. Vol. 1, N 6. P. 269–276. doi: 10.1038/s42256-019-0057-9
28. Blokhin I., Gombolevskiy V., Chernina V., et al. Inter-observer agreement between low-dose and standard-dose CT with soft and sharp convolution kernels in COVID-19 Pneumonia // *J Clin Med*. 2022. Vol. 11, N 669. doi: 10.3390/jcm11030669
29. Филатова Д.А., Синицын В.Е., Мершина Е.А. Возможности снижения лучевой нагрузки при проведении компьютерной томографии для оценки изменений в легких, характерных для COVID-19: использование адаптивной статистической итеративной реконструкции // *Digital Diagnostics*. 2021. Т. 2, № 2. С. 94–104. doi: 10.17816/DD62477
30. Afshar P., Rafiee M.J., Naderkhani F., et al. Human-level COVID-19 diagnosis from low-dose CT scans using a two-stage time-distributed capsule network // *Sci Rep*. 2022. Vol. 12, N 1. P. 4827. doi: 10.1038/s41598-022-08796-8
31. Fukumoto W., Nakamura Y., Yoshimura K., et al. Triaging of COVID-19 patients using low dose chest CT: Incidence and factor analysis of lung involvement on CT images // *J Infect Chemother*. 2022. Vol. 28, N 6. P. 797–801. doi: 10.1016/j.jiac.2022.02.025
32. Bieba C.M., Desmet J.N., Dubbeldam A., et al. Radiological findings in low-dose CT for COVID-19 pneumonia in 182 patients: Correlation of signs and severity with patient outcome // *Medicine (Baltimore)*. 2022. Vol. 101, N 9. P. e28950. doi: 10.1097/MD.00000000000028950
33. Piqueras B.M., Casajús E.A., Iriarte U.C., et al. Low-dose chest CT for preoperative screening for SARS-CoV-2 infection // *Radiologia (Engl.)*. 2022. Vol. 64, N 4. P. 317–323. doi: 10.1016/j.rxeng.2021.11.004
34. Thieß H.M., Bressen K.K., Adams L., et al. Do submillisievert chest CT protocols impact diagnostic quality in suspected COVID-19 patients? // *Acta Radiol Open*. 2022. Vol. 11, N 1. P. 20584601211073864. doi: 10.1177/20584601211073864
35. Greffier J., Hoballah A., Sadate A., et al. Ultra-low-dose chest CT performance for the detection of viral pneumonia patterns during the COVID-19 outbreak period: A monocentric experience // *Quant Imaging Med Surg*. 2021. Vol. 11, N 7. P. 3190–3199. doi: 10.21037/qims-20-1176
36. Karakaş H.M., Yıldırım G., Çiçek E.D. The reliability of low-dose chest CT for the initial imaging of COVID-19: Comparison of structured findings, categorical diagnoses and dose levels // *Diagn Interv Radiol*. 2021. Vol. 27, N 5. P. 607–614. doi: 10.5152/dir.2021.20802
37. Finance J., Zieleskewicz L., Habert P., et al. Low dose chest CT and lung ultrasound for the diagnosis and management of COVID-19 // *J Clinic Med*. 2021. Vol. 10, N 10. P. 2196. doi: 10.3390/jcm10102196
38. Desmet J., Bieba C., De Wever W., et al. Performance of low-dose chest CT as a triage tool for suspected COVID-19 patients // *J Belgian Society Radiology*. 2021. Vol. 105, N 1. P. 9. doi: 10.5334/jbsr.2319
39. Aslan S., Bekçi T., Çakır İ.M., et al. Diagnostic performance of low-dose chest CT to detect COVID-19: A Turkish population study // *Diagn Interv Radiol*. 2021. Vol. 27, N 2. P. 181–187. doi: 10.5152/dir.2020.20350
40. Stoleriu M.G., Gerckens M., Obereisenbuchner F., et al. Automated quantitative thin slice volumetric low dose CT analysis predicts disease severity in COVID-19 patients // *Clin Imaging*. 2021. Vol. 79. P. 96–101. doi: 10.1016/j.clinimag.2021.04.008
41. Bai L., Zhou J., Shen C., et al. Assessment of radiation doses and image quality of multiple low-dose CT exams in COVID-19 clinical management // *Chin J Acad Radiol*. 2021. Vol. 4, N 4. P. 257–261. doi: 10.1007/s42058-021-00083-1
42. Agostini A., Borgheresi A., Carotti M., et al. Third-generation iterative reconstruction on a dual-source, high-pitch, low-dose chest CT protocol with tin filter for spectral shaping at 100 kV: A study on a small series of COVID-19 patients // *Radiol Med*. 2021. Vol. 126, N 3. P. 388–398. doi: 10.1007/s11547-020-01298-5
43. Zali A., Sohrabi M.R., Mahdavi A., et al. Correlation between low-dose chest computed tomography and RT-PCR results for the diagnosis of COVID-19: A report of 27,824 cases in Tehran, Iran // *Acad Radiol*. 2021. Vol. 28, N 12. P. 1654–1661. doi: 10.1016/j.acra.2020.09.003
44. Argentieri G., Bellesi L., Pagnamenta A., et al. Diagnostic yield, safety, and advantages of ultra-low dose chest CT compared to chest radiography in early stage suspected SARS-CoV-2 pneumonia: A retrospective observational study // *Medicine (Baltimore)*. 2021. Vol. 100, N 21. P. e26034. doi: 10.1097/MD.00000000000026034
45. Leger T., Jacquier A., Barral P.A., et al. Low-dose chest CT for diagnosing and assessing the extent of lung involvement of SARS-CoV-2 pneumonia using a semi quantitative score // *PLoS One*. 2020. Vol. 15, N 11. P. e0241407. doi: 10.1371/journal.pone.0241407
46. Hamper C.M., Fleckenstein F.N., Büttner L., et al. Submillisievert chest CT in patients with COVID-19: Experiences of a German Level-I center // *Eur J Radiol Open*. 2020. Vol. 7. P. 100283. doi: 10.1016/j.ejro.2020.100283
47. Li J., Wang X., Huang X., et al. Application of Care Dose 4D combined with Karl 3D technology in the low dose computed tomography for the follow-up of COVID-19 // *BMC Med Imaging*. 2020. Vol. 20, N 1. P. 56. doi: 10.1186/s12880-020-00456-5
48. Dangis A., Gieraerts C., De Bruecker Y., et al. Accuracy and reproducibility of low-dose submillisievert chest CT for the diagnosis of COVID-19 // *Radiol Cardiothorac Imaging*. 2020. Vol. 2, N 2. P. e200196. doi: 10.1148/ryct.2020200196
49. Radpour A., Bahrami-Motlagh H., Taaghi M.T., et al. COVID-19 evaluation by low-dose high resolution CT scans protocol // *Acad Radiol*. 2020. Vol. 27, N 6. P. 901. doi: 10.1016/j.acra.2020.04.016
50. Tofighi S., Najafi S., Johnston S.K., Gholamrezanezhad A. Low-dose CT in COVID-19 outbreak: Radiation safety, image wisely, and image gently pledge // *Emerg Radiol*. 2020. Vol. 27, N 6. P. 601–605. doi: 10.1007/s10140-020-01784-3

- 51.** Tabatabaei S.M., Talari H., Gholamrezanezhad A., et al. A low-dose chest CT protocol for the diagnosis of COVID-19 pneumonia: A prospective study // *Emerg Radiol.* 2020. Vol. 27, N 6. P. 607–615. doi: 10.1007/s10140-020-01838-6
- 52.** Schulze-Hagen M., Hübel C., Meier-Schroers M., et al. Low-dose chest CT for the diagnosis of COVID-19: A systematic, prospective comparison with PCR // *Dtsch Arztebl Int.* 2020. Vol. 117, N 22–23. P. 389–395. doi: 10.3238/arztebl.2020.0389
- 53.** Zhao Y., Wang Y., Duan W., et al. Low-dose chest CT presentation and dynamic changes in patients with novel coronavirus disease 2019 // *Radiol Infect Dis.* 2020. Vol. 7, N 4. P. 186–194. doi: 10.1016/j.jrid.2020.08.001
- 54.** Castelli M., Maurin A., Bartoli A., et al. Prevalence and risk factors for lung involvement on low-dose chest CT (LDCT) in a paucisymptomatic population of 247 patients affected by COVID-19 // *Insights Imaging.* 2020. Vol. 11, N 1. P. 117. doi: 10.1186/s13244-020-00939-7
- 55.** Морозов С.П., Кузьмина Е.С., Ветшева Н.Н., и др. Московский скрининг: скрининг рака легкого с помощью низкодозовой компьютерной томографии // *Проблемы социальной гигиены, здравоохранения и истории медицины.* 2019. Т. 27, № 5. С. 630–636. doi: 10.32687/0869-866X-2019-27-si1-630-636
- 56.** Патент РФ № 2701922 С1. Гомболевский В.А., Морозов С.П., Чернина В.Ю., и др. Способ скрининга рака легкого с помощью ультранизкодозной компьютерной томографии у пациентов с массой тела до 69 кг. Режим доступа: <https://patents.google.com/patent/RU2701922C1/ru>. Дата обращения: 15.01.2023.
- 57.** Gombolevskiy V., Morozov S., Chernina V., et al. A phantom study to optimise the automatic tube current modulation for chest CT in COVID-19 // *Eur Radiol Exp.* 2021. Vol. 5, N 1. P. 21. doi: 10.1186/s41747-021-00218-0
- 58.** Kim Y.K., Lee B.E., Lee S.J., et al. Ultra-low-dose CT of the thorax using iterative reconstruction: Evaluation of image quality and radiation dose reduction // *Am J Roentgenol.* 2015. Vol. 204, N 6. P. 1197–1202. doi: 10.2214/AJR.14.13629
- 59.** Блохин И.А., Гончар А.П., Коденко М.Р., и др. Влияние индекса массы тела на надёжность шкалы КТ0–4: сравнение протоколов компьютерной томографии // *Digital Diagnostics.* 2022. Т. 3, № 2. С. 108–118. doi: 10.17816/DD104358
- 60.** Gierada D.S., Bierhals A.J., Choong C.K., et al. Effects of CT section thickness and reconstruction kernel on emphysema quantification // *Academic Radiology.* 2010. Vol. 17, N 2. P. 146–156. doi: 10.1016/j.acra.2009.08.007
- 61.** Gao Y., Hua M., Lv J., et al. Reproducibility of radiomic features of pulmonary nodules between low-dose CT and conventional-dose CT // *Quant Imaging Med Surg.* 2022. Vol. 12, N 4. P. 2368–2377. doi: 10.21037/qims-21-609
- 62.** Blokhin I.A., Solovov A.V., Vladzimirskiy AV., et al. Automated analysis of lung lesions in COVID-19: Comparison of standard and low-dose CT // *SJCEM.* 2023. Vol. 37, N 4. P. 114–123. doi: 10.29001/2073-8552-2022-37-4-114-123
- 63.** Bak S.H., Kim J.H., Jin H., et al. Emphysema quantification using low-dose computed tomography with deep learning-based kernel conversion comparison // *Eur Radiol.* 2020. Vol. 30, N 12. P. 6779–6787. doi: 10.1007/s00330-020-07020-3

AUTHORS' INFO

* Ivan A. Blokhin;

address: 24/1 Petrovka street, 127051 Moscow, Russia;
ORCID: <https://orcid.org/0000-0002-2681-9378>;
eLibrary SPIN: 3306-1387; e-mail: BlockhinIA@zdrav.mos.ru

Denis A. Rumyantsev;

ORCID: <https://orcid.org/0000-0001-7670-7385>;
eLibrary SPIN: 8734-2085; e-mail: x.radiology@mail.ru

Maria M. Suchilova;

ORCID: <https://orcid.org/0000-0003-1117-0294>;
eLibrary SPIN: 4922-1894; e-mail: SuchilovaMM@zdrav.mos.ru

Anna P. Gonchar;

ORCID: <https://orcid.org/0000-0001-5161-6540>;
eLibrary SPIN: 3513-9531; e-mail: GoncharAP@zdrav.mos.ru

Olga V. Omelyanskaya;

ORCID: <https://orcid.org/0000-0002-0245-4431>;
eLibrary SPIN: 8948-6152;
e-mail: OmelyanskayaOV@zdrav.mos.ru

ОБ АВТОРАХ

* Блохин Иван Андреевич;

адрес: Россия, 127051, Москва, ул. Петровка, д. 24, стр. 1;
ORCID: <https://orcid.org/0000-0002-2681-9378>;
eLibrary SPIN: 3306-1387; e-mail: BlockhinIA@zdrav.mos.ru

Румянцев Денис Андреевич;

ORCID: <https://orcid.org/0000-0001-7670-7385>;
eLibrary SPIN: 8734-2085; e-mail: x.radiology@mail.ru

Сучилова Мария Максимовна;

ORCID: <https://orcid.org/0000-0003-1117-0294>;
eLibrary SPIN: 4922-1894; e-mail: SuchilovaMM@zdrav.mos.ru

Гончар Анна Павловна;

ORCID: <https://orcid.org/0000-0001-5161-6540>;
eLibrary SPIN: 3513-9531; e-mail: GoncharAP@zdrav.mos.ru

Омелянская Ольга Васильевна;

ORCID: <https://orcid.org/0000-0002-0245-4431>;
eLibrary SPIN: 8948-6152;
e-mail: OmelyanskayaOV@zdrav.mos.ru

* Corresponding author / Автор, ответственный за переписку

DOI: <https://doi.org/10.17816/DD123543>

Основные импульсные последовательности в диагностике абдоминальной патологии

Е.М. Сыркашев^{1,2}, Ф.З. Кадырбердиева², Л.Р. Абуладзе¹,
Д.С. Семенов¹, Е.Г. Привалова¹

¹ Научно-практический клинический центр диагностики и телемедицинских технологий, Москва, Российская Федерация

² Национальный медицинский исследовательский центр акушерства, гинекологии и перинатологии имени академика В.И. Кулакова, Москва, Российская Федерация

АННОТАЦИЯ

Магнитно-резонансная томография является одним из основных методов диагностики заболеваний органов брюшной полости и забрюшинного пространства, который позволяет с высокой диагностической точностью и воспроизводимостью визуализировать очаговые или диффузные изменения паренхиматозных и полых органов. Магнитно-резонансная томография имеет определённые преимущества перед компьютерной томографией в чувствительности и специфичности определения патологических изменений паренхиматозных органов, желчевыводящих путей и протоков поджелудочной железы, брюшины и органов забрюшинного пространства.

Мультипараметрический протокол сканирования предоставляет информацию не только о взаимной топографии органов и их структуре, но и о функциональном состоянии тканей, что позволяет перейти от структурной к функциональной оценке изображений. В большинстве случаев стандартный протокол включает сканирование органов брюшной полости (T1-/T2- и диффузионно-взвешенные режимы) и желчевыводящих протоков (магнитно-резонансная холангиопанкреатография), при этом данный протокол может быть значительно сокращён или дополнен в зависимости от целей исследования и состояния пациента.

Существующие технические разработки и достижения позволяют упростить процесс сканирования и сократить время на получение изображений, повышая при этом воспроизводимость методик в разных учреждениях здравоохранения.

Ключевые слова: магнитно-резонансная томография; МРТ; протокол сканирования; МРТ органов брюшной полости и забрюшинного пространства.

Как цитировать

Сырцашев Е.М., Кадырбердиева Ф.З., Абуладзе Л.Р., Семенов Д.С., Привалова Е.Г. Основные импульсные последовательности в диагностике абдоминальной патологии // *Digital Diagnostics*. 2023. Т. 4, № 1. С. 39–50. DOI: <https://doi.org/10.17816/DD123543>

DOI: <https://doi.org/10.17816/DD123543>

Basic pulse sequences in the diagnosis of abdominal pathology

Egor M. Syrkashev^{1, 2}, Faina Z. Kadyrberdieva², Liya R. Abuladze¹,
Dmitriy S. Semenov¹, Ekaterina G. Privalova¹

¹ Moscow Center for Diagnostics and Telemedicine, Moscow, Russian Federation

² National Medical Research Center for Obstetrics, Gynecology and Perinatology, Moscow, Russian Federation

ABSTRACT

Magnetic resonance imaging is used for diagnosing abdominal and retroperitoneal space pathology, which allows visualizing focal or diffuse lesions in the parenchymal and hollow viscera with high diagnostic accuracy and reproducibility. Magnetic resonance imaging has advantages over computed tomography in the sensitivity and specificity of determining pathological changes in parenchymal organs, bile ducts and ducts of the pancreas, peritoneum, and retroperitoneal space.

The multiparametric protocol provides information about the mutual topography of organs and their structure and the functional state of tissues. This allows to move from structural to functional evaluation. In most cases, the standard abdominal protocol includes T1-weighted images, T2-weighted images, diffusion-weighted images, and magnetic resonance cholangiopancreatography. Depending on the objectives and patient's condition, this protocol can be significantly reduced or supplemented.

Existing technical developments and achievements make it possible to simplify the scanning process and reduce the time for obtaining images while increasing the reproducibility of techniques in different healthcare institutions.

Keywords: magnetic resonance imaging; MRI; scanning protocol; abdominal and retroperitoneal MRI.

To cite this article

Syrkashev EM, Kadyrberdieva FZ, Abuladze LR, Semenov DS, Privalova EG. Basic pulse sequences in the diagnosis of abdominal pathology. *Digital Diagnostics*. 2023;4(1):39–50. DOI: <https://doi.org/10.17816/DD123543>

Received: 18.01.2023

Accepted: 10.03.2023

Published: 04.04.2023

DOI: <https://doi.org/10.17816/DD123543>

腹部病理诊断中的关键脉冲序列

Egor M. Syrkashev^{1,2}, Faina Z. Kadyrberdieva², Liya R. Abuladze¹,
Dmitriy S. Semenov¹, Ekaterina G. Privalova¹

¹ Moscow Center for Diagnostics and Telemedicine, Moscow, Russian Federation

² National Medical Research Center for Obstetrics, Gynecology and Perinatology, Moscow, Russian Federation

简评

磁共振成像是诊断腹部和腹膜后器官疾病的主要方法之一，它允许显示出实质器官和空腔脏器的病灶或弥漫性变化，具有很高的诊断准确度和可重复性。与计算机断层扫描相比，磁共振成像在确定实质器官、胆道和胰管、腹膜和腹膜后器官的病理变化的敏感性和特异性方面有明显优势。

多参数扫描方案不仅提供器官的相互形貌及其结构的信息，而且提供组织的功能状态，使图像从结构评估过渡到功能评估。在大多数情况下，标准方案包括腹部扫描（T1-/T2-和扩散加权模式）和胆道扫描（磁共振胆胰管成像），但根据检查的目的和病人的情况，这个方案可以大大缩短或补充。

现有的技术发展和成果允许简化扫描过程和缩短成像时间，同时提高技术在不同医疗机构的方法重复性。

关键词：磁共振成像，MRI，扫描方案，腹部和腹膜后的MRI。

To cite this article

Syrkashev EM, Kadyrberdieva FZ, Abuladze LR, Semenov DS, Privalova EG. 腹部病理诊断中的关键脉冲序列. *Digital Diagnostics*. 2023;4(1):39–50.

DOI: <https://doi.org/10.17816/DD123543>

收到: 18.01.2023

接受: 10.03.2023

发布日期: 04.04.2023

INTRODUCTION

Magnetic resonance imaging (MRI) is one of the most important radiodiagnostic modalities, with an increasing role in the routine diagnosis of abdominal organ diseases. In addition to the absence of ionizing radiation and the high natural soft tissue contrast, MRI allows for image analysis in any plane and three-dimensional (3D) reconstruction of areas of interest. Diffusion and perfusion techniques provide information not only on the structure of tissues but also on their functional state, such as determining the diffusion rate of water molecules and the accumulation and leaching of contrast agents.

Currently, MRI is one of the primary diagnostic methods, with advantages over computed tomography in terms of sensitivity and specificity in determining pathological changes in parenchymal organs, biliary tract and pancreatic ducts, peritoneum, and retroperitoneal organs [1].

BASIC PULSE SEQUENCES

Abdominal MRI can be challenging when obtaining images with a high signal-to-noise ratio (SNR) from tissues in motion due to the patient's breathing, intestinal motility, heart contractions, and pulsation of large vessels. Initially, MRI was performed using standard spin-echo (SE) sequences to obtain T1- and T2-weighted images (WIs). However, the lengthy data-collection process necessitated additional respiratory gating, which significantly increased the scanning time (in some cases, the study protocol exceeded 60 min) [2, 3]. Moreover, even minor respiratory desynchronization resulted in image interpretation difficulties in some cases.

Currently, the standard abdominal MRI protocol includes techniques based on shorter breath-hold sequences. These include T1-WIs with spoiled gradient echo (SGE) and half-Fourier acquisition single-shot turbo SE imaging (HASTE) or single-shot fast SE (SSFSE) [4, 5] (Table 1).

T1- and T2-wi

Obtaining one T2-WI slice using a single-shot SE takes approximately 1 s with a central filling of the k-space. Because image contrast is determined by the central regions of the k-space, single-shot techniques are much less sensitive to patient movements, which is critical for unconscious patients. T1-WIs with SGE are much more sensitive to movements; even brief movements during scanning result in image artifacts that affect all slices. Moreover, less motion sensitive techniques are also available. They are based on the same principles that are used for single-shot T2-WIs: fast filling of the central k-space by analyzing one slice per pulse (e.g., turbo fast low angle shot and fast inversion-recovery motion-insensitive [FIRM]).

Another approach is to use angiography-specific-modified 3D gradient echo sequences. Their names vary depending on the manufacturer (initially, volumetric interpolated breath-hold examination) [6]. These sequences provide images with high resolution (2–3 mm) and nearly isotropic voxel size, which is critical in the diagnosis of liver pathology and vascular anatomy. This technique is also used for multiplanar image reconstruction.

Another important aspect of T1-WIs is the use of intravenous contrast enhancement, including hepatospecific contrast agents. For example, gadoxetic acid has a high affinity for hepatocytes and thus allows for better visualization of liver pathologies (Fig. 1).

Contrast agents shorten the T1 relaxation time, resulting in higher signal intensity on T1-WIs. Depending on the blood supply to focal or diffuse lesions in parenchymal organs, various contrasting patterns are distinguished, which in general differ from those in adjacent unaffected tissues. Arterial phase imaging is accomplished by short sequences immediately after the administration of gadolinium-based contrast agents.

The main method involves dynamic multiphase 2D or 3D SGE sequences, which can be used to analyze signal intensity-time curves in areas of interest. Most focal lesions (e.g.,

Table 1. Names of basic pulse sequences used by major magnetic resonance imaging scanner manufacturers

Manufacturer	TOSHIBA	PHILIPS	GE	SIEMENS
Spin-echo	SE	SE	SE	SE
Fast spin-echo	FSE	TSE	FSE	TSE
Single-shot fast spin-echo	FASE	SSh TSE	SSFSE/RARE	HASTE
Gradient echo	FE	FFE	GRASSE, GRE	FISP, GRE
	T1-FE	CE-FFE T1	SPGR	FLASH
	-	CE-FFE T2	SSFP	PSIF
Steady-state fast-field echo	TrueSSFP	Balanced FFE (BFFE)	FIESTA	True FISP
Fast scan	FFE	TFE	Rapid SPGR	TurboFlash
Saturation bands	PreSat	REST	SAT	PreSAT
Fat, water, and background suppression	FatSat	SPIR	CHEMSAT	FATSAT

Note. Spin-echo, fast spin-echo, single-shot fast spin-echo, gradient echo, steady-state fast-field echo, fast scan, saturation bands, and fat, water, and background suppression.

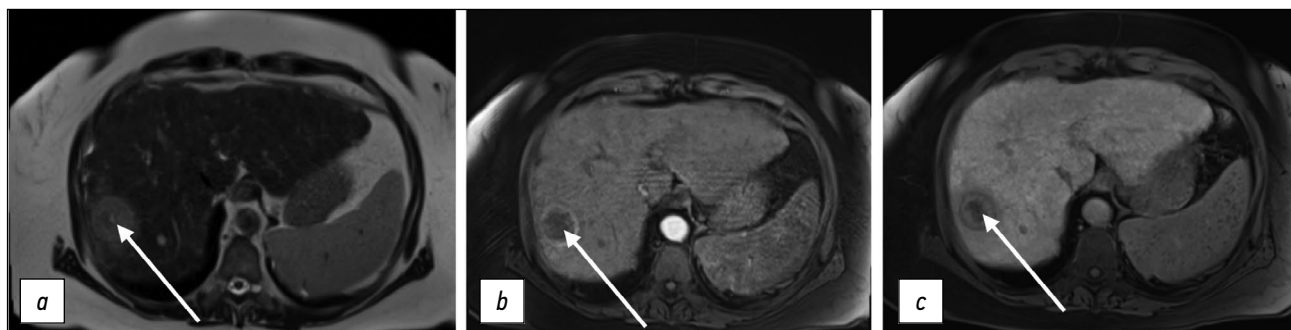


Figure 1. Liver magnetic resonance imaging with a hepatospecific contrast agent. A hepatocellular carcinoma nodule (arrows): *a* T2-weighted image: a hyperintense nodule is visualized; *b* T1-weighted image, arterial phase: a ring-like contrast uptake is visualized; *c* T1-weighted image, hepatospecific phase, 20 min after contrast agent injection.

those in the spleen, liver, or pancreas) are best visualized during the arterial phase. Images taken 1.5–10 min after contrast agent injection are in the equilibrium contrast phase, with an optimal window of 2–5 min after injection. As a rule, 5 min after contrast agent injection, a delayed or excretory phase begins. Many inflammatory or neoplastic diseases are better visualized during this phase, and the addition of fat suppression aids in the detection of these changes (e.g., peritoneal implants, cholangiocarcinoma, inflammatory bowel disease, and adrenal masses) [7–9].

Increasing the difference in signal intensity from lesions compared with unaffected tissues helps in disease detection: lesions localized in adipose tissue can be easily detected by varying the fat signal intensity on T1-WIs and T2-WIs. For example, fibrotic changes or peritoneal fluid with low signal intensity on T1-WIs are easier to detect on images without fat suppression. On the contrary, pathologies with high signal intensity, such as a subacute hematoma or a protein-rich fluid, are easier to visualize with fat suppression.

Diffusion-weighted images

DWIs are based on differences in the movement of water molecules (diffusion) in the extracellular and intracellular

spaces and are used for visualization without exogenous contrast agents. This technique allows for quantitative and qualitative analyses of not only cell density but also cell membrane integrity, making it a type of functional image assessment [10]. Therefore, it should be included in standard abdominal and retroperitoneal MRI protocols (Figs. 2 and 3).

DWIs were initially used to diagnose brain pathology, primarily strokes: signal changes in a given pulse sequence allow for the detection of ischemic changes long before they are visible on T2-WIs. DWIs are now used to diagnose various extracranial pathologies owing to advancements in high-amplitude gradients, multichannel surface coils, and parallel imaging.

Diffusion is proportional to cell density and cell membrane integrity: restricted diffusion is observed in tissues with increased cellularity or decreased extracellular fluid volume (e.g., some tumors and abscesses; Fig. 4) and in the presence of cytotoxic edema. Relatively free diffusion is observed in tissues with low cell density or when their membranes are damaged, such as cysts or necrotic tissues.

DWI sensitivity to water molecule movement can be altered by varying the gradient amplitude and duration and the time interval between gradient pairs. For this purpose, A

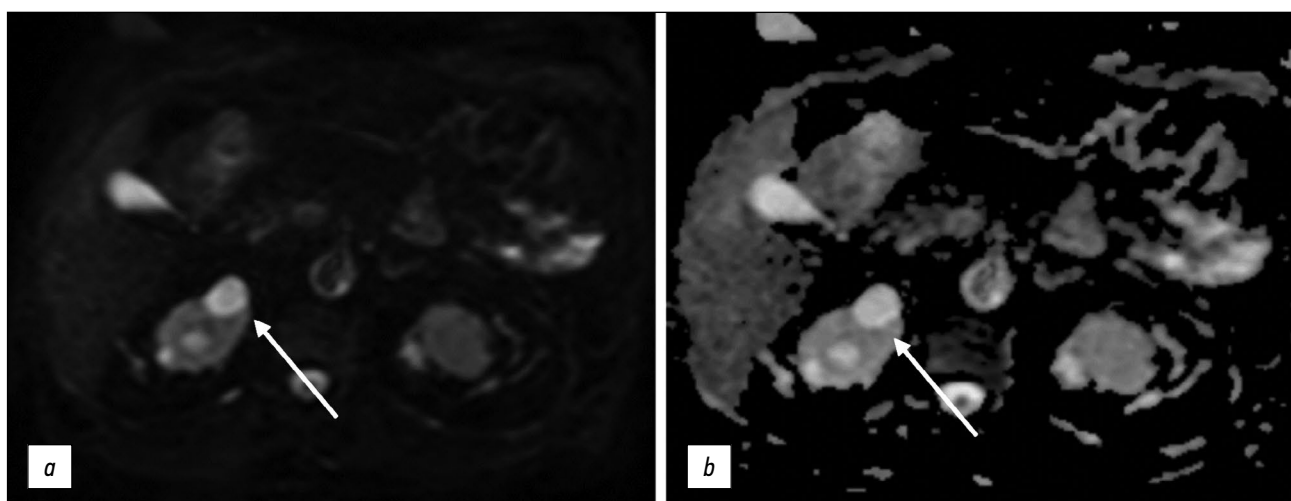


Figure 2. Abdominal magnetic resonance imaging, simple renal cortical cysts (arrows): *a* a diffusion-weighted image; *b* map of the apparent diffusion coefficient. False restricted diffusion.

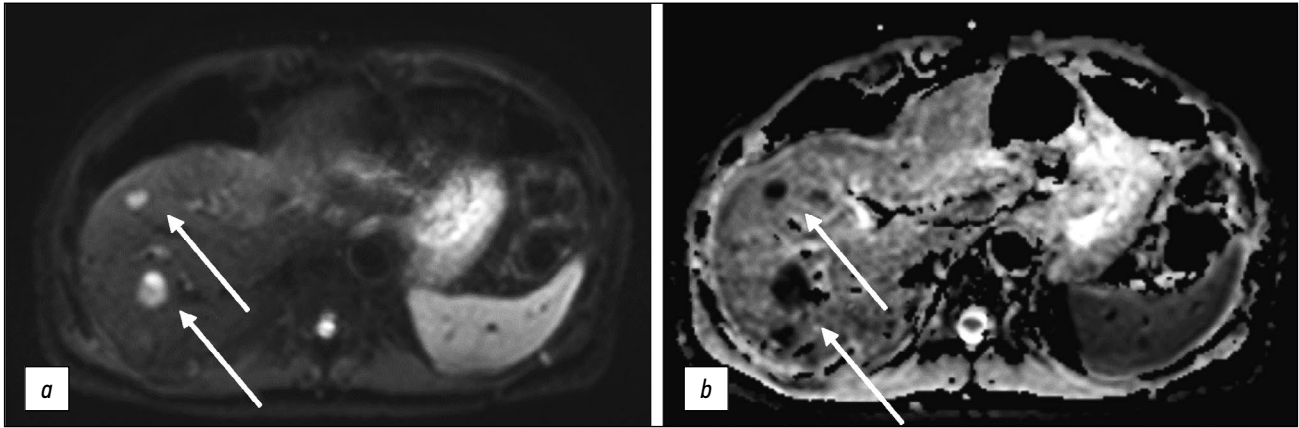


Figure 3. Abdominal magnetic resonance imaging, secondary hepatic lesions (arrows): *a* a diffusion-weighted image; *b* map of the apparent diffusion coefficient. True restricted diffusion.

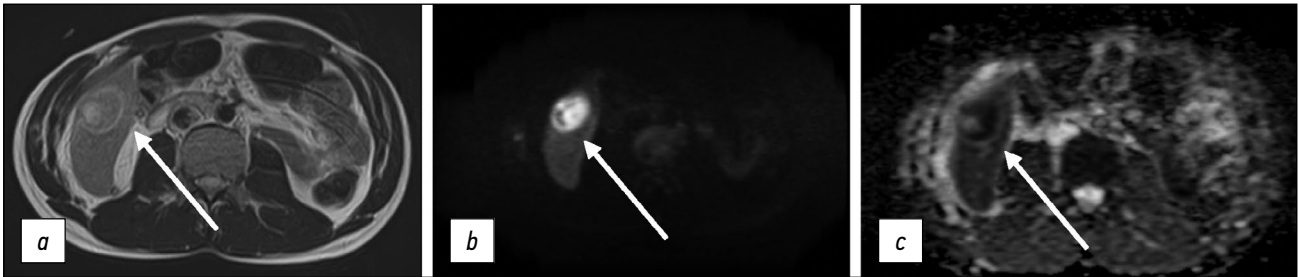


Figure 4. Abdominal magnetic resonance imaging, encapsulated liver mass (abscess) (arrows): *a* T2-weighted image; *b* apparent diffusion coefficient; *c* map of apparent diffusion coefficient.

b-factor is used, which is proportional to the criteria described above. Water molecules with high mobility or long diffusion distance (e.g., in the intravascular space) exhibit signal attenuation at low b-factor values (e.g., $b = 50\text{--}100\text{ mm}^2/\text{s}$). Conversely, high b-factor values (e.g., $b = 1,000\text{ mm}^2/\text{s}$) are typically used to visualize slow-moving water molecules or short diffusion distances because they exhibit slower signal attenuation (as the b-factor increases). For a correct interpretation, DWIs must be taken with at least two b-factors, namely, $b = 0\text{ mm}^2/\text{s}$ and $b = 100\text{--}1,000\text{ mm}^2/\text{s}$, because DWIs obtained with $b = 0\text{ mm}^2/\text{s}$ are T2-weighted sequences. At low b-factor values (e.g., $\leq 200\text{ mm}^2/\text{s}$), the apparent diffusion coefficient depends on tissue perfusion and water diffusion. As the b-factor increases, the effects of perfusion decrease. In general, the higher the b-factor, the more sensitive the sequence is to diffusion effects; in addition, high b-factor values (e.g., $100\text{--}1,000\text{ mm}^2/\text{s}$) are better for suppressing the background signal [10, 14].

ROUTINE IMAGING PROTOCOL

In most cases, the abdominal MRI protocol includes T2-WIs, pre- and postcontrast T1-WIs, including those with fat suppression, DWIs, and MR cholangiopancreatography (MRCP). These sequences enable accurate visualization of lesions not only in the parenchymal organs, walls of hollow organs, and bile ducts but also in the peritoneum, retroperitoneal organs, and cellular spaces (Table 2).

However, this protocol can be supplemented or shortened depending on the clinical situation and the study goals and objectives. The American College of Radiology recommends that slice thickness should not exceed 8 mm, slice spacing should not exceed 2 mm, and thinner slices are preferred [15].

Standard T2-WIs are taken in the frontal and axial planes using SE. These sequences have a relatively long acquisition time but provide a high SNR. The routine use of this approach in abdominal radiology is limited by the patient's breathing, pulsation of large vessels, and intestinal motility. In such cases, respiratory gating can be performed, which increases scan time (up to 5–7 min); however, motion correction is not absolute: in most cases, there is a blurring effect at the border of organs, which can make diagnosing various pathologies difficult. As a result, T2-WIs are now more commonly obtained using accelerated fast SE, single-shot accelerated fast SE or steady-state free precession sequences (Fig. 5).

Images can be taken with or without breath-holding. When taking images without breath-holding, every effort should be made to reduce respiratory motion artifacts by multiple signal averaging and/or respiratory compensation/trigging. The main difference between this and standard SE is the relative decrease in tissue contrast, which can lead to diagnostic errors, particularly small changes compared with unaffected parenchymal organ tissue (e.g., small hepatocellular carcinoma). Conversely, T1-WIs

Table 2. Basic pulse sequences and their role in the diagnosis of abdominal organ and retroperitoneal space diseases

Pulse sequences	Main role
T1 FS	It is used to identify lesions that are mostly fatty or have adipose tissue or a hemorrhagic component (e.g., angiomyolipomas, teratomas, pancreatic steatosis, and renal corticomedullary differentiation). It is used as a general sequence in abdominal organ examinations and for contrast agent injection
T1 in-phase, out-of-phase	They are used for affected tissue visualization when a combination of fat and water protons is observed in the same voxel (fatty liver, adrenal adenoma, hemochromatosis, and hemosiderosis) and provide information about abnormally elevated fluid or fibrous tissue (subacute hemorrhage, fat, or high protein content)
T2, T2 FS	They are used to detect elevated serous fluid, hemangiomas, biliary hamartomas, tissue edema, hemorrhagic or high protein cysts, and fibrous changes, can be used for iron detection in combination without-of-phase T1, and are used as general sequences in abdominal organ examinations
DWI	Primary and secondary abdominal and retroperitoneal tumors, including not visualized on T1 and T2 (e.g., peritoneal disseminations)
MRCP	Pancreatobiliary system examination for strictures, cysts of intrahepatic bile ducts, choledocholithiasis, and pancreatic cysts

compensate for this disadvantage: these areas, on average, have a longer T1 time relative to the unaffected tissue and are well visualized on nonenhanced SGE sequences or early (arterial) postcontrast images as focal lesions with a reduced signal.

MRCP is based on a modified SE sequence with a time of echo (TE) of 250–500 ms that produces heavily T2-WIs. TE elongation causes soft tissue opacity, and the fluid in the bile and pancreatic ducts serves as its contrast agent.

The fluid-filled structures in the abdomen appear hyperintense against the surrounding soft tissues because they have a longer T2 relaxation time. When using hepatospecific contrast agents, MRCP should be performed before the contrast agent enters the bile ducts because gadolinium shortens T2, resulting in poor visualization of

the biliary system. Thus, MRCP is performed before or no later than 5 min after contrast agent injection (DWIs, e.g., can be taken even ≥ 5 min after contrast agent injection, to save time). Furthermore, multiplanar reconstruction and maximum intensity projection of the obtained images can be performed for optimal visualization.

T1-WIs are taken with SE sequences (turbo SE [TSE] or fast SE [FSE]), although SGE is usually preferred because of its much shorter acquisition time.

For a more accurate assessment of hepatic steatosis or signs of hemochromatosis, in-phase and opposed-phase T1-WIs should also be included in the standard MRI protocol. Furthermore, this sequence is useful in the diagnosis of adrenal adenoma (Fig. 6), clear-cell renal cell carcinoma, and pancreatic fatty infiltration (Fig. 7). These sequences must

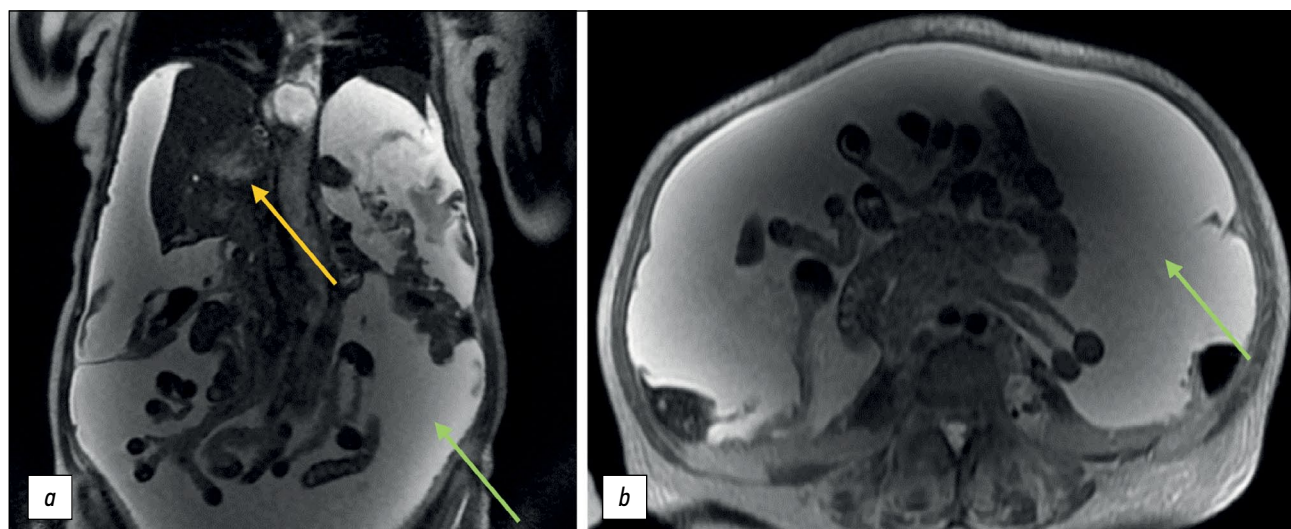


Figure 5. Single-shot fast spin-echo mode: hepatocellular carcinoma with inferior vena cava invasion (yellow arrow) and tense ascites (green arrow): *a* coronal plane; *b* axial plane.

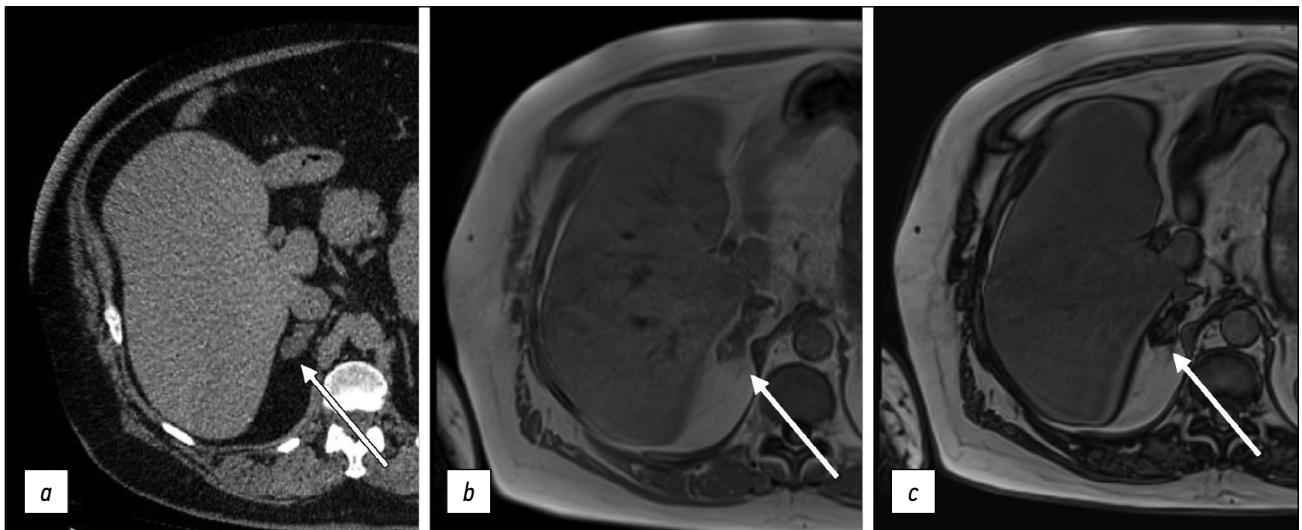


Figure 6. Abdominal computed tomography, axial plane (a): a right adrenal mass of nonuniform density is visualized (arrow); abdominal magnetic resonance imaging (b, c), in-phase (b) and opposed-phase (c): a typical signal loss from the adenoma fat component in the opposed-phase is detected (arrows).

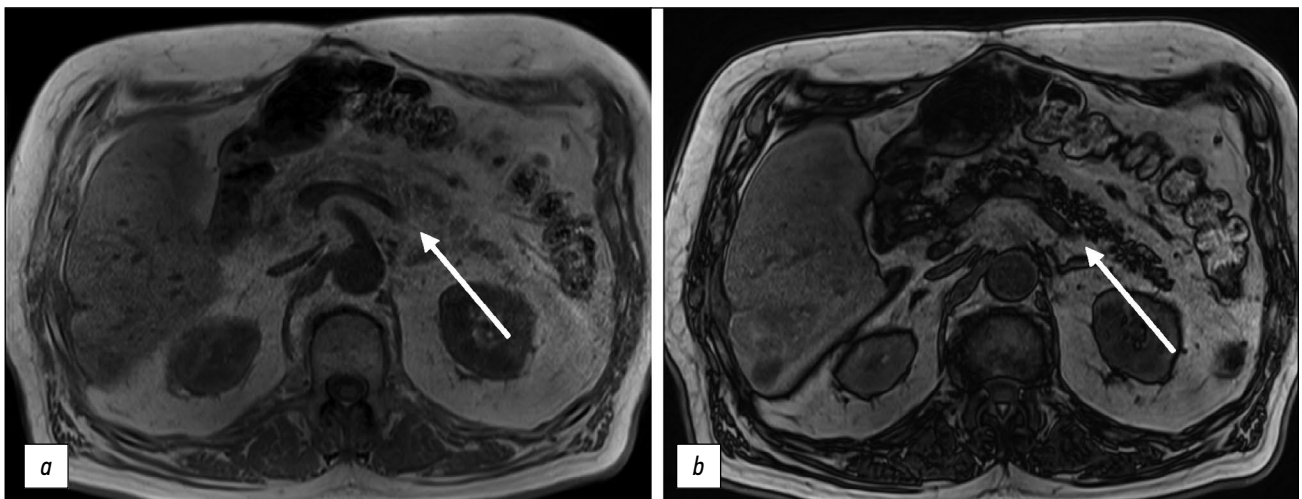


Figure 7. Abdominal magnetic resonance imaging, pancreatic lipomatosis (arrows): a in-phase, b opposed-phase. In the opposite phase, a signal loss from the pancreas with a normal signal from the liver is detected.

be obtained before contrast agent injection. Out-of-phase images allow for the assessment of signal loss from adipose tissue and fat-containing lesions such as liver adenomas or hepatocellular carcinoma. Moreover, the determination of the proton density fat fraction is the gold standard for noninvasive quantitative assessment of hepatic steatosis. However, this sequence is not included in the routine protocol.

Dynamic pre- and postcontrast T1-WIs can be obtained using 2D or 3D pulse sequences [6], with 3D sequences preferred because minimizing slice thickness reduces truncation artifacts. 3D SGE sequences were initially used to visualize vascular anatomy (MR angiography; Fig. 8). This technique is currently widely used to visualize soft tissue structures in the abdominal cavity and small pelvis. Short repetition time and TE values allow for the acquisition of many thin sections in a single breath-hold. The relatively low SNR of this sequence may be a limitation; however, this disadvantage is offset by the use of intravenous contrast.

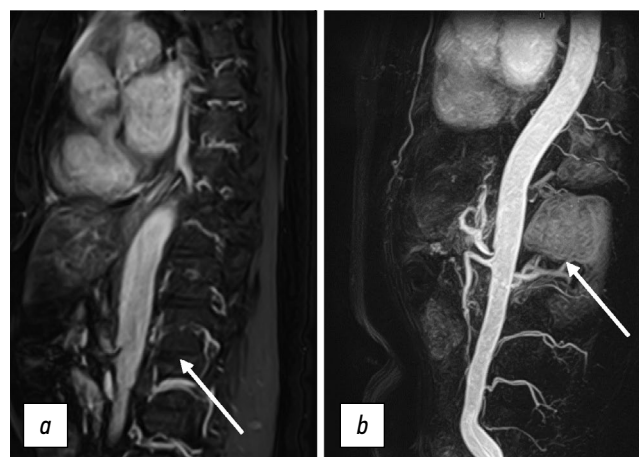


Figure 8. Contrast-enhanced magnetic resonance imaging of the abdominal aorta and its branches. Extravascular compression of the celiac trunk by crus diaphragm (arrows): a SSFE; b contrast-enhanced 3D mode.

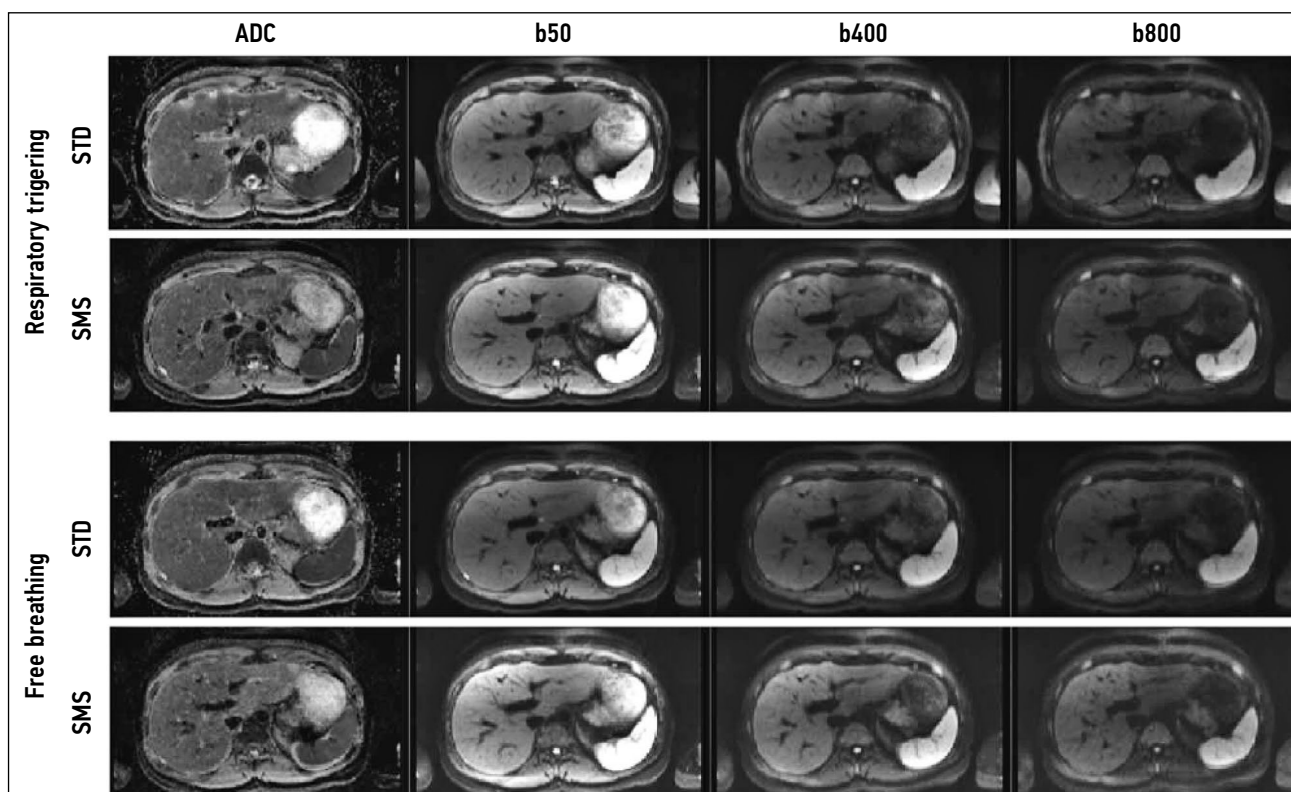


Figure 9. Comparison of standard (STD DWI) and simultaneous (SMS DWI) multislice diffusion-weighted images with free breathing and respiratory triggering using various b-factors (50, 400, and 800 s/mm²) and corresponding apparent diffusion coefficients. The mean scan time was 10:30 min (5:56–18:13) for STD DWIs and 3:29 min (2:19–4:27) for SMS-DWIs [16].

In patients unable to cooperate, SGE can be performed without breath-holding; such sequences include magnetization prepared rapid acquisition gradient and turbo fast low angle shot. The relatively low T1-weighted tissue contrast (compared with standard SGEs) is a limitation of this approach. In addition, this technique cannot be used for dynamic liver contrast, particularly in the early arterial phase: it takes approximately 1.5 s to obtain one slice; thus, the time difference between scanning the upper and lower sections of the liver does not allow capturing all sections within a single (arterial) phase. By contrast, despite being motion sensitive, standard SGE sequences have a high temporal resolution to visualize the desired tissue volume.

DWIs are widely used in abdominal radiology. The most common are single-shot echoplanar sequences with or without breath-holding. Parallel data acquisition is used to reduce scan time and more accurately calculate the apparent diffusion coefficient, and modern techniques allow for taking DWIs with high spatial resolution in <1 min (simultaneous multislice imaging DWI) [16] (Fig. 9).

CONCLUSION

MRI is one of the main methods for diagnosing abdominal organ and retroperitoneal space diseases, and it allows for the visualization of focal or diffuse lesions

in parenchymal and hollow organs with high diagnostic accuracy and reproducibility. The multiparametric MRI protocol provides information not only on the mutual topography and structure of organs but also on tissue function, allowing for the transition from structural to functional image evaluation.

In most cases, the standard abdominal MRI protocol includes T1-WIs, T2-WIs, DWIs, and MRCP, although this protocol can be shortened or supplemented depending on the study goals and patient condition.

Many pulse sequences are now available, and current technological advances are simplifying the scanning process and shortening the time to image acquisition while increasing the reproducibility of techniques in various healthcare settings, even among novice users.

ADDITIONAL INFORMATION

Funding source. This article was not supported by any external sources of funding.

Competing interests. The authors declare that they have no competing interests.

Authors' contribution. All authors made a substantial contribution to the conception of the work, acquisition, analysis, interpretation of data for the work, drafting and revising the work, final approval of the version to be published and agree to be accountable for all aspects of the work.

REFERENCES

- Hussain SM, Sorrell MF. Liver MRI: Correlation with other imaging modalities and histopathology, second edition. Springer; 2015. doi: 10.1007/978-3-319-06004-0
- Runge VM, Clanton JA, Partain CL, James AE. Respiratory gating in magnetic resonance imaging at 0.5 Tesla. *Radiology*. 1984;151(2):521–523. doi: 10.1148/radiology.151.2.6709928
- Bailes DR, Gilderdale DJ, Bydder GM, et al. Respiratory ordered phase encoding (ROPE): A method for reducing respiratory motion artefacts in MR imaging. *J Comput Assist Tomogr*. 1985;9(4):835–838.
- American College of Radiology [online]. ACR-SAR-SPR practice parameter for the performance of magnetic resonance (MR) Enterography. Available from: <https://www.acr.org/-/media/ACR/Files/Practice-Parameters/MR-Enterog.pdf>. Accessed: 17.01.2023.
- Semelka RC, Kelekis NL, Thomasson D, et al. HASTE MR imaging: Description of technique and preliminary results in the abdomen. *J Mag Reson Imaging*. 1996;6(4):698–699. doi: 10.1002/jmri.1880060420
- Rofsky NM, Lee VS, Laub G, et al. Abdominal MR imaging with a volumetric interpolated breath-hold examination. *Radiology*. 1999;212(3):876–884. doi: 10.1148/radiology.212.3.r99se34876
- Syrkashev EM, Solopova A, Kulabukhova EA. Magnetic resonance imaging in the diagnosis of peritoneal carcinomatosis indissemated ovarian cancer. *Obstetrics Gynecology*. 2020;(9):38–47. doi: 10.18565/aig.2020.9.38-47
- Vanderveen KA, Hussain HK. Magnetic resonance imaging of cholangiocarcinoma. *Cancer Imaging*. 2004;4(2):104–115. doi: 10.1102/1470-7330.2004.0018
- Kilcoyne A, Kaplan JL, Gee MS. Inflammatory bowel disease imaging: Current practice and future directions. *World J Gastroenterol*. 2016;22(3):917–932. doi: 10.3748/wjg.v22.i3.917
- Koh DM, Collins DJ. Diffusion-weighted MRI in the body: Applications and challenges in oncology. *AJR Am J Roentgenol*. 2007;188(6):1622–1635. doi: 10.2214/AJR.06.1403
- Abuladze LR, Semenov DS, Panina OY, Vasilev YA. Optimized biparametric magnetic resonance imaging protocol for prostate cancer detection. *Digit Diagnostics*. 2022;3(3):166–177. doi: 10.17816/dd108484
- Thoeny HC, De Keyzer F. Extracranial applications of diffusion-weighted magnetic resonance imaging. *Eur Radiol*. 2007;17(6):1385–1393. doi: 10.1007/s00330-006-0547-0
- Charles-Edwards EM, De Souza NM. Diffusion-weighted magnetic resonance imaging and its application to cancer. *Cancer Imaging*. 2006;6(1):135–143. doi: 10.1102/1470-7330.2006.0021
- Kele PG, van der Jagt EJ. Diffusion weighted imaging in the liver. *World J Gastroenterol*. 2010;16(13):1567–1576. doi: 10.3748/wjg.v16.i13.1567
- Monticciolo L, Podberesky DJ, Pollack MS, et al. ACR-SAR-SPR practice parameter for the performance of magnetic resonance imaging (MRI) of the abdomen (Excluding the Liver). Semantic Scholar; 2015. Available from: [https://www.semanticscholar.org/paper/ACR-%E2%80%93SAR-%E2%80%93SPR-PRACTICE-PARAMETER-FOR-THE-OF-\(-MRI-Monticciolo-Podberesky/7dc9771a1b5aaec215c99fd74ab5e659738cf4fd](https://www.semanticscholar.org/paper/ACR-%E2%80%93SAR-%E2%80%93SPR-PRACTICE-PARAMETER-FOR-THE-OF-(-MRI-Monticciolo-Podberesky/7dc9771a1b5aaec215c99fd74ab5e659738cf4fd). Accessed: 17.01.2023.
- Taron J, Martirosian P, Erb M, et al. Simultaneous multislice diffusion-weighted MRI of the liver: Analysis of different breathing schemes in comparison to standard sequences. *J Magn Reson Imaging*. 2016;44(4):865–879. doi: 10.1002/jmri.25204

СПИСОК ЛИТЕРАТУРЫ

- Hussain S.M., Sorrell M.F. Liver MRI: Correlation with other imaging modalities and histopathology, second edition. Springer, 2015. doi: 10.1007/978-3-319-06004-0
- Runge V.M., Clanton J.A., Partain C.L., James A.E. Respiratory gating in magnetic resonance imaging at 0.5 Tesla // *Radiology*. 1984. Vol. 151, N 2. P. 521–523. doi: 10.1148/radiology.151.2.6709928
- Bailes D.R., Gilderdale D.J., Bydder G.M., et al. Respiratory ordered phase encoding (ROPE): A method for reducing respiratory motion artefacts in MR imaging // *J Comput Assist Tomogr*. 1985. Vol. 9, N 4. P. 835–838.
- American College of Radiology [интернет-ресурс]. ACR-SAR-SPR practice parameter for the performance of magnetic resonance (MR) Enterography. Режим доступа: <https://www.acr.org/-/media/ACR/Files/Practice-Parameters/MR-Enterog.pdf>. Дата обращения: 17.01.2023.
- Semelka R.C., Kelekis N.L., Thomasson D., et al. HASTE MR imaging: Description of technique and preliminary results in the abdomen // *J Mag Reson Imaging*. 1996. Vol. 6, N 4. P. 698–699. doi: 10.1002/jmri.1880060420
- Rofsky N.M., Lee V.S., Laub G., et al. Abdominal MR imaging with a volumetric interpolated breath-hold examination // *Radiology*. 1999. Vol. 212, N 3. P. 876–884. doi: 10.1148/radiology.212.3.r99se34876
- Syrkashev E.M., Solopova A.E., Kulabukhova E.A. Magnetic resonance imaging in the diagnosis of peritoneal carcinomatosis indissemated ovarian cancer // *Obstetrics Gynecology*. 2020. N 9. P. 38–47. doi: 10.18565/aig.2020.9.38-47
- Vanderveen K.A., Hussain H.K. Magnetic resonance imaging of cholangiocarcinoma // *Cancer Imaging*. 2004. Vol. 4, N 2. P. 104–115. doi: 10.1102/1470-7330.2004.0018
- Kilcoyne A., Kaplan J.L., Gee M.S. Inflammatory bowel disease imaging: Current practice and future directions // *World J Gastroenterol*. 2016. Vol. 22, N 3. P. 917–932. doi: 10.3748/wjg.v22.i3.917
- Koh D.M., Collins D.J. Diffusion-weighted MRI in the body: Applications and challenges in oncology // *AJR Am J Roentgenol*. 2007. Vol. 188, N 6. P. 1622–1635. doi: 10.2214/AJR.06.1403
- Abuladze L.R., Semenov D.S., Panina O.Y., Vasilev Y.A. Optimized biparametric magnetic resonance imaging protocol for prostate cancer detection // *Digit Diagnostics*. 2022. Vol. 3, N 3. P. 166–177. doi: 10.17816/dd108484
- Thoeny H.C., De Keyzer F. Extracranial applications of diffusion-weighted magnetic resonance imaging // *Eur Radiol*. 2007. Vol. 17, N 6. P. 1385–1393. doi: 10.1007/s00330-006-0547-0
- Charles-Edwards E.M., De Souza N.M. Diffusion-weighted magnetic resonance imaging and its application to cancer // *Cancer Imaging*. 2006. Vol. 6, N 1. P. 135–143. doi: 10.1102/1470-7330.2006.0021
- Kele P.G., van der Jagt E.J. Diffusion weighted imaging in the liver // *World J Gastroenterol*. 2010. Vol. 16, N 13. P. 1567–1576. doi: 10.3748/wjg.v16.i13.1567

15. Monticciolo L., Podberesky D.J., Pollack M.S., et al. ACR-SAR-SPR practice parameter for the performance of magnetic resonance imaging (MRI) of the abdomen (Excluding the Liver). Semantic Scholar; 2015. Режим доступа: [https://www.semanticscholar.org/paper/ACR-%E2%80%93-SAR-%E2%80%93-SPR-PRACTICE-PARAMETER-FOR-THE-OF-\(-MRI-Monticciolo-Podberesky/7dc](https://www.semanticscholar.org/paper/ACR-%E2%80%93-SAR-%E2%80%93-SPR-PRACTICE-PARAMETER-FOR-THE-OF-(-MRI-Monticciolo-Podberesky/7dc)

9771a1b5aaec215c99fd74ab5e659738cf4fd. Дата обращения: 17.01.2023.

16. Taron J., Martirosian P., Erb M., et al. Simultaneous multislice diffusion-weighted MRI of the liver: Analysis of different breathing schemes in comparison to standard sequences // J Magn Reson Imaging. 2016. Vol. 44, N 4. P. 865–879. doi: 10.1002/jmri.25204

AUTHORS' INFO

* **Egor M. Syrkashev**, MD, Cand Sci (Med.);
address: 24/1 Petrovka street, 127051 Moscow, Russia;
ORCID: <https://orcid.org/0000-0003-4043-907X>;
eLibrary SPIN: 1901-5364; e-mail: egorsrkshv@mail.ru

Faina Z. Kadyrberdieva, MD, Cand Sci (Med.);
ORCID: <https://orcid.org/0009-0004-7787-3413>;
e-mail: k.faina1992@mail.ru

Liya R. Abuladze, MD;
ORCID: <https://orcid.org/0000-0001-6745-1672>;
eLibrary SPIN: 8640-9989; e-mail: AbuladzeLR@zdrav.mos.ru

Dmitriy S. Semenov;
ORCID: <https://orcid.org/0000-0002-4293-2514>;
eLibrary SPIN: 2278-7290; e-mail: semenovds4@zdrav.mos.ru

Ekaterina G. Privalova, MD, Dr.Sci. (Med.);
ORCID: <https://orcid.org/0000-0002-9851-9390>;
eLibrary SPIN: 6546-5135; e-mail: e-privalova@mail.ru

ОБ АВТОРАХ

* **Сыркашев Егор Михайлович**, к.м.н.;
адрес: Россия, 127051, Москва, ул. Петровка, д. 24, стр. 1;
ORCID: <https://orcid.org/0000-0003-4043-907X>;
eLibrary SPIN: 1901-5364; e-mail: egorsrkshv@mail.ru

Кадырбердиева Фаина Залимхановна, к.м.н.;
ORCID: <https://orcid.org/0009-0004-7787-3413>;
e-mail: k.faina1992@mail.ru

Абуладзе Лия Руслановна;
ORCID: <https://orcid.org/0000-0001-6745-1672>;
eLibrary SPIN: 8640-9989; e-mail: AbuladzeLR@zdrav.mos.ru

Семенов Дмитрий Сергеевич;
ORCID: <https://orcid.org/0000-0002-4293-2514>;
eLibrary SPIN: 2278-7290; e-mail: semenovds4@zdrav.mos.ru

Привалова Екатерина Геннадьевна, д.м.н.;
ORCID: <https://orcid.org/0000-0002-9851-9390>;
eLibrary SPIN: 6546-5135; e-mail: e-privalova@mail.ru

* Corresponding author / Автор, ответственный за переписку

DOI: <https://doi.org/10.17816/DD112093>

Диагностика патологии и аномалии сосково-ареолярного комплекса: серия клинических случаев

Е.Н. Каранадзе¹, В.Е. Синицын², М.А. Каранадзе³

¹ Клинико-диагностический центр МЕДСИ на Красной Пресне, Москва, Российская Федерация

² Московский государственный университет имени М.В. Ломоносова, Медицинский научно-образовательный центр, Москва, Российская Федерация

³ Российский национальный исследовательский медицинский университет имени Н.И. Пирогова, Москва, Российская Федерация

АННОТАЦИЯ

Сосково-ареолярный комплекс — особая анатомическая и гистологическая структура. Вариабельность нормального строения, широкий спектр патологических процессов и сложность диагностической визуализации вызывают трудности у врачей лучевой диагностики и клиницистов.

Наиболее часто в диагностике патологии сосково-ареолярного комплекса используют ультразвуковую диагностику и маммографию. При неоднозначных результатах предшествующих методов и для оценки распространённости процесса применяют магнитно-резонансную томографию с внутривенным контрастированием.

Магнитно-резонансная томография молочной железы — наиболее чувствительный метод выявления особенностей строения, диагностики доброкачественных и злокачественных заболеваний, затрагивающих сосково-ареолярный комплекс. Магнитно-резонансная томография полезна в качестве дополнительного диагностического инструмента при неоднозначных результатах маммографии и ультразвукового исследования. Магнитно-резонансная томография позволяет визуализировать ретроареолярную зону, подходит для диагностики папиллом, аденом, болезни Педжета, протоковой карциномы *in situ* и инвазивного рака.

В статье дано описание клинических случаев диагностики патологии и аномалий сосково-ареолярного комплекса, что может быть полезно для врачей лучевой диагностики, гинекологов, клинических ординаторов.

Ключевые слова: клинический случай; рак молочной железы; сосково-ареолярный комплекс; маммография.

Как цитировать

Каранадзе Е.Н., Синицын В.Е., Каранадзе М.А. Диагностика патологии и аномалии сосково-ареолярного комплекса: серия клинических случаев // *Digital Diagnostics*. 2023. Т. 4, № 1. С. 51–60. DOI: <https://doi.org/10.17816/DD112093>

DOI: <https://doi.org/10.17816/DD112093>

Diseases and abnormalities of the nipple-areolar complex: a case report series

Elena N. Karanadze¹, Valentin E. Sinitsyn², Mariia A. Karanadze³

¹ Clinical Diagnostic Center MEDSI on Krasnaya Presnya, Moscow, Russian Federation

² Lomonosov Moscow State University, Medical Scientific and Educational Center, Moscow, Russian Federation

³ The Russian National Research Medical University named after N.I. Pirogov, Moscow, Russian Federation

ABSTRACT

The nipple-areolar complex is a specific anatomical and histological structure. Normal structure and pathological process variabilities and the complexity of diagnostic imaging cause difficulties for radiologists and physicians. Breast magnetic resonance imaging is highly sensitive for structural features and nipple-areolar complex cancer detection. Magnetic resonance imaging is a useful diagnostic tool when mammography and ultrasound findings are inconclusive. It allows visualization of the retroareolar region, suitable for the diagnosis of papillomas, adenomas, Paget's disease, ductal carcinoma in situ, and invasive ductal carcinoma.

This is a case report on identifying the pathology and anomalies of the nipple-areolar complex, which may benefit radiologists, gynecologists, and residents.

Keywords: case report, breast disease, nipple-areolar complex, mammography.

To cite this article

Karanadze EN, Sinitsyn VE, Karanadze MA. Diseases and abnormalities of the nipple-areolar complex: a case report series. *Digital Diagnostics*. 2023;4(1):51–60.

DOI: <https://doi.org/10.17816/DD112093>

Received: 26.10.2022

Accepted: 24.03.2023

Published: 03.04.2023

DOI: <https://doi.org/10.17816/DD112093>

乳头乳晕复合体的病理和异常的诊断： 一系列临床病例

Elena N. Karanadze¹, Valentin E. Sinitsyn², Mariia A. Karanadze³

¹ Clinical Diagnostic Center MEDSI on Krasnaya Presnya, Moscow, Russian Federation

² Lomonosov Moscow State University, Medical Scientific and Educational Center, Moscow, Russian Federation

³ The Russian National Research Medical University named after N.I. Pirogov, Moscow, Russian Federation

简评

乳头乳晕复合体是一种特殊的解剖学和组织学结构。正常结构的变异性、病理过程的广泛性和诊断成像的复杂性给放射科医生和临床医生带来困难。乳房磁共振成像是检测结构特征、诊断涉及乳头乳晕复合体的良性和恶性疾病的最灵敏方法。在乳腺钼靶和超声检查结果不明确的情况下，磁共振成像作为一种额外的诊断工具非常有用。磁共振成像允许看到乳腺后区，适合诊断乳头瘤、腺瘤、佩吉特氏病、导管原位癌和浸润性癌。

我们在这篇文章中描述了乳头乳晕复合体的病理和异常的临床病例，这可能会对放射科医生、妇科医生和临床住院医师有用。

关键词： 临床病例，乳腺癌，乳头乳晕复合体，乳腺钼靶。

To cite this article

Karanadze EN, Sinitsyn VE, Karanadze MA. 乳头乳晕复合体的病理和异常的诊断：一系列临床病例. *Digital Diagnostics*. 2023;4(1):51–60. DOI: <https://doi.org/10.17816/DD112093>

收到: 26.10.2022

接受: 24.03.2023

发布日期: 03.04.2023

BACKGROUND

The nipple–areolar complex (NAC) is a unique breast area. NAC consists of various cells and specific tissues that are responsible for the outflow and secretion of breast milk during lactation. [1] NAC is susceptible to a wide range of conditions including developmental anomalies, benign processes (inflammation, infection, and benign tumors), and invasive and non-invasive cancers. [2]

The evaluation of the NAC is a challenging task for clinicians and radiologists. In this area, pathological processes often have nonspecific clinical and radiological signs, which make establishing a correct diagnosis difficult and time consuming.

The differential diagnosis of NAC conditions requires the review of a patient's medical history and visual assessment of the skin, abnormal nipple discharge, nipple retraction, inversion, palpable formations, etc.

Imaging is an important component of diagnosing NAC conditions. Standard mammography and ultrasonography have some limitations. Images are especially difficult to interpret because of mobility, superficial location, and varying density of breast structures. The retroareolar region is difficult to assess on mammograms; thus, in this area, abnormalities often remain unnoticed. This is why magnetic resonance imaging (MRI) is increasingly important for the diagnosis of NAC conditions.

While planning the surgical treatment, it is important to detect whether the NAC is involved in the tumor process. When breast cancer involves the NAC, the tumor is classified as T4, which determines the disease stage (prognosis) and makes it impossible to save the nipple during mastectomy. On the contrary, precise determination of tumor borders with uninvolved NAC provides new opportunities for organ-preserving breast surgeries. [3]

Contrast-enhanced MRI is the most sensitive method of diagnosing breast cancer. [4] Breast MRI is performed for confirming the results of mammography and ultrasonography, breast cancer staging, evaluating the effectiveness of neoadjuvant chemotherapy, and determining the more precise localization of the lesion during biopsy. [5] MRI may be used in patients with abnormal nipple discharge as an additional diagnostic tool when standard mammography and ultrasonography are inconclusive. [6]

CASE REPORTS

Case Report 1

A 59-year-old patient complained of erosive changes in the nipple (Fig. 1). Physical examination revealed erythema, erosion, and nipple retraction. Doppler ultrasonography with color flow mapping revealed increased blood flow in the nipple projection (Fig. 2). Mammography findings were normal. To assess the extent of disease spread, breast MRI with contrast enhancement was performed. The



Figure 1. Erosive nipple changes in Paget's disease.

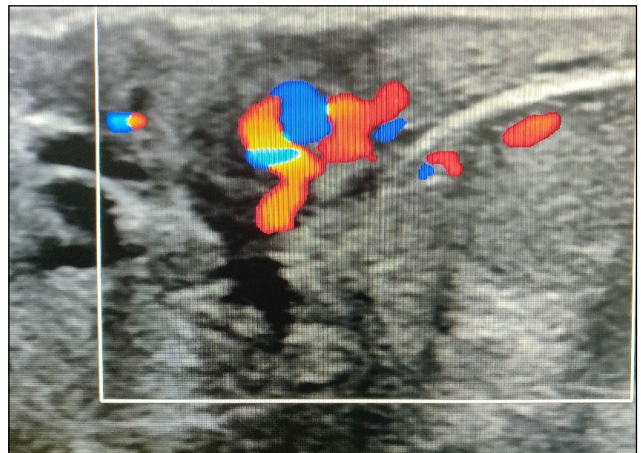


Figure 2. Paget's disease: increased blood flow on color Doppler imaging.

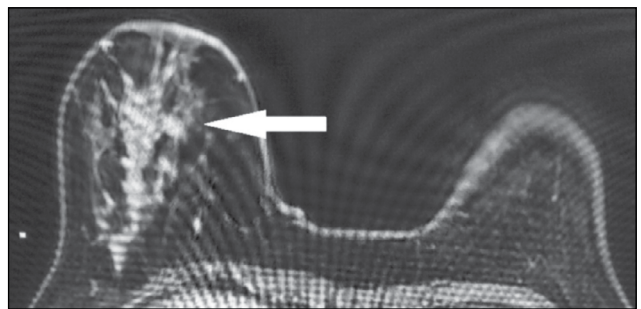


Figure 3. Magnetic resonance imaging of Paget's disease (early enhancement phase): the retroareolar area of segmental enhancement from the nipple level to the posterior breast (arrow).

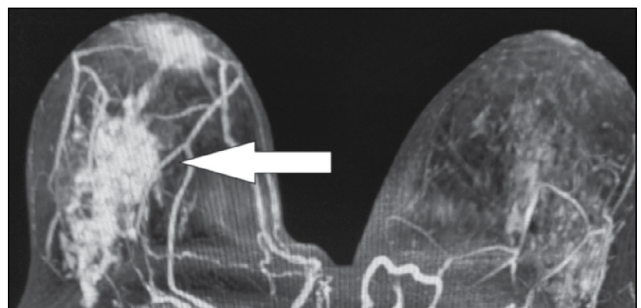


Figure 4. Magnetic resonance imaging of Paget's disease (maximum intensity projection): the retroareolar area of segmental enhancement from the nipple level to the posterior breast (arrow).

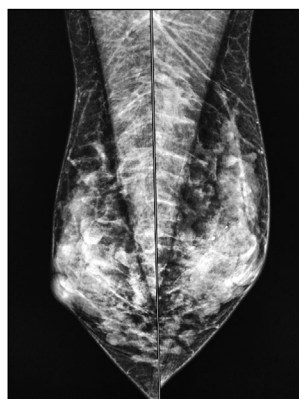


Figure 5. A nipple adenoma: mammography (mediolateral oblique projection).

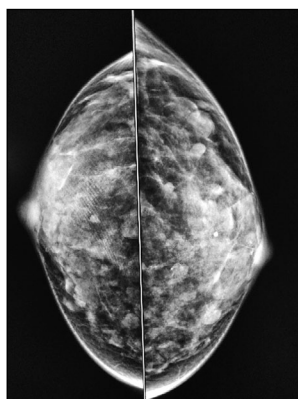


Figure 6. A nipple adenoma: mammography (craniocaudal oblique projection).

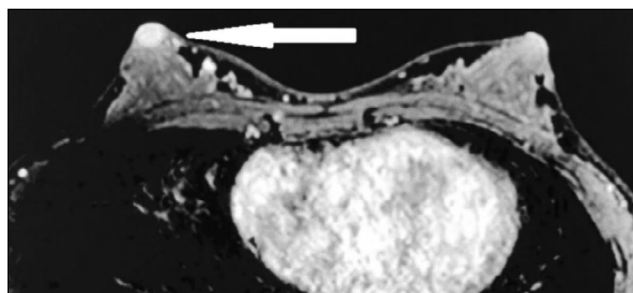


Figure 7. Magnetic resonance imaging of a nipple adenoma (early postcontrast series): a right nipple mass homogeneously accumulating a contrast agent (arrow).

early postcontrast series (Fig. 3) and maximum intensity projection (MIP) images (Fig. 4) showed a segmental contrast retroareolar area from the nipple level to posterior breast sections. Ultrasound-guided core biopsy followed by immunohistochemical analysis revealed Paget's disease of the nipple with high-grade intraductal carcinoma in situ. Receptors for estrogen (G3 ER) and progesterone (PR) were negative. Oncogenic protein Ki-67 was 45%.

Case Report 2

A 38-year-old patient complained of 1-month itching of the right nipple and skin discoloration. Breast ultrasonography and mammography findings (Figs. 5 and 6) were normal. The

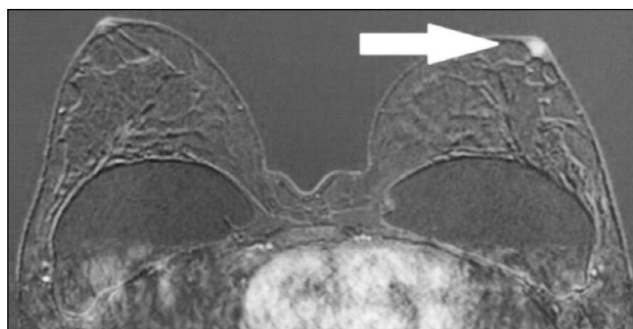


Figure 9. Magnetic resonance imaging (early postcontrast series): asymmetric contrast accumulation in the left nipple; normal finding (arrow).

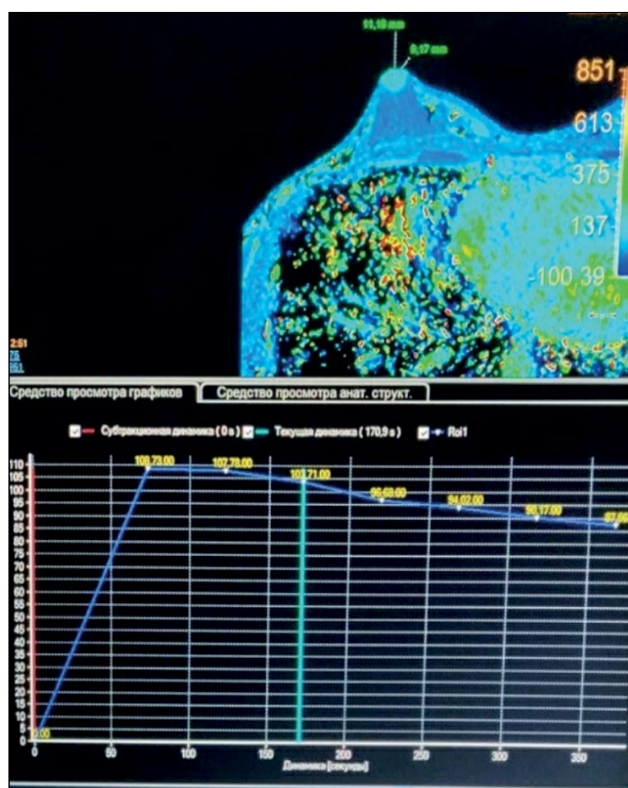


Figure 8. Magnetic resonance imaging of a nipple adenoma (parametric map): a right nipple mass with rapid contrast enhancement and subsequent elimination, type III graphic curve.

breast was examined by contrast-enhanced MRI. The early postcontrast series revealed a right nipple mass homogeneously accumulating a contrast agent (Fig. 7). A parametric map showed a nipple mass with rapid contrast enhancement and subsequent elimination, a type III graphic curve (Fig. 8). Morphological verification revealed nipple adenoma.

Case Report 3

In a 43-year-old patient who had no complaints, the breast was examined by MRI to assess the integrity of implants. The asymmetric enhancement of the left nipple was accidentally found (Figs. 9 and 10). Three-year dynamic observation did not reveal any unfavorable changes.

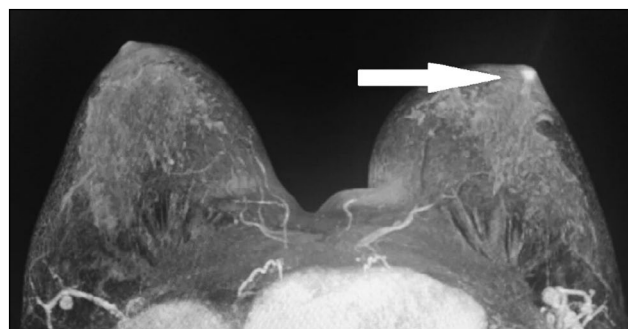


Figure 10. Magnetic resonance imaging (MIP): asymmetric contrast accumulation in the left nipple; normal finding (arrow).

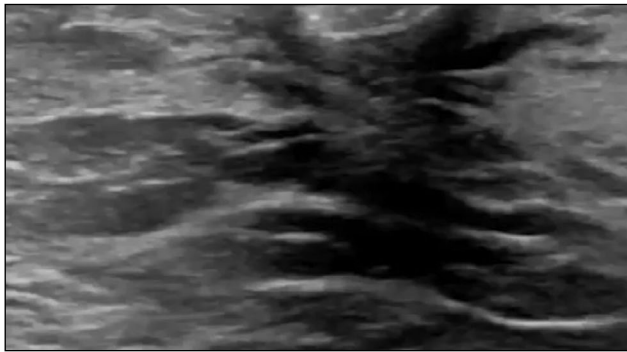


Figure 11. Ultrasound image of the left breast with the inverted nipple.

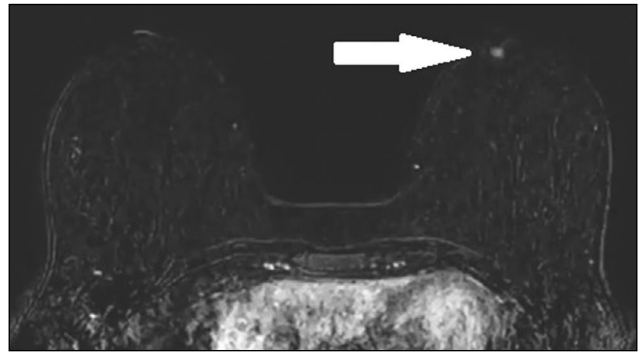


Figure 12. Magnetic resonance imaging (subtraction): a retroareolar mass with accumulation of contrast agent (inverted nipple, arrow).

Case Report 4

In a 38-year-old patient who had no complaints, a routine medical examination showed a left nipple inversion. Ultrasonography of the left breast revealed no abnormalities (Fig. 11). MRI with intravenous contrast (Fig. 12) showed asymmetric contrast accumulation with a retroareolar mass accumulating the contrast agent (inverted nipple). No focal breast pathology was detected.

DISCUSSION

The NAC is a pigmented area in the most protruding part of the breast, the site where milk ducts converge, draining 15–20 breast lobes. [7] Given its complex anatomy, [8] superficial location, and mobility, this area requires special attention during clinical examination and imaging.

In clinical practice, ultrasonography and mammography are the most used methods for NAC pathology detection. If imaging modalities revealed conflicting findings, MRI with intravenous contrast enhancement is used to assess the extent of disease spread.

Ultrasonography has some advantages as a method of NAC examination. In addition to being widely available and not requiring ionizing radiation, ultrasonography provides a good spatial resolution of this superficial region, making it possible to characterize small lesions in the retroareolar region. [9]

Mammography is the most sensitive technique for detecting calcifications. In the NAC, calcifications are uncommon and usually benign, such as cutaneous, calcified intraductal detritus, and calcifications due to fat necrosis. Microcalcifications can be seen in relation to intraductal carcinoma, sometimes associated with Paget's disease. [10] Mammography is less sensitive than ultrasonography because of the greater density and mobility of this part of the breast. [11]

For mammography, the breast must be positioned correctly. [10] The nipple must be located tangentially at least in one projection, ideally in both craniocaudal and mediolateral projections. In patients with inverted nipples (normal variation), nipples should be tangential and symmetrical.

Dynamic contrast-enhanced MRI is the most sensitive method for diagnosing breast diseases. In breast cancer, MRI provides valuable information on the extent of disease spread and can be used to plan the treatment and establish a prognosis. [12] When evaluating a NAC tumor, MRI has high sensitivity (90%–100%), moderate specificity (80%–90%), and high negative predictive value (98%) [3]; thus, it can be used for establishing a diagnosis if mammography and ultrasonography results are conflicting and the clinical presentation is nonspecific. [13] The advantages of MRI include providing high-resolution images and possibility for dynamic contrast enhancement. If contrast accumulation is early, intense, asymmetric, and heterogeneous with subsequent contrast elimination, it may be indicative of a malignant neoplasm. [14] MRI is required for preoperative planning to determine the extent of nipple-sparing mastectomy in breast cancer treatment. [15–17] Finally, MRI can be used as a supplementary method to mammography and ultrasonography in the diagnosis of abnormal nipple discharge and percutaneous biopsy. [18]

We describe a clinical case of diagnosis of Paget's disease with a false-negative mammography result. MRI with intravenous contrast enhancement allowed us to determine the real extent of the disease spread. Paget's disease accounts for 1%–3% of all breast carcinomas. It is characterized by the presence of neoplastic cells in the nipple epidermis [19] and clinically manifested as erythema, erosion, and ulceration of the nipple, sometimes combined with a palpable retroareolar mass and/or nipple retraction or discharge. Differential diagnosis includes atopic or contact dermatitis, malignant melanoma, Merkel cell carcinoma, mycosis fungoides, nipple adenoma, and ductal exocrine carcinoma. As in our case, to establish the final diagnosis, skin biopsy and immunohistochemistry are required.

Imaging techniques are of critical importance because in 90% of cases, Paget's disease is associated with ductal carcinoma in situ or invasive cancer. [13, 20] In primary mammography, images with enlarged NAC and anterior breast third are important. Skin thickening, retroareolar masses, or pleomorphic microcalcifications may be detected. Ultrasonography showed no characteristic signs. It may help

identify dilated subareolar ducts, calcifications, and nipple changes.

In 22%–71% of cases, mammography provides a false-negative result [21], and in this case, breast MRI is indicated to identify abnormalities and deter the extent of disease spread. [20] Characteristic MRI findings include asymmetry, thickening, flattening, retraction of the NAC, and uneven contrast accumulation in this area. MRI allows evaluating adjacent structures and axillary lymph nodes.

Case 2 demonstrates the complexity of the diagnostic search in a nipple adenoma. Ultrasonography and mammography revealed no abnormalities, and the correct diagnosis was established only by MRI followed by biopsy. A nipple adenoma (erosive adenomatosis or subareolar papillomatosis) is a rare variant of intraductal papilloma. Clinical manifestations include a small palpable nodule under the skin of the nipple, which is usually associated with inflammatory nipple changes (pain, redness, and swelling). Skin involvement results from the growth of glandular epithelium toward the skin surface. Skin manifestations are similar to Paget's disease, squamous cell carcinoma, eczema, psoriasis, or infection. Histological verification is the gold standard for definitive diagnosis. Mammography and ultrasonography usually do not provide valuable information. Ultrasonography may show a hypoechoic nodule in the nipple or subareolar region. [22]

Cases 3 and 4 prove that asymmetric contrast accumulation in MRI is not necessarily a sign of pathology. Normally, in MRI, both nipples accumulate the contrast agent at the same rate and intensity. However, nipple asymmetry may be the normal variation. Possible reasons include special NAC anatomy, breast size, breast compression and friction with clothing, blood flow variations, and local inflammation. [12] Some physiological features and differences are involved in contrast accumulation in NAC structures. Both breasts usually show symmetrical thin rings of enhancement. In some cases, enhancement is asymmetrical in the early phase and becomes symmetrical in later phases. In a study of 530 normal nipples in 265 asymptomatic women, Gao et al. used T1-weighted NAC images to describe three areas of enhancement. [12]

Nipple inversion is a benign condition associated with the insufficient ability of the mesenchymal tissue to fix the nipple in the right position. [12] It occurs in 4% of women and men. Nipples are convex in 75% of women, flat in 23%,

and inverted in 2%. MIP images are well suited for assessing the morphology and symmetry of the NAC. On postcontrast images, the nipple should be hypo- or isointense compared with the enhanced parenchymal tissue in the background. [12]

Nipple inversion, retraction, and asymmetry are normal but may also be indicative of pathology. In differential diagnosis, obtaining a detailed medical history, comparing with results of previous examinations, and providing ongoing monitoring are recommended.

CONCLUSION

The complex anatomy of the NAC requires a special multimodal approach to diagnosing pathologies in this area. In many cases, such conditions have nonspecific clinical and radiological manifestations, which can complicate the diagnostic process. Imaging techniques play an important role in this process. Clinicians and radiologists must be aware of the advantages and disadvantages of each technique and interpret the results of various modalities. To make a precise diagnosis, clinical, radiological, and histological data must be comprehensively evaluated. Our case reports show examples of asymmetric NAC changes in normal and pathological conditions.

ADDITIONAL INFORMATION

Funding source. This article was not supported by any external sources of funding.

Competing interests. The authors declare that they have no competing interests.

Authors' contribution. All authors made a substantial contribution to the conception of the work, acquisition, analysis, interpretation of data for the work, drafting and revising the work, final approval of the version to be published and agree to be accountable for all aspects of the work. V.E. Sinitsyn — concept and design of the work, editing and approval the final version of the manuscript; E.N. Karanadze — concept and design of the work, data analysis, writing the text of the article, editing and approval the final version of the manuscript; M.A. Karanadze — writing the text of the article, editing.

Consent for publication. Written consent was obtained from the patients for publication of relevant medical information and all of accompanying images within the manuscript in Digital Diagnostics journal.

REFERENCES

1. Stone K, Wheeler A. A Review of anatomy, physiology, and benign pathology of the nipple. *Ann Surg Oncol*. 2015;22(10):3236–3240. doi: 10.1245/s10434-015-4760-4
2. Reisenbichler E, Hanley KZ. Seminars in diagnostic pathology developmental disorders and malformations of the breast. *Semin Diagn Pathol*. 2019;36(1):11–15. doi: 10.1053/j.semmp.2018.11.007
3. Liao CY, Wu YT, Wu WP, et al. Role of breast magnetic resonance imaging in predicting malignant invasion of the nipple-areolar complex: Potential predictors and reliability between inter-observers. *Medicine (Baltimore)*. 2017;96(28):e7170. doi: 10.1097/MD.0000000000007170
4. Milon A, Wahab CA, Kermarrec E, et al. Breast MRI: Is faster better? *AJR Am J Roentgenol*. 2020;214(2):282–95. doi: 10.2214/AJR.19.21924

5. Acrpractice parameter for the performance of contrast-enhanced magnetic resonance imaging (MRI) of the breast. ACoR; 2018. Available from: <https://www.acr.org/-/media/ACR/Files/Practice-Parameters/MR-Contrast-Breast.pdf>. Accessed: 15.01.2023.
6. Lee SJ, Trikha S, Moy L, et al. ACR appropriateness criteria evaluation of nipple discharge. *J Am Coll Radiol*. 2017;14(5s):S138–53. doi: 10.1016/j.jacr.2017.01.030
7. Ferris-James DM, Iuanow E, Mehta TS, et al. Imaging approaches to diagnosis and management of common ductal abnormalities. *Radiographics*. 2012;32(4):1009–1030. doi: 10.1148/rg.324115150
8. Del Riego J, Pitarch M, Codina C, et al. Multimodality approach to the nipple-areolar complex: A pictorial review and diagnostic algorithm. *Insights Imaging*. 2020 5;11(1):89. doi: 10.1186/s13244-020-00896-1
9. Yoon JH, Yoon H, Kim EK, et al. Ultrasonographic evaluation of women with pathologic nipple discharge. *Ultrasonography*. 2017;36(4):310–320. doi: 10.14366/usg.17013
10. Horvat JV, Keating DM, Rodrigues-Duarte H, et al. Calcifications at digital breast tomosynthesis: Imaging features and biopsy techniques. *Radiographics*. 2019;39(2):307–318. doi: 10.1148/rg.2019180124
11. Huppe AI, Overman KL, Gatewood JB, et al. Mammography positioning standards in the digital era: Is the status quo acceptable? *AJR Am J Roentgenol*. 2017;209(6):1419–1425. doi: 10.2214/AJR.16.17522
12. Gao Y, Brachtel EF, Hernandez O, Heller SL. An analysis of nipple enhancement at breast MRI with radiologic-pathologic correlation. *Radiographics*. 2019;39(1):10–27. doi: 10.1148/rg.2019180039
13. Lim HS, Jeong SJ, Lee JS, et al. Paget disease of the breast: Mammographic, US, and MR Imaging findings with pathologic correlation. *Radiographics*. 2011;31(7):1973–1987. doi: 10.1148/rg.317115070
14. Geffroy D, Doutriaux-Dumoulin I. Clinical abnormalities of the nipple-areola complex: The role of imaging. *Diagn Interv Imaging*. 2015;96(10):1033–1044. doi: 10.1016/j.diii.2015.07.001
15. Moon JY, Chang YW, Lee EH, Seo DY. Malignant invasion of the nipple-areolar complex of the breast: Usefulness of breast MRI. *AJR Am J Roentgenol*. 2013;201(2):448–455. doi: 10.2214/AJR.12.9186
16. Maksimov DA, Sergeev AN, Morozov AM, et al. About modern types of surgical treatment for breast cancer (literature review). *Journal of new medical technologies, eEdition*. 2021;(1):7–13. (In Russ). doi: 10.24412/2075-4094-2021-1-1-1
17. Zikiryakhodzhayev AD, Volchenko NN, Saribekyan EK, Rasskazova EA. Lesion of the nipple-areola complex in patients with breast cancer. *Problems in oncology*. 2017;63(4):593–597. (In Russ).
18. Levchuk AL, Khodyrev SA, Shabaev RM. Current state of breast reconstructive surgery. *Bulletin of Pirogov National Medical & Surgical Center*. 2021;16(2):122–127. (In Russ). doi: 10.25881/20728255-2021-16-2-122
19. Berger N, Luparia A, Di Leo G, et al. Diagnostic performance of MRI versus galactography in women with pathologic nipple discharge: A systematic review and meta-analysis. *AJR Am J Roentgenol*. 2017;209(2):465–471. doi: 10.2214/AJR.16.16682
20. Sripathi S, Ayachit A, Kadavigere R, et al. Spectrum of imaging findings in Paget's disease of the breast: A pictorial review. *Insights Imaging*. 2015;6(4):419–429. doi: 10.1007/s13244-015-0415-z
21. Da Costa D, Taddese A, Cure ML, et al. Common and unusual diseases of the nipple-areolar complex. *Radiographics*. 2007;27(Suppl. 1):S65–S77. doi: 10.1148/rg.27si075512
22. Alhajo ST, Edirimanne S. Clinically challenging case of nipple adenoma. *Breast J*. 2018;24(6):1084–1085. doi: 10.1111/tbj.13089

СПИСОК ЛИТЕРАТУРЫ

1. Stone K., Wheeler A. A review of anatomy, physiology, and benign pathology of the nipple // *Ann Surg Oncol*. 2015. Vol. 22, N 10. P. 3236–3240. doi: 10.1245/s10434-015-4760-4
2. Reisenbichler E., Hanley K.Z. Seminars in diagnostic pathology developmental disorders and malformations of the breast // *Semin Diagn Pathol*. 2019. Vol. 36, N 1. P. 11–15. doi: 10.1053/j.semmp.2018.11.007
3. Liao C.Y., Wu Y.T., Wu W.P., et al. Role of breast magnetic resonance imaging in predicting malignant invasion of the nipple-areolar complex: Potential predictors and reliability between inter-observers // *Medicine (Baltimore)*. 2017. Vol. 96, N 28. P. e7170. doi: 10.1097/MD.00000000000007170
4. Milon A., Wahab C.A., Kermarrec E., et al. Breast MRI: Is faster better? // *AJR Am J Roentgenol*. 2020. Vol. 214, N 2. P. 282–295. doi: 10.2214/AJR.19.21924
5. Acrpractice parameter for the performance of contrast-enhanced magnetic resonance imaging (MRI) of the breast. ACoR, 2018. Режим доступа: <https://www.acr.org/-/media/ACR/Files/Practice-Parameters/MR-Contrast-Breast.pdf>. Дата обращения: 15.01.2023.
6. Lee S.J., Trikha S., Moy L., et al. ACR appropriateness criteria evaluation of nipple discharge // *J Am Coll Radiol*. 2017. Vol. 14, N 5s. P. 138–153. doi: 10.1016/j.jacr.2017.01.030
7. Ferris-James D.M., Iuanow E., Mehta T.S., et al. Imaging approaches to diagnosis and management of common ductal abnormalities // *Radiographics*. 2012. Vol. 32, N 4. P. 1009–1030. doi: 10.1148/rg.324115150
8. Del Riego J., Pitarch M., Codina C., et al. Multimodality approach to the nipple-areolar complex: A pictorial review and diagnostic algorithm // *Insights Imaging*. 2020. Vol. 11, N 4. P. 89. doi: 10.1186/s13244-020-00896-1
9. Yoon J.H., Yoon H., Kim E.K., et al. Ultrasonographic evaluation of women with pathologic nipple discharge // *Ultrasonography*. 2017. Vol. 36, N 4. P. 310–320. doi: 10.14366/usg.17013
10. Huppe A.I., Overman K.L., Gatewood J.B., et al. Mammography positioning standards in the digital era: Is the status quo acceptable? // *AJR Am J Roentgenol*. 2017. Vol. 209, N 6. P. 1419–1425. doi: 10.2214/AJR.16.17522
11. Horvat J.V., Keating D.M., Rodrigues-Duarte H., et al. Calcifications at digital breast tomosynthesis: imaging features and biopsy techniques // *Radiographics*. 2019. Vol. 39, N 2. P. 307–318. doi: 10.1148/rg.2019180124
12. Gao Y., Brachtel E.F., Hernandez O., Heller S.L. An analysis of nipple enhancement at breast MRI with radiologic-pathologic correlation // *Radiographics*. 2019. Vol. 39, N 1. P. 10–27. doi: 10.1148/rg.2019180039
13. Lim H.S., Jeong S.J., Lee J.S., et al. Paget disease of the breast: Mammographic, US, and MR Imaging findings with pathologic correlation // *Radiographics*. 2011. Vol. 31, N 7. P. 1973–1987. doi: 10.1148/rg.317115070

14. Geffroy D., Doutriaux-Dumoulin I. Clinical abnormalities of the nipple-areola complex: The role of imaging // *Diagn Interv Imaging*. 2015. Vol. 96, N 10. P. 1033–1044. doi: 10.1016/j.diii.2015.07.001
15. Moon J.Y., Chang Y.W., Lee E.H., Seo D.Y. Malignant invasion of the nipple-areolar complex of the breast: Usefulness of breast MRI // *AJR Am J Roentgenol*. 2013. Vol. 201, N 2. P. 448–455. doi: 10.2214/AJR.12.9186
16. Максимов Д.А., Сергеев А.Н., Морозов А.М., и др. О современных видах хирургического лечения рака молочной железы (обзор литературы) // *Вестник новых медицинских технологий. Электронное издание*. 2021. № 1. С. 7–13. doi: 10.24412/2075-4094-2021-1-1-1
17. Зирияходжаев А.Д., Волченко Н.Н., Сарибекян Э.К., Расказова Е.А. Поражение сосково-ареолярного комплекса при раке молочной железы // *Вопросы онкологии*. 2017. Т. 63, № 4. С. 593–597.
18. Левчук А.Л., Ходырев С.А., Шабаетов Р.М. Современное состояние реконструктивно-восстановительной хирургии молочных желёз // *Вестник Национального медико-хирургического центра им. Н.И. Пирогова*. 2021. Т. 16, № 2. С. 122–127. doi: 10.25881/20728255-2021-16-2-122
19. Berger N., Luparia A., Di Leo G., et al. Diagnostic performance of MRI versus galactography in women with pathologic nipple discharge: A systematic review and meta-analysis // *AJR Am J Roentgenol*. 2017. Vol. 209, N 2. P. 465–471. doi: 10.2214/AJR.16.16682
20. Sripathi S., Ayachit A., Kadavigere R., et al. Spectrum of imaging findings in Paget's disease of the breast: A pictorial review // *Insights Imaging*. 2015. Vol. 6, N 4. P. 419–429. doi: 10.1007/s13244-015-0415-z
21. Da Costa D., Taddese A., Cure M.L., et al. Common and unusual diseases of the nipple-areolar complex // *Radiographics*. 2007. Vol. 27, Suppl. 1. P. S65–S77. doi: 10.1148/rg.27si075512
22. Alhaya S.T., Edirimanne S. Clinically challenging case of nipple adenoma // *Breast J*. 2018. Vol. 24, N 6. P. 1084–1085. doi: 10.1111/tbj.13089

AUTHORS' INFO

* **Elena N. Karanadze**, MD, Cand. Sci. (Med.);
address: 16 Krasnaya Presnia street, 123242 Moscow, Russia;
ORCID: <https://orcid.org/0000-0001-6745-1672>;
e-mail: ekaranadze@mail.ru

Valentin E. Sinitsyn, MD, Dr. Sci. (Med), Professor;
ORCID: <https://orcid.org/0000-0002-5649-2193>;
eLibrary SPIN: 8449-6590; e-mail: info@npcmr.ru

Mariia A. Karanadze, MD;
ORCID: <https://orcid.org/0009-0008-1723-6796>;
e-mail: ekaranadze@mail.ru

ОБ АВТОРАХ

* **Каранадзе Елена Николаевна**, к.м.н.;
адрес: Россия, 123242, Москва, ул. Красная Пресня, д. 16;
ORCID: <https://orcid.org/0000-0001-5147-4095>;
e-mail: ekaranadze@mail.ru

Синицын Валентин Евгеньевич, д.м.н., профессор;
ORCID: <https://orcid.org/0000-0002-5649-2193>;
eLibrary SPIN: 8449-6590; e-mail: info@npcmr.ru

Каранадзе Мария Алексеевна;
ORCID: <https://orcid.org/0009-0008-1723-6796>;
e-mail: ekaranadze@mail.ru

* Corresponding author / Автор, ответственный за переписку

DOI: <https://doi.org/10.17816/DD227288>

Магнитно-резонансная томография в диагностике некроза низведённого сегмента толстой кишки после брюшно-анальной резекции прямой кишки по поводу рака

С.А. Мялина¹, К.И. Пазюк², Т.П. Березовская¹, А.А. Невольских^{1, 2},
А.Л. Потапов¹, С.А. Иванов^{1, 2, 3}

¹ Национальный медицинский исследовательский центр радиологии, Медицинский радиологический научный центр имени А.Ф. Цыба, Обнинск, Российская Федерация

² Обнинский институт атомной энергетики — филиал Национального исследовательского ядерного университета «МИФИ», Обнинск, Российская Федерация

³ Российский университет дружбы народов, Москва, Российская Федерация

АННОТАЦИЯ

В работе представлен случай некроза низведённой толстой кишки после брюшно-анальной резекции прямой кишки, для диагностики которого была использована магнитно-резонансная томография.

Пациенту (мужчина, 47 лет) в ходе комбинированного лечения местно-распространённого рака прямой кишки выполнена лапароскопически ассистированная брюшно-анальная резекция прямой кишки с формированием колопластического резервуара и трансверзостомы. Послеоперационный период осложнился развитием синдрома воспалительной реакции. На 3-й послеоперационный день методом магнитно-резонансной томографии с контрастным усилением выявлен отёк 15-сантиметрового сегмента низведённой толстой кишки до колоанального анастомоза с резко ослабленным контрастированием; при ректоскопии изменений не выявлено. На 6-й послеоперационный день методом магнитно-резонансной томографии обнаружен дефект передней стенки колопластического резервуара с формированием пристеночной воздушной полости, при ректоскопии — признаки некроза стенки кишки. На 10-й послеоперационный день картина магнитно-резонансной томографии без динамики. В связи с нарастающими признаками воспаления выполнена релапаротомия с разобщением анастомоза и резекцией некротизированного сегмента кишки.

Ишемия низведённой толстой кишки после операций на прямой кишке является редким, но крайне серьёзным осложнением. Наше клиническое наблюдение демонстрирует возможности магнитно-резонансной томографии с контрастным усилением в качестве неинвазивного метода динамического наблюдения пациентов с осложнённым послеоперационным периодом с целью ранней диагностики ишемии и дефектов стенки кишки, что способствует принятию верной тактики ведения пациента.

Ключевые слова: магнитно-резонансная томография; рак прямой кишки; брюшно-анальная резекция прямой кишки; диагностика послеоперационных осложнений; ишемия толстой кишки; некроз толстой кишки; клинический случай.

Как цитировать

Мялина С.А., Пазюк К.И., Березовская Т.П., Невольских А.А., Потапов А.Л., Иванов С.А. Магнитно-резонансная томография в диагностике некроза низведённого сегмента толстой кишки после брюшно-анальной резекции прямой кишки по поводу рака // *Digital Diagnostics*. 2023. Т. 4, № 1. С. 61–69. DOI: <https://doi.org/10.17816/DD227288>

DOI: <https://doi.org/10.17816/DD227288>

Magnetic resonance imaging in the diagnosis of necrosis of a pulled-through colon segment after abdomino-anal resection of the rectum for cancer

Sofiya A. Myalina¹, Ksenia I. Paziuk², Tatiana P. Berezovskaya¹, Alexey A. Nevolskikh^{1,2}, Aleksandr L. Potapov¹, Sergey A. Ivanov^{1,2,3}

¹ National Medical Research Radiological Center, A. Tsyb Medical Radiological Research Centre, Obninsk, Russian Federation

² Obninsk Institute for Nuclear Power Engineering — National Research Nuclear University MEPhI, Obninsk, Russian Federation

³ Peoples' Friendship University of Russia, Moscow, Russian Federation

ABSTRACT

This study presents a case of necrosis of the pulled-through colon after abdomino-anal resection of the rectum, which was diagnosed by magnetic resonance imaging.

A 47-year-old man underwent laparoscopically assisted abdomino-anal resection of the rectum with reconstruction of a coloplasty pouch and transverse colostomy in the course of combination treatment for locally advanced rectal cancer. The postoperative period was complicated by the development of an inflammatory response syndrome. On postoperative day 3, contrast-enhanced magnetic resonance imaging revealed swelling of the 15-cm segment of pulled-through colon up to the coloanal anastomosis with sharply attenuated contrast enhancement, whereas rectoscopy showed no changes. On postoperative day 6, a magnetic resonance imaging scan revealed a defect in the anterior wall of the coloplasty pouch with a parietal aerocele, and rectoscopy showed signs of necrosis of the bowel wall. On postoperative day 10, the magnetic resonance imaging scan presented no changes. Because of increasing signs of inflammation, relaparotomy with anastomosis disconnection and resection of the necrotized bowel segment were performed.

Ischemia of the pulled-through colon after rectal surgery is a rare but serious complication. Our clinical case report demonstrates the potential of contrast-enhanced magnetic resonance imaging as a non-invasive method in case follow-up in patients with a complicated postoperative period for early diagnosis of ischemia and bowel wall defects, which helps to make the appropriate patient management plan.

Keywords: magnetic resonance imaging; rectal cancer; abdomino-anal resection of the rectum; diagnosis of postoperative complications; colonic ischemia; colonic necrosis; case report.

To cite this article

Myalina SA, Paziuk KI, Berezovskaya TP, Nevolskikh AA, Potapov AL, Ivanov SA. Magnetic resonance imaging in the diagnosis of necrosis of a pulled-through colon segment after abdomino-anal resection of the rectum for cancer. *Digital Diagnostics*. 2023;4(1):61–69. DOI: <https://doi.org/10.17816/DD227288>

Received: 13.02.2023

Accepted: 10.03.2023

Published: 30.03.2023

DOI: <https://doi.org/10.17816/DD227288>

磁共振成像在腹腔肛管直肠癌切除术后降结肠坏死的诊断中的作用

Sofiya A. Myalina¹, Ksenia I. Paziuk², Tatiana P. Berezovskaya¹,
Alexey A. Nevolskikh^{1,2}, Aleksandr L. Potapov¹, Sergey A. Ivanov^{1,2,3}

¹ National Medical Research Radiological Center, A. Tsyb Medical Radiological Research Centre, Obninsk, Russian Federation

² Obninsk Institute for Nuclear Power Engineering — National Research Nuclear University MEPhI, Obninsk, Russian Federation

³ Peoples' Friendship University of Russia, Moscow, Russian Federation

简评

本文介绍了一个通过磁共振成像诊断的腹腔直肠切除术后降结肠坏死的病例。

一名47岁的男性患者在局部晚期直肠癌的联合治疗期间接受了腹腔镜辅助下的腹腔肛管直肠切除术，并医生形成了结肠贮袋和横结肠造口。手术后发生了并发症，即炎症反应综合征。手术后第3天，造影剂增强磁共振成像显示了降结肠至结肠肛门吻合的15厘米处肿胀，造影剂急剧减少；直肠镜检查没显示变化。手术后第6天，磁共振成像显示了结肠贮袋前壁有缺陷，形成了壁性气腔；直肠镜检查显示了肠壁有坏死迹象。手术后第10天，磁共振成像检查结果没有任何动态变化。由于炎症的迹象越来越明显，因此重新进行了吻合口隔绝术，并切除了坏死的肠段。

直肠手术后降结肠缺血是一种罕见但非常严重的并发症。我们的临床观察表明造影剂增强磁共振成像的优点，具体来说，作为一种对手术后有并发症的患者进行动态监测的非侵入性方法，为了早期诊断缺血和肠壁缺陷，造影剂增强磁共振成像有助于采取正确的患者管理策略。

关键词：磁共振成像，直肠癌，腹腔肛管直肠切除术，术后并发症的诊断，结肠缺血，结肠坏死，临床病例。

To cite this article

Myalina SA, Paziuk KI, Berezovskaya TP, Nevolskikh AA, Potapov AL, Ivanov SA. 磁共振成像在腹腔肛管直肠癌切除术后降结肠坏死的诊断中的作用. *Digital Diagnostics*. 2023;4(1):61–69. DOI: <https://doi.org/10.17816/DD227288>

收到: 13.02.2023

接受: 10.03.2023

发布日期: 30.03.2023

BACKGROUND

Significant progress has been made over the last few decades in the development of surgical techniques for rectal cancer with the goal of improving treatment outcomes and lowering the risk of perioperative complications [1]. The number of sphincter-preserving surgeries, such as low anterior resection and abdominoanal resection of the rectum [2,3] with coloanal anastomosis, has increased dramatically. Nevertheless, according to various authors, the proportion of early postoperative complications is 20% or higher. Necrosis of a pulled-through colon segment is the second most common severe complication after an enteroenteric anastomosis leak [3,4]. Thus, identifying noninvasive methods to detect complications early and for case follow-up during the postoperative period is particularly important.

Proctography, ultrasound, and computed tomography have been used to diagnose postoperative complications. However, these methods have some disadvantages due to limited visualization of the pelvic area and radiation exposure. Magnetic resonance imaging (MRI) without radiation exposure has become more widely available, making it a promising method for detecting and controlling postoperative complications in patients undergoing rectal resection. This method has several advantages, such as good soft tissue contrast, which allows for assessing the continuity of the colorectal anastomosis and detecting the accumulation of fluid/blood/pus/gas in the pelvic area, including the presacral space, and the ability to assess the blood supply to a pulled-through colon segment on post-contrast images.

We present a clinical case of colon necrosis following laparoscopic-assisted abdominoanal resection of the rectum with a coloplasty pouch and coloanal anastomosis to demonstrate the utility of MRI in the diagnosis of this complication.

CLINICAL CASE

About the patient

The patient was a 47-year-old man admitted to the A. F. Tsyb Medical Radiological Research Center (Obninsk) with the diagnosis of C20 cT4bN1aM0 stage IIIB malignant rectal neoplasm. The patient received combined therapy, including preoperative chemoradiotherapy (total radiation dose 50 Gy + capecitabine), 4 cycles of FOLFOX6 neoadjuvant chemotherapy, laparoscopic-assisted abdominoanal resection of the rectum with a coloplasty pouch and coloanal anastomosis, and transverse colostomy. The entire left half of the colon with the splenic flexure was mobilized by ligating the inferior mesenteric artery at the base and the inferior mesenteric vein at the ligament of Treitz. The rectum was mobilized along all walls up to the anal canal. This procedure has been associated with technical difficulties due to post-radiation changes in the pelvic cavity (soft tissue edema and

fibrotic changes) and anthropometric parameters. The large intestine was transected at the middle third of the sigmoid colon. The rectal mucosa was dissected along the dental line border, and the rectum was mobilized by resecting the internal sphincter. The surgical specimen was removed via the abdominal cavity. The descending colon was fully mobilized and pulled-through the anal canal, followed by the formation of a coloplasty pouch and a hand-sewn coloanal anastomosis. The histological examination of the surgical specimen revealed a complete pathomorphological response to neoadjuvant therapy.

Case follow-up

Intermittent low-grade fever and a high serum C-reactive protein (CRP) level were detected starting on postoperative day (POD) 1 (Fig. 1). Due to this clinical pattern, imaging studies, including MRI and rectoscopy, were performed on POD 3. Pelvic MRI included high-resolution T2-weighted images (WIs) in three orthogonal planes and T1WIs with fat suppression and intravenous gadolinium enhancement. Diffuse edema was present on the wall of the colon 15 cm proximal to the coloanal anastomosis, with sharply reduced contrast uptake, which was interpreted as a disturbance in blood supply in the pulled-through distal colon segment (Fig. 2). The pulled-through colon mucosa was pink on rectoscopy, with no signs of ischemia or necrosis; mucus was in the lumen.

During the case follow-up, the patient received conservative therapy, including infusion therapy, antibiotics, and anticoagulants.

Hyperthermia (37.6°C) and a high CRP level (up to 114.6 mg/L) persisted on POD 6, necessitating another imaging study.

On the follow-up non-contrast-enhanced MRI, the previously detected changes (diffuse edema of the distal colon wall) were accompanied by a defect in the anterior wall of the coloplasty pouch, with a parietal air-filled cavity at the bottom in which a small amount of exudate was detected (Fig. 3). There were signs of necrosis in the pulled-through colon on rectoscopy (Fig. 4): the mucosa was violet-gray and dull; the lumen was deformed, and the folds were absent; the lumen contained blood and necrotic masses, and there was a putrid odor.

The case conference determined that the only surgical option, in this case, was to disconnect the anastomosis and resect the necrotic portion of the pulled-through colon. However, in the absence of a clinical picture of total necrosis of the pulled-through colon and purulent-septic complications, positive changes in body temperature and the CRP level, and the patient's relatively satisfactory condition, conservative treatment was continued with laboratory test monitoring.

Fever up to 37.8°C persisted on POD 10, but the CRP level decreased to 78.8 mg/L. A persistent defect in the wall of the coloplasty pouch with a parietal air-filled cavity was

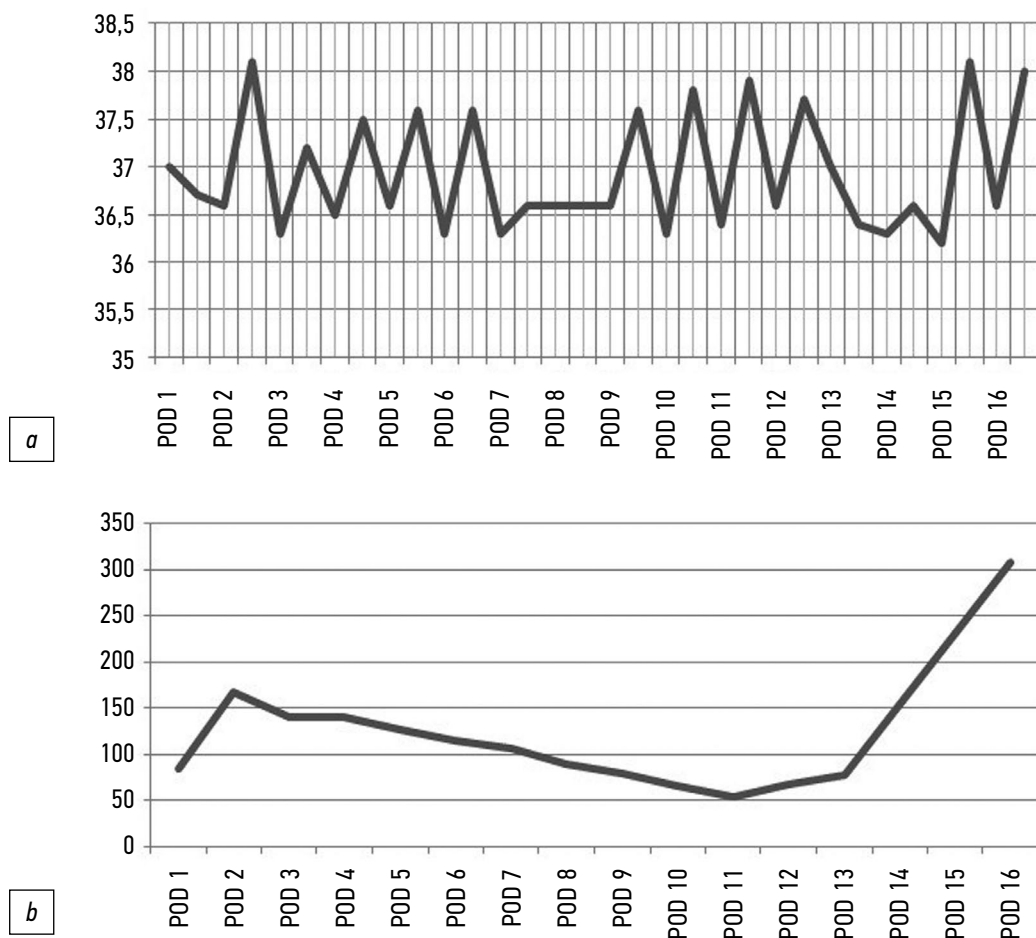


Figure 1. Body temperature (*a*; °C) and serum C-reactive protein (*b*; mg/L) on postoperative day (POD) 1 to the relaparotomy (POD 16).

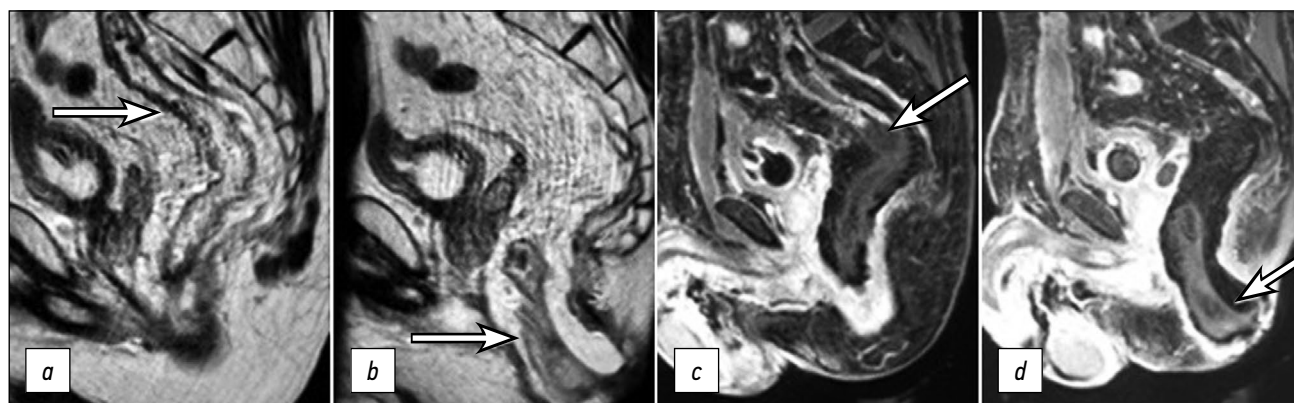


Figure 2. MRI scans of two adjacent sagittal sections of the pelvis in T2 mode (*a*, *b*) and 1-FS mode with contrast enhancement (*c*, *d*) on POD 3: the upper (*a*, *c*) and lower (*b*, *d*) segments of the pulled-through colon with thickened walls and sharply reduced contrast uptake, 15 cm long, with a distinct boundary between the ischemic and normal colon segments (arrows).

observed on a follow-up contrast-enhanced MRI; no contrast uptake was observed in the pulled-through colon segment (Fig. 5).

Because of persistent signs of a disturbance in blood supply in the pulled-through colon segment, a high CRP level of 307.5 mg/L, and an increase in body temperature to 38.1°C, surgery was performed on POD 17 including resection of the pulled-through colon, disconnection of the

coloanal anastomosis, an end colostomy, and pelvic lavage and drainage.

No effusion was detected in the abdominal cavity during the revision surgery. A greater omentum segment plugged the pelvic inlet, and there were no signs of ischemia or necrosis in the colon at the pelvic inlet level. The left half of the colon was mobilized to the stoma, the colon was transected at the level of the transverse colostoma, the distal segment of the colon

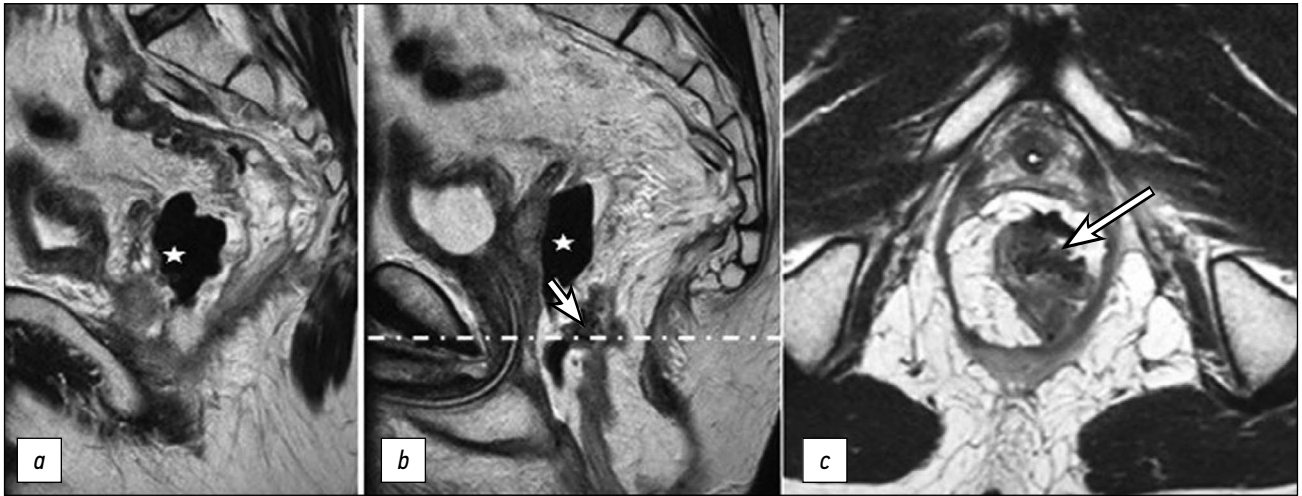


Figure 3. Pelvic MRI scans in T2 mode on POD 6: two adjacent sagittal sections including the upper (a) and lower (b) segments of the pulled-through colon, with persistent diffuse edema of the walls; axial section (c) at the level of the dashed-dotted line. A defect in the anterior wall of the coloplasty pouch (arrow) with a parietal air-filled cavity (asterisk).

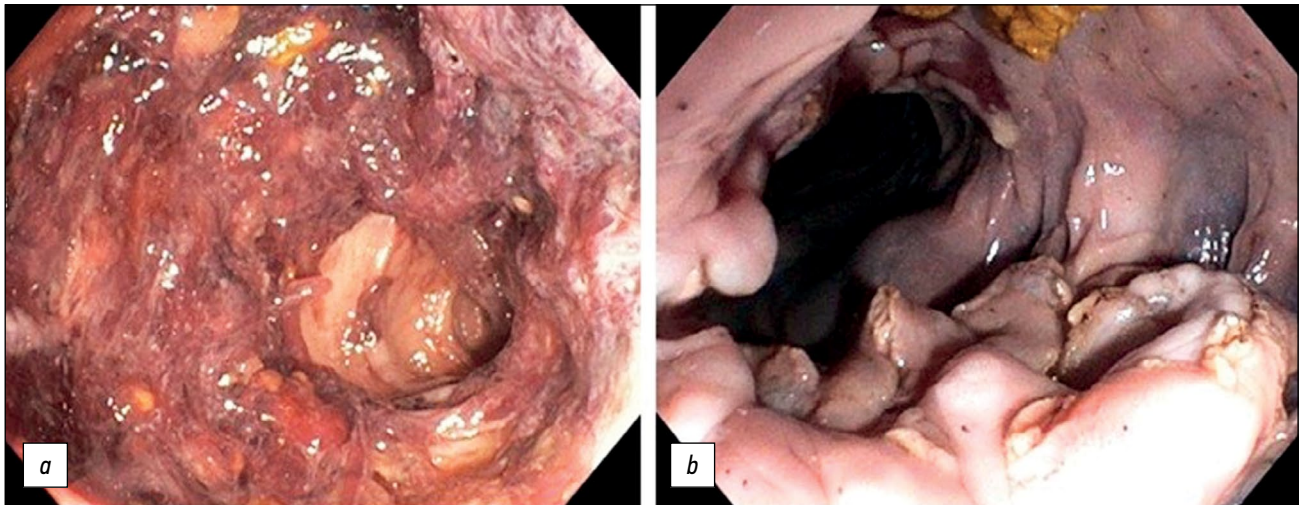


Figure 4. Endoscopic photograph on POD 6: areas of necrotic changes (a); intestinal wall deformation; mucosa is violet-gray and dull (b).

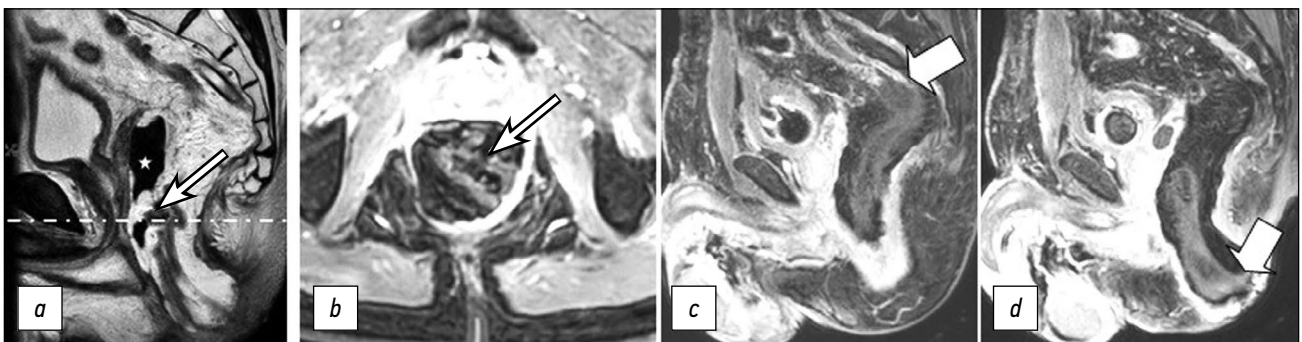


Figure 5. Pelvic MRI scans in T2 mode (a) and 1-FS mode with contrast enhancement at the level of the dashed-dotted line in the axial plane (b) on POD 10: a defect in the wall of the coloplasty pouch (arrow) and an air-filled cavity (asterisk); two adjacent sagittal sections in 1-FS mode with contrast enhancement (c, d): the upper and lower edges of the ischemic colon segment (arrows).

with signs of ischemia was isolated from the pelvic cavity, the coloanal anastomosis was disconnected, and the surgical specimen was removed. Pelvic lavage and tamponade through the anus were performed. An end transverse colostomy was performed in the left hypochondrium.

The pathological examination of the surgical specimen revealed necrotic mucosal foci in the left half of the colon, some of which extended the entire thickness of the colon wall. Lipoxanthogranulomas and necrotic foci were detected in the adjacent fatty tissue of the mesentery. Fibrin deposits

and detritus were found on the serous membrane of the large intestine and adjacent mesentery. The postoperative period was uneventful.

DISCUSSION

The pulled-through colon segment has a high risk of acute ischemia after abdominoanal resection of the rectum with coloanal anastomosis and neoadjuvant chemoradiotherapy in patients with rectal cancer, which can result in serious complications during the postoperative period. Although the colon may appear normal immediately following the anastomosis, the possibility of ischemia during the early postoperative period cannot be excluded.

Preoperative radiation therapy, older age, male gender, and cardiovascular diseases are important risk factors for colonic ischemia. High ligation of the inferior mesenteric artery and excessive colonic tension during anastomosis are perioperative risk factors [5, 6]. Furthermore, laparoscopic access has been associated with colonic ischemia because pneumoperitoneum and increased intraabdominal pressure reduce mesenteric venous blood flow [7]. Of the listed risk factors, our patient was male and had undergone neoadjuvant chemoradiotherapy, laparoscopic access, and high ligation of the inferior mesenteric artery.

In our clinical case, the signs of ischemia in the pulled-through colon segment, which was detected by MRI on POD 3, included nonspecific manifestations of non-enhanced T2-WIs in the form of edema and thickening of the colon wall, as well as the absence of contrast uptake above the anastomosis with a distinct upper boundary on the post-contrast images. The involvement of a significant area (6–15 cm) from the anastomosis level is a characteristic feature of this type of colonic ischemia [5], which we also observed in our patient.

Necrosis was not observed on endoscopy at the time of the primary postoperative MRI, which justified conservative therapy. In most cases, a 2-week conservative treatment of ischemia (antibiotic therapy) allows the patient to be discharged in a satisfactory condition; however, the patient will almost certainly develop an ischemic area stricture after a few months [5].

Necrosis of the pulled-through colon segment, which necessitates emergency surgery, is an unfavorable outcome of acute ischemia. In our case, a follow-up MRI (POD 6) revealed diffuse edema in the pulled-through colon segment wall that persisted and an area of tissue destruction appeared. A defect containing fluid and gas formed in the wall of the coloplasty pouch. Changes in the MRI pattern

were detected on POD 10 despite ongoing conservative therapy. A follow-up endoscopic examination confirmed the MRI findings of necrotic changes. Additionally, signs of a general inflammatory response increased, necessitating relaparotomy with disconnection of the anastomosis and resection of the necrotic portion of the colon.

CONCLUSION

The presented clinical case demonstrates that ischemia of the pulled-through colon segment following abdominoanal resection can be diagnosed using contrast-enhanced MRI in the absence of contrast uptake in a large area of the small pulled-through colon with distinct boundaries. Non-enhanced T2-WIs showed thickening and edema of the entire intestinal wall in the affected area.

Follow-up MRI revealed signs of total necrosis of the entire intestinal wall with destruction and the formation of a parietal cavity containing fluid and gas. MRI signs of total intestinal wall necrosis in combination with relevant clinical and laboratory findings should be considered an indication for relaparotomy.

Thus, MRI with intravenous contrast enhancement is recommended as a noninvasive method for detecting and monitoring acute ischemia of the pulled-through colon segment following the formation of colorectal anastomoses.

ADDITIONAL INFORMATION

Funding source. This article was not supported by any external sources of funding.

Competing interests. The authors declare that they have no competing interests.

Authors' contribution. All authors made a substantial contribution to the conception of the work, acquisition, analysis, interpretation of data for the work, drafting and revising the work, final approval of the version to be published and agree to be accountable for all aspects of the work. S.A. Myalina — data sources collection and analysis, manuscript preparation, illustrations creating; K.I. Paziuk — data sources collection and analysis, manuscript preparation; T.P. Berezovskaya — conception of the work, revising and editing the manuscript; A.A. Nevolskikh, A.L. Potapov — editing the manuscript; S.A. Ivanov — approved the final version of the work.

Consent for publication. Written consent was obtained from the patient for publication of relevant medical information and all of accompanying images within the manuscript in Digital Diagnostics journal.

REFERENCES

1. Berdov BA, Nevolskikh AA, Yerygin DV, Lantsov DS. Current approaches to preventing local relapses in the surgical treatment of rectal cancer. *Russ J Oncol.* 2007;(5):51–55. (In Russ).
2. Krot VS, Ryliuk AF. Causes of necrosis in operations with descending sigmoid intestine. *Health Ecology Issues.* 2011;(2):55–60. (In Russ).

3. Basheev VK. Optimization of tactics of treatment of cancer of the lower ampullary rectum [dissertation abstract]. Donetsk; 2003. 32 p. (In Russ).
4. Tsepilova IYa, Trunov GV, Vinnik YA, et al. Study of microcirculation in the graft after abdominal-anal resection of the rectum. *Vrachebnaya praktika*. 2000;(6):44–45. (In Russ).
5. Lim DR, Hur H, Min BS, et al. Colon stricture after ischemia following a robot-assisted ultra-low anterior resection

- with coloanal anastomosis. *Ann Coloproctol*. 2015;31(4):57. doi: 10.3393/ac.2015.31.4.157
6. Toiyama Y, Hiro J, Ichikawa T, et al. Colonic necrosis following laparoscopic high anterior resection for sigmoid colon cancer: Case report and review of the literature. *Int Surg*. 2017;102(3-4):109–114. doi: 10.9738/intsurg-d-17-1.1
7. Jakimowicz J, Stultiens G, Smulders F. Laparoscopic insufflation of the abdomen reduces portal venous flow. *Surg Endoscopy*. 1998;12(2):129–132. doi: 10.1007/s004649900612

СПИСОК ЛИТЕРАТУРЫ

1. Бердов Б.А., Невольских А.А., Ерыгин Д.В., Ланцов Д.С. Современные подходы к профилактике местных рецидивов при оперативном лечении рака прямой кишки (обзор литературы) // Российский онкологический журнал. 2007. № 5. С. 51–55.
2. Крот В.С., Рылюк А.Ф. Причины некрозов при операциях с низведением сигмовидной кишки // Проблемы здоровья и экологии. 2011. № 2. С. 55–60.
3. Башеев В.Х. Оптимизация тактики лечения рака нижеампулярного отдела прямой кишки: Автореф. дис. ... канд. мед. наук. Донецк, 2003. 32 с.
4. Цепилова И.Я., Трунов Г.В., Винник Ю.А., и др. Изучение микроциркуляции в трансплантате после брюшно-анальной

- резекции прямой кишки // Врачебная практика. 2000. № 6. С. 44–45.
5. Lim D.R., Hur H., Min B.S., et al. Colon stricture after ischemia following a robot-assisted ultra-low anterior resection with coloanal anastomosis // *Ann Coloproctol*. 2015. Vol. 31, N 4. P. 157–162. doi: 10.3393/ac.2015.31.4.157
6. Toiyama Y., Hiro J., Ichikawa T., et al. Colonic necrosis following laparoscopic high anterior resection for sigmoid colon cancer: Case report and review of the literature // *Int Surg*. 2017. Vol. 102, N 3-4. P. 109–114. doi: 10.9738/intsurg-d-17-1.1
7. Jakimowicz J., Stultiens G., Smulders F. Laparoscopic insufflation of the abdomen reduces portal venous flow // *Surg Endoscopy*. 1998. Vol. 12, N 2. P. 129–132. doi: 10.1007/s004649900612

AUTHORS' INFO

* Ksenia I. Paziuk;

address: 1 Studgorodok, 249039 Obninsk, Russia;
ORCID: <https://orcid.org/0009-0000-0036-9877>;
e-mail: komolovaksusha@yandex.ru

Sofiya A. Myalina;

ORCID: <https://orcid.org/0000-0001-6686-5419>;
eLibrary SPIN: 9668-3834; e-mail: samyalina@mail.ru

Tatiana P. Berezovskaya, MD, Dr. Sci. (Med.), Professor;

ORCID: <https://orcid.org/0000-0002-3549-4499>;
eLibrary SPIN: 5837-3465; e-mail: berez@mrrc.obninsk.ru

Alexey A. Nevolskikh, MD, Dr. Sci. (Med.);

ORCID: <https://orcid.org/0000-0001-5961-2958>;
eLibrary SPIN: 3787-6139; e-mail: nevol@mrrc.obninsk.ru

Aleksandr L. Potapov, MD, Dr. Sci. (Med.), Professor;

ORCID: <https://orcid.org/0000-0003-3752-3107>;
eLibrary SPIN: 9189-4126; e-mail: ALP8@yandex.ru

Sergey A. Ivanov, MD, Dr. Sci. (Med.), Professor;

ORCID: <https://orcid.org/0000-0001-7689-6032>;
eLibrary SPIN: 4264-5167; e-mail: oncurolog@gmail.com

ОБ АВТОРАХ

* Пазюк Ксения Игоревна;

адрес: Россия, 249039, Обнинск, Студгородок, д. 1;
ORCID: <https://orcid.org/0009-0000-0036-9877>;
e-mail: komolovaksusha@yandex.ru

Мялина София Анатольевна;

ORCID: <https://orcid.org/0000-0001-6686-5419>;
eLibrary SPIN: 9668-3834; e-mail: samyalina@mail.ru

Березовская Татьяна Павловна, д.м.н., профессор;

ORCID: <https://orcid.org/0000-0002-3549-4499>;
eLibrary SPIN: 5837-3465; e-mail: berez@mrrc.obninsk.ru

Невольских Алексей Алексеевич, д.м.н.;

ORCID: <https://orcid.org/0000-0001-5961-2958>;
eLibrary SPIN: 3787-6139; e-mail: nevol@mrrc.obninsk.ru

Потапов Александр Леонидович, д.м.н., профессор;

ORCID: <https://orcid.org/0000-0003-3752-3107>;
eLibrary SPIN: 9189-4126; e-mail: ALP8@yandex.ru

Иванов Сергей Анатольевич, д.м.н., профессор;

ORCID: <https://orcid.org/0000-0001-7689-6032>;
eLibrary SPIN: 4264-5167; e-mail: oncurolog@gmail.com

* Corresponding author / Автор, ответственный за переписку

DOI: <https://doi.org/10.17816/DD114723>

Динамическая магнитно-резонансная томография лёгких у пациентов с COVID-19: серия клинических случаев

Ю.А. Васильев¹, Е.А. Грик², О.Ю. Панина^{1, 3, 4}, А.Н. Хоружая¹, Д.С. Семенов¹,
А.В. Бажин¹, Ю.Н. Васильева⁴

¹ Научно-практический клинический центр диагностики и телемедицинских технологий, Москва, Российская Федерация

² Lincoln Medical Center, Бронкс, Нью-Йорк, США

³ Городская клиническая онкологическая больница № 1, Москва, Российская Федерация

⁴ Московский государственный медико-стоматологический университет имени А.И. Евдокимова, Москва, Российская Федерация

АННОТАЦИЯ

Широкое распространение новой коронавирусной инфекции (COVID-19) привело к активному изучению её диагностических особенностей. Острая вирусная пневмония, связанная с COVID-19, уже подробно описана по результатам компьютерной томографии, рентгенографии и статической магнитно-резонансной томографии, однако картина, наблюдаемая при динамической магнитно-резонансной томографии, не получила достаточного освещения в специализированной литературе.

Учитывая комплексный диагностический подход, важно, чтобы врачи-рентгенологи имели возможность правильно распознавать и интерпретировать COVID-19 по изображениям магнитно-резонансной томографии.

В представленной серии клинических случаев продемонстрированы возможности методики динамической магнитно-резонансной томографии в обнаружении признака «облачного неба» и его отличия от консолидации у пациентов с COVID-19, что позволяет предположительно разграничить раннее или лёгкое изменение от прогрессирующего клинического течения.

Таким образом, динамическая магнитно-резонансная томография может оказаться чрезвычайно полезным инструментом, к тому же без лучевой нагрузки, в случаях, когда доступ к компьютерной томографии ограничен и требуется динамическая морфофункциональная визуализация.

Ключевые слова: магнитно-резонансная томография; динамическая МРТ; МРТ в режиме реального времени; пневмония; COVID-19.

Как цитировать

Васильев Ю.А., Грик Е.А., Панина О.Ю., Хоружая А.Н., Семенов Д.С., Бажин А.В., Васильева Ю.Н. Динамическая магнитно-резонансная томография лёгких у пациентов с COVID-19: серия клинических случаев // *Digital Diagnostics*. 2023. Т. 4, № 1. С. 71–79. DOI: <https://doi.org/10.17816/DD114723>

DOI: <https://doi.org/10.17816/DD114723>

Dynamic MRI in a COVID-19 patient: a case series

Yuriy A. Vasilev¹, Evgeniia A. Grik², Olga Yu. Panina^{1, 3, 4}, Anna N. Khoruzhaya¹,
Dmitriy S. Semenov¹, Alexander V. Bazhin¹, Yulia N. Vasileva⁴

¹ Moscow Center for Diagnostics and Telemedicine, Moscow, Russian Federation

² Lincoln Medical Center, The Bronx, NY, United States

³ City Clinical Oncological Hospital 1 of the Department of healthcare of the city of Moscow, Moscow, Russian Federation

⁴ Moscow State University of Medicine and Dentistry named after A.I. Evdokimov, Moscow, Russian Federation

ABSTRACT

Extensive spread of the coronavirus disease (COVID-19) prompted an investigation of its diagnostic features. Acute viral pneumonia associated with COVID-19 has been described in detail using CT, radiography, and MRI. There is no data in the literature on the descriptive picture observed with dynamic MRI. Considering a comprehensive diagnostic approach, radiologists should know how to correctly recognize and interpret COVID-19 on MRI. This case series demonstrated the ability of dynamic MRI to detect the cloudy sky sign and distinguish it from consolidation in COVID-19 patients, thus presumably distinguishing between early or mild changes and a progressive clinical course. These changes in dynamic lung images on MRI can be recorded depending on the phase of the respiratory cycle. Thus, MRI, as a radiation-free tool that can be used to examine a patient with acute viral pneumonia COVID-19, can be useful in cases where access to computed tomography is limited and dynamic morphofunctional imaging is required.

Keywords: dynamic MR, real-time MRI, pneumonia; COVID-19; magnetic resonance imaging.

To cite this article

Vasilev YuA, Grik EA, Panina OYu, Khoruzhaya AN, Semenov DS, Bazhin AV, Vasileva YuN. Dynamic MRI in a COVID-19 patient: a case series. *Digital Diagnostics*. 2023;4(1):71–79. DOI: <https://doi.org/10.17816/DD114723>

Received: 19.11.2022

Accepted: 17.03.2023

Published: 04.04.2023

DOI: <https://doi.org/10.17816/DD114723>

COVID-19患者的肺部动态磁共振成像： 一系列临床病例

Yuriy A. Vasilev¹, Evgeniia A. Grik², Olga Yu. Panina^{1, 3, 4}, Anna N. Khoruzhaya¹,
Dmitriy S. Semenov¹, Alexander V. Bazhin¹, Yulia N. Vasileva⁴

¹ Moscow Center for Diagnostics and Telemedicine, Moscow, Russian Federation

² Lincoln Medical Center, The Bronx, NY, United States

³ City Clinical Oncological Hospital 1 of the Department of healthcare of the city of Moscow, Moscow, Russian Federation

⁴ Moscow State University of Medicine and Dentistry named after A.I. Evdokimov, Moscow, Russian Federation

简评

一场新型冠状病毒感染（COVID-19）的广泛流行导致了对其诊断特征的积极性研究。与COVID-19相关的急性病毒性肺炎是已经在计算机断层扫描（CT）、辐射成像和静态磁共振成像（MRI）的研究中详细描述。然而，文献中有很少关于通过动态MRI观察到的描述性图片的数据。鉴于综合诊断方法，放射科医生知道如何通过MRI正确识别和解释COVID-19是很重要的。在这一系列临床病例中，我们展示了动态MRI工作方法的威力，使我们能够看到“cloudy sky”的迹象，并将其与COVID-19患者的固结区分开来，使我们能够推测区分早期或轻微的变化和渐进的临床过程。因此，MRI作为一种无辐射的工具，在进行CT扫描的机会有限和需要动态形态功能成像的情况下是非常有用的。

关键词：磁共振成像，动态MRI，实时MRI，肺炎，COVID-19。

To cite this article

Vasilev YuA, Grik EA, Panina OYu, Khoruzhaya AN, Semenov DS, Bazhin AV, Vasileva YuN. COVID-19患者的肺部动态磁共振成像：一系列临床病例. *Digital Diagnostics*. 2023;4(1):71-79. DOI: <https://doi.org/10.17816/DD114723>

收到: 19.11.2022

接受: 17.03.2023

发布日期: 04.04.2023

BACKGROUND

Over the last 2 years, a novel coronavirus infection (COVID-19) caused by SARS-CoV-2 has become an important research focus due to the prevalence of pulmonary symptoms. The computed tomography (CT) is used to detect the primary chest symptoms of COVID-19, which include localized unilateral or diffuse bilateral ground-glass opacity (GGO) progressing to lung parenchyma consolidation.[1,2]

Due to a paucity of laboratory diagnostics funding at the start of the pandemic, a chest CT scan was considered as a possible factor in deciding whether a patient should be tested for COVID-19 using laboratory methods. This screening approach was later cancelled, and currently, chest CT is only recommended if clinical signs and symptoms of COVID-19 are observed.[3,4] In severe cases, chest CT scans are performed several times for condition monitoring, resulting in high radiation exposure. Software for magnetic resonance imaging (MRI) of the chest is continually being improved and is regarded as a promising area of imaging development for lung conditions. Lung MRI may be considered the method of choice in some cases due to some advantages, such as the lack of radiation exposure.[5-7]

Our case reports describe the use of dynamic lung MRI in SARS-CoV-2-positive patients. An MRI was performed within the first few days after the onset of viral pneumonia symptoms (subfebrile/febrile fever, dry cough, and weakness). This study focuses on abnormal changes revealed by dynamic MRI using three-dimensional cinematic chest imaging in COVID-19 patients with acute viral pneumonia.

CASE REPORTS

MRI scan

A patient was examined in the supine position using abdominal and vertebral radiofrequency (RF) coils built into the tabletop of a 3T MRI scanner (Signa Pioneer, General Electric, USA). Under free-breathing conditions, the scan was performed without a respiratory trigger. The RF coil

was fixed to reduce dynamic artifacts associated with respiratory movements. The study was conducted under free-breathing conditions using automatic synchronization of diaphragm movement to optimize the time of data collection. For cinematic MRI, a single fast spin echo was used with additional parameters as follows: TR 1,460 ms, TE 108.6 ms, rotation angle 90°, FOV 450 × 450 mm, matrix 384 × 256, slice thickness 6 mm, slice spacing 6 mm, average number 0.6, and non-Cartesian k-space filling method. To obtain these scans, we asked the patient to take a slow breath while mentally counting to 10 and then exhale slowly in the same manner. Three dynamic images in three orthogonal planes were obtained for each patient.

MRI analysis

The search focused on polysegmented sites with increased signal intensity (hyperintense compared with muscle tissue but hypointense compared with pulmonary consolidation sites, i.e., with less intense signal compared with consolidation sites), which could represent a “cloudy sky” sign. We also noted changes in the signal intensity of the lesions during inhalation and exhalation.

Case Report 1

A patient (female, 45 years old) presented to the clinic on the fifth day after the onset of dry cough and mild fever up to 37.5°C. Dynamic lung MRI in the coronal plane (Fig. 1) showed an area of hyperintense signal in the lower lobe of the right lung (S9–S10), interpreted as an area of central induration (more intense signal) with a surrounding “cloudy sky” (less intense signal) during inhalation. A hyperintense signal was found in the corresponding area in the axial and sagittal planes, indicating consolidation with a “cloudy sky” along the edge of the area. At the end of exhalation, increased signal intensity was observed in the described area in the coronal plane (Fig. 2) with decreased visual size of the affected areas due to lung tissue contraction. During exhalation, no changes in signal intensity were observed in the axial and sagittal planes.

If the same hyperintense signal is observed regardless of respiration phases, this could indicate alveolar infiltration

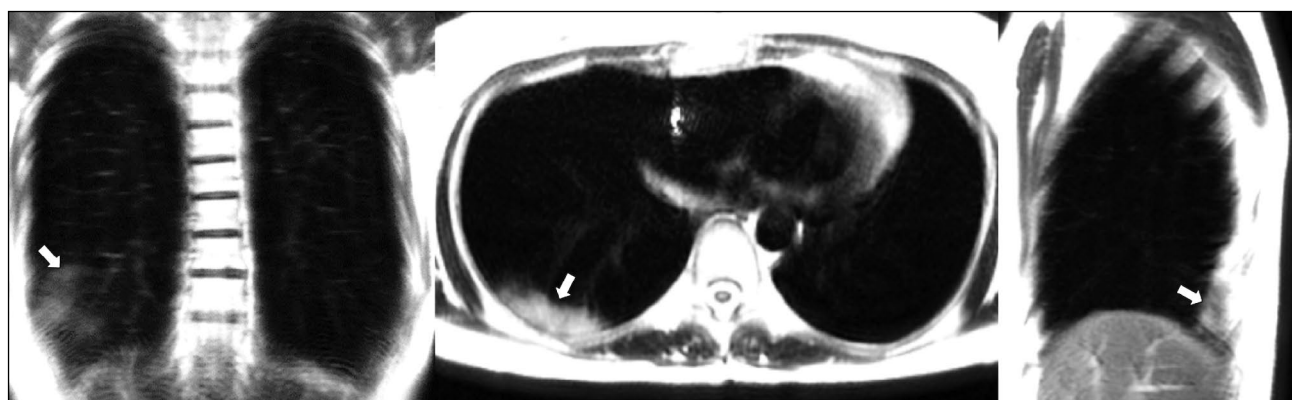


Figure 1. Dynamic magnetic resonance imaging of the lungs during inhalation in the coronal, axial, and sagittal planes. In the axial and sagittal planes, arrows point to areas of compaction. In the coronal plane, the arrow points to a “cloudy sky” (S9–S10).



Figure 2. Dynamic magnetic resonance imaging of the lungs during exhalation in the coronal, axial, and sagittal planes. Arrows indicate the areas of consolidation (S9–S10).

(consolidation), but a less intense signal during exhalation could indicate intermediate changes (cloudy sky”).

Case Report 2

A patient (female, 25 years old) complained of a dry cough, high fever (up to 39°C), chills, and chest heaviness. She went to the hospital on the sixth day after the onset of the first symptoms, when they became extremely pronounced. Dynamic MRI showed a large area of increased signal in segments S6,

S8, and S9 of the left lung’s lower lobe. An inhomogeneous increased signal was found during inhalation in the coronal, axial, and sagittal planes (Fig. 3). The signal intensity increased in the coronal and sagittal planes during exhalation (Fig. 4), with the increased visual size of the affected areas and the expanded “cloudy sky” area. These findings may be attributed to expiratory contraction of lung tissue during exhalation.

Chest breathing movements can also influence scanning and thus the observed pattern. The “cloudy sky” observed

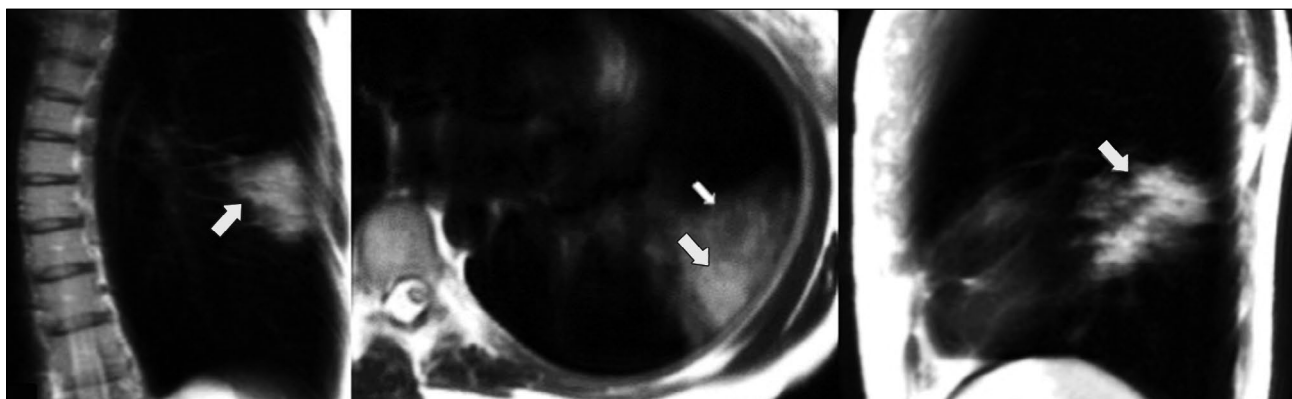


Figure 3. Dynamic magnetic resonance imaging of the lungs during inhalation in the coronal, axial, and sagittal planes. Orange arrows point to consolidation areas visible during inhalation (S6, S8, and S9). The white arrow points to the area with the “cloudy sky.”

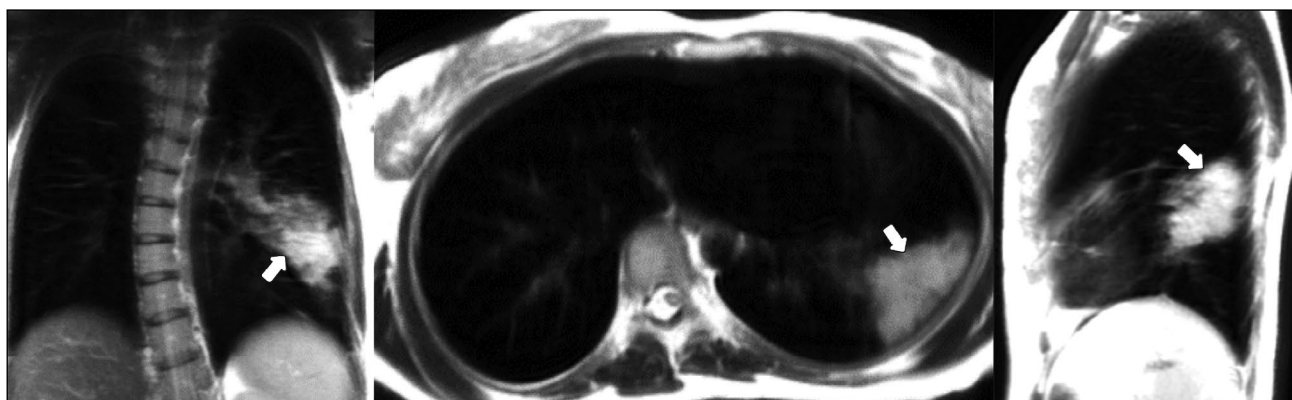


Figure 4. Dynamic magnetic resonance imaging of the lungs during exhalation in the coronal, axial, and sagittal planes. Arrows point to lesions with areas of both marked interstitial changes (the sign of the “cloudy sky”) and alveolar (compaction) changes that can be differentiated during inhalation (see Figure 3).

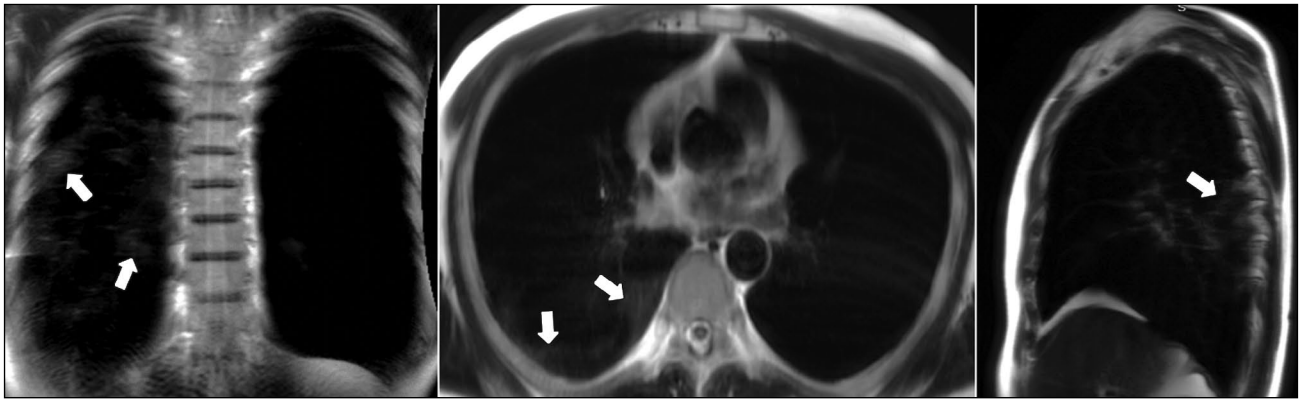


Figure 5. Dynamic magnetic resonance imaging of the lungs during inhalation in the coronal, axial, and sagittal planes. Arrows point to areas of low-intensity signal with the “cloudy sky” pattern (S6, S9, and S10).

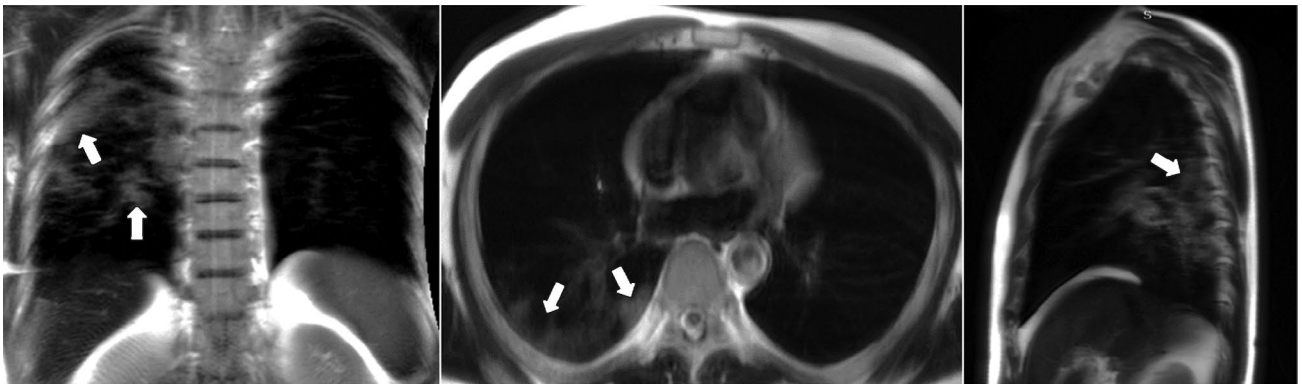


Figure 6. Dynamic magnetic resonance imaging of the lungs during exhalation in the coronal, axial, and sagittal planes. Arrows point to an increase in low-intensity signal areas with the “cloudy sky” pattern (S6, S9, and S10).

at the periphery of the signal enhancement area during inhalation becomes more intense during exhalation, most likely due to increasing density of the lung parenchyma.

Case Report 3

A patient (male, 49 years old) with a mild cough and subfebrile fever up to 37.5°C consulted a doctor on the second day after the onset of symptoms. Dynamic lung MRI showed the predominant “cloudy sky,” which was confirmed by different signal intensities and signal change area sizes depending on the respiratory cycle phase. During inhalation, a weak signal was detected in the lower lobe of the right lung (S6, S9, and S10) in the coronal, axial, and sagittal planes (Fig. 5). Increased signal intensities and area sizes were observed in the coronal and sagittal planes at the end of exhalation (Fig. 6) compared with the areas described. The “cloudy sky” was more prominent in the axial plane during exhalation, whereas the area of visible lung damage was wider.

DISCUSSION

CT scanning is the gold standard for lung evaluation in COVID-19 pneumonia and other viral pneumonias. In most cases, early signs of acute coronavirus pneumonia caused by SARS-CoV-2 present as GGO on chest CT scans. Consolidation

areas indicating an alveolar lesion typically appear in the later stages of the disease.

MRI changes in patients with viral pneumonia are associated with inflamed parenchyma, leading to an increased signal. Viral pneumonia is also characterized by the presence of the “cloudy sky” sign, which is similar to GGO. [5] During dynamic MRI, we observed signal concentration with “cloudy sky” sign during exhalation and pronounced rarefaction during inhalation, which may be indicative of early lung changes in acute viral pneumonia. The consolidation pattern, which is characteristic of alveolar involvement, does not change significantly during respiration. Therefore, dynamic lung MRI allows us to differentiate areas of consolidation and GGO, which is not always possible with static lung MRI.

Previously, our authors examined patients using an MRI-LUNG protocol [5] (static scanning) and found that the visible parenchyma lesions are similar to the pattern of CT lesions. Real-time tests showed that MRI enables for rapid and painless lung imaging under free-breathing conditions. A limitation of our study was the lack of CT data to compare identified patterns.

The use of MRI in COVID-19 patients has already been studied.[6, 8-14] Dong et al. [8] suggested that MRI may be used to diagnose pregnant women and children. This suggestion was confirmed by Fields et al. [9] compared with various diagnostic methods, such as CT, MRI, and positron

emission tomography with CT. Langenbach et al. [10] from Germany reported a case of a patient referred to MRI for primary lung cancer with characteristic changes in the lower lung lobes. In this case, COVID-19 was subsequently confirmed. Szarf et al. [11] presented a case report describing MRI data on perilobular opacities similar to the sign of “cloudy sky” and consolidation, which could indicate the presence of organized pneumonia. Akhlaghpour et al. [12] performed a similar MRI imaging of viral pneumonia caused by COVID-19, demonstrating and describing 8 case reports. In addition to these changes, Dheir et al. [13] reported MRI-detected nodules in 11 patients and CT-detected nodules in 12 patients, with sensitivity and specificity of 91.67% and 100%, respectively.

CONCLUSION

Several case reports have clearly demonstrated that dynamic MRI can be used to detect “cloudy sky” sign (as the GGO pattern in CT) and differentiate it from consolidation in COVID-19 patients.

The study showed that dynamic lung examination may be superior to standard static scans. Despite its high potential, lung MRI remains an experimental technique that needs more research to understand its role in the management of COVID-19 patients. However, the observed patterns can be applied to other lung conditions.

REFERENCES

1. Shi H, Han X, Jiang N, et al. Radiological findings from 81 patients with COVID-19 pneumonia in Wuhan, China: A descriptive study. *Lancet Infectious Dis.* 2020;20(4):425–434. doi: 10.1016/S1473-3099(20)30086-4
2. Salehi S, Abedi A, Balakrishnan S, Gholamrezaezhad A. Coronavirus Disease 2019 (COVID-19): A systematic review of imaging findings in 919 patients. *Am J Roentgenol.* 2020;215(1):87–93. doi: 10.2214/AJR.20.23034
3. ACR Recommendations for the use of chest radiography and computed tomography (CT) for suspected COVID-19 infection [cited March 11, 2020]. Available from: <https://www.acr.org/Advocacy-and-Economics/ACR-Position-Statements/Recommendations-for-Chest-Radiography-and-CT-for-Suspected-COVID19-Infection>. Accessed: 15.01.2023.
4. Temporary guidelines “Prevention, diagnosis and treatment of new coronavirus infection (COVID-19)”. Version 16 (08/18/2022). Moscow; 2022. 249 p. (In Russ).
5. Vasilev YA, Sergunova KA, Bazhin AV, et al. Chest MRI of patients with COVID-19. *Magn Reson Imaging.* 2021;(79):13–19. doi: 10.1016/j.mri.2021.03.005
6. Vasilev YuA, Sergunova KA, BazhinAV, et al. Chest MRI of a pregnant woman with COVID-19 pneumonia. *Digital Diagnostics.* 2020;1(1):61–68. doi: 10.17816/DD46800
7. Vasiliev YuA, Panina OYu, Kudryavtsev ND, et al. Magnetic resonance imaging of the lungs: methodological recommendations.

ADDITIONAL INFORMATION

Funding source. The article was prepared with the support of the Moscow Department of Health as part of the research work (No. EGISU: AAAA-A21-123031500007-6) in accordance with the program “Scientific support of the capital’s healthcare” for 2023–2025.

Competing interests. The authors declare that they have no competing interests.

Authors’ contribution. All authors made a substantial contribution to the conception of the work, acquisition, analysis, interpretation of data for the work, drafting and revising the work, final approval of the version to be published and agree to be accountable for all aspects of the work. Yu.A. Vasiliev, A.V. Bazhin, Yu.N. Vasilyeva, D.S. Semenov — concept and design of the study, editing and approval of the final version of the manuscript text, advisory support for clinical and technical parts; E.A. Grik, O.Yu. Panina — study concept and design, analysis of MRI studies, description of clinical cases; A.N. Khoruzhaya — literature analysis, writing the text of the article, editing.

Consent for publication. Written consent was obtained from the patients for publication of relevant medical information and all of accompanying images within the manuscript Digital Diagnostics journal.

Acknowledgments. The authors are grateful for the help in developing the concept of the study, as well as for the organizational and methodological support of K.A. Sergunova, S.P. Morozov, A.G. Masri, A.V. Midaev and E.A. Suleimanov.

Issue 92. Moscow; 2022. 102 p. (Series «The best practices of radiation and instrumental diagnostics»). (In Russ).

8. Dong D, Tang Z, Wang S, et al. The role of imaging in the detection and management of COVID-19: A review. *IEEE Rev Biomed Eng.* 2021;(14):16–29. doi: 10.1109/RBME.2020.2990959

9. Fields BK, Demirjian NL, Dadgar H, Gholamrezaezhad A. Imaging of COVID-19: CT, MRI, and PET. *Semin Nucl Med.* 2021;51(4):312–320. doi: 10.1053/j.semnuclmed.2020.11.003

10. Langenbach MC, Hokamp GN, Persigehl T, Bratke G. MRI appearance of COVID-19 infection. *Diagn Interv Radiol.* 2020;26(4):377–378. doi: 10.5152/dir.2020.20152

11. Fonseca EK, Chate RC, Neto RS, et al. Findings of COVID-19 on magnetic resonance imaging. *Radiology Cardiothoracic Imaging.* 2020;2(2):e200193. doi: 10.1148/ryct.2020200193

12. Torkian P, Rajebi H, Zamani T, et al. Magnetic resonance imaging features of coronavirus disease 2019 (COVID-19) pneumonia: The first preliminary case series. *Clin Imaging.* 2021;(69):261–265. doi: 10.1016/j.clinimag.2020.09.002

13. Ates OF, Taydas O, Dheir H. Thorax magnetic resonance imaging findings in patients with coronavirus disease (COVID-19). *Acad Radiol.* 2020;27(10):1373–1378. doi: 10.1016/j.acra.2020.08.009

14. Ussov WY, Nudnov NV, Ignatenko G, et al. Primary and prospective imaging of the chest using magnetic resonance imaging in patients with viral lung damage in COVID-19. *Med Visualizat.* 2020;24(4):11–26. (In Russ). doi: 10.24835/1607-0763-2020-4-11-26

СПИСОК ЛИТЕРАТУРЫ

1. Shi H., Han X., Jiang N., et al. Radiological findings from 81 patients with COVID-19 pneumonia in Wuhan, China: A descriptive study // *Lancet Infectious Dis.* 2020. Vol. 20, N 4. P. 425–434. doi: 10.1016/S1473-3099(20)30086-4
2. Salehi S., Abedi A., Balakrishnan S., Gholamrezanezhad A. Coronavirus Disease 2019 (COVID-19): A systematic review of imaging findings in 919 patients // *Am J Roentgenol.* 2020. Vol. 215, N 1. P. 87–93. doi: 10.2214/AJR.20.23034
3. ACR Recommendations for the use of chest radiography and computed tomography (CT) for suspected COVID-19 infection [cited March 11, 2020]. Режим доступа: <https://www.acr.org/Advocacy-and-Economics/ACR-Position-Statements/Recommendations-for-Chest-Radiography-and-CT-for-Suspected-COVID19-Infection>. Дата обращения: 15.01.2023.
4. Временные методические рекомендации. Профилактика, диагностика и лечение новой коронавирусной инфекции (COVID-19). Версия 16 (18.08.2022). Москва, 2022. 249 с.
5. Vasilev Y.A., Sergunova K.A., Bazhin A.V., et al. Chest MRI of patients with COVID-19 // *Magn Reson Imaging.* 2021. N 79. P. 13–19. doi: 10.1016/j.mri.2021.03.005
6. Vasilev Y.A., Sergunova K.A., Bazhin A.V., et al. Chest MRI of a pregnant woman with COVID-19 pneumonia // *Digital Diagnostics.* 2020. Vol. 1, N 1. P. 61–68. doi: 10.17816/DD46800
7. Васильев Ю.А., Панина О.Ю., Кудрявцев Н.Д., и др. Магнитно-резонансная томография легких. Методические рекомендации. Вып. 92. Москва, 2022. 102 с. (Серия «Лучшие практики лучевой и инструментальной диагностики»).
8. Dong D., Tang Z., Wang S., et al. The role of imaging in the detection and management of COVID-19: A review // *IEEE Rev Biomed Eng.* 2020. N 14. P. 16–29. doi: 10.1109/RBME.2020.2990959
9. Fields B.K., Demirjian N.L., Dadgar H., Gholamrezanezhad A. Imaging of COVID-19: CT, MRI, and PET // *Semin Nucl Med.* 2021. Vol. 51, N 4. P. 312–320. doi: 10.1053/j.semnuclmed.2020.11.003
10. Langenbach M.C., Hokamp G.N., Persigehl T., Bratke G. MRI appearance of COVID-19 infection // *Diagn Interv Radiol.* 2020. Vol. 26, N 4. P. 377–378. doi: 10.5152/dir.2020.20152
11. Fonseca E.K., Chate R.C., Neto R.S., et al. Findings of COVID-19 on magnetic resonance imaging // *Radiology Cardiothoracic Imaging.* 2020. Vol. 2, N 2. P. e200193. doi: 10.1148/ryct.2020200193
12. Torkian P., Rajebi H., Zamani T., et al. Magnetic resonance imaging features of coronavirus disease 2019 (COVID-19) pneumonia: The first preliminary case series // *Clin Imaging.* 2021. Vol. 69. P. 261–265. doi: 10.1016/j.clinimag.2020.09.002
13. Ates O.F., Taydas O., Dheir H. Thorax magnetic resonance imaging findings in patients with coronavirus disease (COVID-19) // *Acad Radiol.* 2020. Vol. 27, N 10. P. 1373–1378. doi: 10.1016/j.acra.2020.08.009
14. Ussov W.Y., Nudnov N.V., Ignatenko G.A., et al. Primary and prospective imaging of the chest using magnetic resonance imaging in patients with viral lung damage in COVID-19 // *Med Visualizat.* 2020. T. 24, N 4. С. 11–26. doi: 10.24835/1607-0763-2020-4-11-26

AUTHORS' INFO

* Anna N. Khoruzhaya;

address: 24/1 Petrovka street, 127051 Moscow, Russia;
ORCID: <https://orcid.org/0000-0003-4857-5404>;
eLibrary SPIN: 7948-6427; e-mail: a.khoruzhaya@npcmr.ru

Yuriy A. Vasilev, MD, Cand. Sci. (Med.);

ORCID: <https://orcid.org/0000-0002-0208-5218>;
eLibrary SPIN: 4458-5608; e-mail: y.vasilev@npcmr.ru

Evgeniia A. Grik;

ORCID: <https://orcid.org/0000-0002-7908-3982>;
eLibrary SPIN: 5558-7307; e-mail: evgeniyagrik@gmail.com

Olga Yu. Panina;

ORCID: <https://orcid.org/0000-0002-8684-775X>;
eLibrary SPIN: 5504-8136; e-mail: o.panina@npcmr.ru

Dmitriy S. Semenov;

ORCID: <https://orcid.org/0000-0002-4293-2514>;
eLibrary SPIN: 2278-7290; e-mail: d.semenov@npcmr.ru

Alexander V. Bazhin;

ORCID: <https://orcid.org/0000-0003-3198-1334>;
eLibrary SPIN: 6122-5786; e-mail: a.bazhin@npcmr.ru

Yulia N. Vasileva, MD, Cand. Sci. (Med.);

ORCID: <https://orcid.org/0000-0002-1066-3989>;
eLibrary SPIN: 9777-2067; e-mail: drugya@yandex.ru

ОБ АВТОРАХ

* Хоружая Анна Николаевна;

адрес: Россия, 127051, Москва, ул. Петровка, д. 24, стр. 1;
ORCID: <https://orcid.org/0000-0003-4857-5404>;
eLibrary SPIN: 7948-6427; e-mail: a.khoruzhaya@npcmr.ru

Васильев Юрий Александрович, к.м.н.;

ORCID: <https://orcid.org/0000-0002-0208-5218>;
eLibrary SPIN: 4458-5608; e-mail: y.vasilev@npcmr.ru

Грик Евгения Андреевна;

ORCID: <https://orcid.org/0000-0002-7908-3982>;
eLibrary SPIN: 5558-7307; e-mail: evgeniyagrik@gmail.com

Панина Ольга Юрьевна;

ORCID: <https://orcid.org/0000-0002-8684-775X>;
eLibrary SPIN: 5504-8136; e-mail: o.panina@npcmr.ru

Семенов Дмитрий Сергеевич;

ORCID: <https://orcid.org/0000-0002-4293-2514>;
eLibrary SPIN: 2278-7290; e-mail: d.semenov@npcmr.ru

Бажин Александр Владимирович;

ORCID: <https://orcid.org/0000-0003-3198-1334>;
eLibrary SPIN: 6122-5786; e-mail: a.bazhin@npcmr.ru

Васильева Юлия Николаевна, к.м.н.;

ORCID: <https://orcid.org/0000-0002-1066-3989>;
eLibrary SPIN: 9777-2067; e-mail: drugya@yandex.ru

* Corresponding author / Автор, ответственный за переписку

DOI: <https://doi.org/10.17816/DD123559>

Системы искусственного интеллекта в клинической физиологии: как сделать их обучение эффективным?

Д.В. Шутов¹, Д.Е. Шарова¹, Л.Р. Абуладзе¹, Д.В. Дроздов²¹ Научно-практический клинический центр диагностики и телемедицинских технологий, Москва, Российская Федерация² Национальный медицинский исследовательский центр кардиологии, Москва, Российская Федерация

АННОТАЦИЯ

Клиническая физиология — раздел медицинских наук о роли и характере изменений физиологических процессов, происходящих в организме при предпатологических и патологических состояниях, — предполагает полное, комплексное, многостороннее исследование функций как поражённых, так и здоровых органов, что позволяет оценить компенсаторные возможности организма.

Программное обеспечение и различные программно-аппаратные комплексы, созданные с использованием технологий искусственного интеллекта, всё активнее применяются в различных отраслях медицины, в том числе и в клинической физиологии. Этому способствуют появление наборов медицинских данных, увеличение вычислительных мощностей, развитие облачных сервисов, а также многочисленные публикации, демонстрирующие эффективность и перспективность применения подобных интеллектуальных решений.

Несмотря на то, что в целом подход к формированию медицинских наборов данных схож, в клинической физиологии имеется целый ряд ключевых особенностей и существенных отличий. Соблюдение предлагаемых нами правил по формированию наборов данных потенциально позволит эффективно обучить системы искусственного интеллекта в области клинической физиологии и применять их на практике.

Вступивший в силу национальный стандарт Российской Федерации ГОСТ Р 59921.9-2022 входит в комплекс стандартов «Системы искусственного интеллекта в клинической медицине» и устанавливает дополнительные требования к алгоритмам анализа данных и методам испытаний систем искусственного интеллекта, применяемых в области клинической физиологии. Важной особенностью нового стандарта является его квазиметрический тип (прилагается обязательный набор демонстрационных данных).

Россия одной из первых стран в мире приступила к разработке квазиметрических стандартов, и уже в текущем году вступят в силу 15 отраслевых стандартов в сфере искусственного интеллекта (из них два — по медицине).

Ключевые слова: набор данных; электрокардиография; клиническая физиология; аннотирование; автоматический анализ ЭКГ.

Как цитировать

Шутов Д.В., Шарова Д.Е., Абуладзе Л.Р., Дроздов Д.В. Системы искусственного интеллекта в клинической физиологии: как сделать их обучение эффективным? // *Digital Diagnostics*. 2023. Т. 4, № 1. С. 81–88. DOI: <https://doi.org/10.17816/DD123559>

DOI: <https://doi.org/10.17816/DD123559>

Artificial intelligence in clinical physiology: How to improve learning agility

Dmitry V. Shutov¹, Dariya E. Sharova¹, Liya R. Abuladze¹, Dmitrii V. Drozdov²

¹ Moscow Center for Diagnostics and Telemedicine, Moscow, Russian Federation

² National Medical Research Center of Cardiology, Moscow, Russian Federation

ABSTRACT

Clinical physiology involves a complete, comprehensive, multilateral study of the functions of both affected and healthy organs, which allows us to assess the compensatory capabilities of the body.

Artificial intelligence is increasingly being used in medicine, including in clinical physiology. This is facilitated by the increase in computing processing power, development of cloud services and datasets, and numerous scientific articles demonstrating the effectiveness and viability of such intelligent solutions.

Although the approach to medical dataset development is generally similar, there are a number of key features and significant differences in clinical physiology. Artificial intelligence systems in clinical physiology may be effectively trained and applied in practice by following the recommendations in this study.

The national standard of the Russian Federation GOST R 59921.9-2022, which has entered into force, is included in the set of standards "Artificial Intelligence systems in clinical medicine" and establishes additional requirements for data analysis algorithms and test methods of artificial intelligence systems used in the field of clinical physiology. A crucial feature of the created standard is its qualimetric type (i.e., it has a mandatory set of demonstration data).

Russia is one of the first countries to start developing quasi-metric standards worldwide, and 15 industry standards in the field of artificial intelligence (2 of them in medicine) will come into force this year.

Keywords: dataset; electrocardiograph; clinical physiology; annotation; automated ECG interpretation.

To cite this article

Shutov DV, Sharova DE, Abuladze LR, Drozdov DV. Artificial intelligence in clinical physiology: How to improve learning agility. *Digital Diagnostics*. 2023;4(1):81–88. DOI: <https://doi.org/10.17816/DD123559>

Received: 18.01.2023

Accepted: 24.01.2023

Published: 24.03.2023

DOI: <https://doi.org/10.17816/DD123559>

临床生理学中的人工智能系统：如何使其训练有效？

Dmitry V. Shutov¹, Dariya E. Sharova¹, Liya R. Abuladze¹, Dmitrii V. Drozdov²

¹ Moscow Center for Diagnostics and Telemedicine, Moscow, Russian Federation

² National Medical Research Center of Cardiology, Moscow, Russian Federation

简评

临床生理学是关于在病理前和病理情况下身体内发生的生理过程变化的作用和性质的一个医学科学分支，它要求对患病和健康器官的功能进行完整、全面、多边的研究，从而允许评估身体的补偿能力。

使用人工智能技术创造的软件和各种硬件系统更积极地被用于医学的各个领域，包括临床生理学。医疗数据集的出现、不断提高的计算能力、云服务的发展以及证明这种智能解决方案的有效性和前景的众多出版物都有助于这个过程。

虽然医学数据集的形成方法大体相似，但临床生理学有一系列关键特征和显著差异。遵守我们提出的数据集形成规则将有可能使临床生理学中的人工智能系统接受有效的训练并得到实际应用。

生效的俄罗斯联邦GOST R 59921.9-2022标准被纳入“临床医学中的人工智能系统”这套标准，这种标准对临床生理学中使用的人工智能系统的数据分析算法和测试方法提出额外要求。新标准的一个重要特点是其拟度量类型（附有一套强制性的示范数据）。

俄罗斯是世界上最早开始制定拟度量标准的国家之一，人工智能方面的15项行业标准（其中两项是与医学方面有关的）将于今年生效。

关键词：数据集，心电描记法，临床生理学，注释，心电图自动分析。

To cite this article

Shutov DV, Sharova DE, Abuladze LR, Drozdov DV. 临床生理学中的人工智能系统：如何使其训练有效？ *Digital Diagnostics*. 2023;4(1):81-88. DOI: <https://doi.org/10.17816/DD123559>

收到: 18.01.2023

接受: 24.01.2023

发布日期: 24.03.2023

INTRODUCTION

Clinical physiology is a branch of medicine that studies the role and nature of physiological changes in the body during pre-pathological and pathological conditions. Clinical physiology is a complete, comprehensive, multifaceted study of the body's functions (not only of affected organs but also of healthy ones), allowing us to assess the body's compensatory capabilities.[1]

Artificial intelligence (AI) systems are increasingly being used in almost all fields of medicine: [2] there is a significant number of works on electrocardiography (ECG) evaluation, including through smart watches, [3–7] and an increasing amount of research in the field of computer vision around the world,[8, 9] as well as the development of various smart solutions¹. PhysioNet², for example, includes a large number of open data sets pertaining to various pathologies. The largest open ECG data sets contain 21,837 [10] and 10,646 ECGs, [11] respectively; however, despite the importance of the issue, the formation of such data sets remains a major challenge that necessitates a thorough approach.

We identified the following major issues while analyzing public open ECG data sets:

1. Differences in technical conditions for ECG recording: sampling rate, least significant digit value, analog-to-digital converter bit depth, recording duration, and number of channels
2. Incompatible descriptive languages (thesauri): different "schools," different patient populations, and different end-user goals
3. Imbalance in ECG disorder classes within the data set and in data sets with the general population
4. Concerns about the quality of the annotation/classification
5. Lack or absence of clinical data (metadata)

These issues can be worsened when other diagnostic and control methods in clinical physiology are used. This is due to the fact that the following data can be used to create a data set and then train AI systems in clinical physiology³:

1. Physiological parameter values (blood pressure, heart rate, and saturation level)
2. Digitized biological signals (electrocardiogram and vessel pressure indicator)
3. Induced and returned signals (neuromyogram, rheogram, Doppler curve, and ultrasound M-scan)
4. Dynamic images (cine loops)
5. Complex data

DATA SET FORMATION METHODOLOGY: ARE THERE ANY DIFFERENCES?

Data set formation methodology in clinical physiology is broadly similar to that of radiodiagnosis [12]: planning; creation of a thesaurus or glossary and inclusion and exclusion criteria; selection of experts and moderators; data analysis for compliance with inclusion criteria; annotation approval; and multilevel moderation. However, there are several key differences as follows:

1. The order in which the data array is processed differs significantly. The work sequence for preparing a data set (number series, graphs, and individual measurements) is as follows:
 - Data segmentation (separation)
 - Data measurement
 - Data annotation: a method of providing verbal (semantics) meaning to an object or set of data
 - Data classification
2. A dictionary (glossary) is sufficient for classifying simple (binary) properties of objects, and a thesaurus is required for multiclass objects.
3. Moreover, some less evident and difficult-to-categorize factors can lead to significant errors when creating a data set^{4, 5}:
 - Highly qualified operators are required to conduct clinical physiology research; one of the most important factors in source data generation is operator dependence.
 - When forming the final data set, the presented array of studies should be analyzed for the following factors: sufficient recording duration, number of channels, disabling signal filtering, as well as compliance with accepted technical parameters, dynamic range, signal-to-noise ratio, and results storage format.
 - Experts and moderators involved in data separation must be qualified: while data anonymization is permissible, details of their qualifications and contributions must be included in the AI system test report.
 - A set of equipment and software for AI system tests in clinical physiology should be developed; at the same time, the characteristics of hardware and software must exceed the minimum requirements set by the AI system manufacturer and consider the typical characteristics of a specific or potential user's computing facilities.

¹ Center for Diagnostics and Telemedicine [Internet]. AI services in radiodiagnosis. Available at <https://mosmed.ai/>.

² PhysioNet [Internet]. The Research Resource for Complex Physiologic Signals. Available at <https://physionet.org/>.

³ GOST R 55036-2012/ISO/TS 25237:2008. National Standard of the Russian Federation. Health informatics. Pseudonymization. Available at <https://docs.cntd.ru/document/1200100339>.

⁴ GOST R 55036-2012/ISO/TS 25237:2008. National Standard of the Russian Federation. Health informatics. Pseudonymization. Available at <https://docs.cntd.ru/document/1200100339>.

⁵ GOST R 59921.5. National Standard of the Russian Federation. Artificial intelligence systems in clinical medicine. Part 5. Requirements for the structure and application of data set for training and testing algorithms. Available at <https://docs.cntd.ru/document/1200183858>.

INCLUSION AND EXCLUSION CRITERIA FOR RECORD SELECTION IN CLINICAL PHYSIOLOGY DATA SET FORMATION

Exclusion criteria (absolute; only one is required):

- The records are provided in a proprietary format, and the manufacturer refuses to create a matching layer
- Noncompliance with technical specifications for saved data (for example, the recording duration for a digital ECG is less than 10 s, the sampling rate is less than 500 Hz, the least significant digit value is greater than 5 μ V, and the analog-to-digital converter bit depth is less than 10 bits).
- Access to metadata is either impossible or significantly restricted
- Less than 70% of the ECGs in the final data set are annotated and classified appropriately

Inclusion criteria (all must be met):

- The records are provided in one of the following formats: WDBF, EDF, aECG (HL-7), SCP-ECG, DICOM-ECG, and XML
- Compliance with the technical specifications for saved data (for example, for a digital ECG, the recording duration must be at least 10 s, the sampling rate must be at least 500 Hz, the least significant digit value must be 5 μ V, and the analog-to-digital converter bit depth must be at least 10 bits)
- Access to metadata is not restricted
- At least 90% of the ECGs in the final data set are annotated and classified appropriately

It appears that data sets for AI system training should include the full range of possible phenomena (syndromes, diagnoses, and outcomes) from the most rare (casual) to the most common. The type of data set determines the need to respect the variability of gender and racial differences in patients (for example, these metadata are required for assessing respiratory function parameters). The incidence of phenomena (syndromes) in a population is given less weight in the data set formation. It is recommended to use additional metrics when using unbalanced data sets for rare (casual) phenomena.

NORMATIVE DOCUMENTS REGULATING THE DEVELOPMENT AND APPLICATION OF DATA ANALYSIS ALGORITHMS AND TEST METHODS OF ARTIFICIAL INTELLIGENCE SYSTEMS IN CLINICAL PHYSIOLOGY

The national standard of the Russian Federation GOST R 59921.9-2022⁶, which became effective on January 1, 2023, is included in the set of standards known as “Artificial

Intelligence Systems in Clinical Medicine” and establishes additional requirements for data analysis algorithms and test methods of AI systems in clinical physiology.

Developers of AI systems for clinical physiology and other interested parties will be able to study the requirements:

- Data set generation, preparation, segmentation, measurement, detection, annotation, and classification for AI system testing
- Data set structure, application procedures, and access conditions
- Organizing terminological resources and presenting data analysis results
- Information exchange between medical devices, intelligent systems, and other healthcare automation systems
- Technical, bench, laborator, and clinical test processes and results, as well as postregistration and operational control of software and hardware–software systems based on artificial intelligence technologies
- The form and content of software and hardware–software systems based on artificial intelligence technologies, in accordance with the tasks being solved in the field of medicine and healthcare

The prescribed requirements for data sets distinguish the new national standard from other GOST R standards and English-language counterparts. Three scenarios are proposed in particular: clinical trials conducted only on a test site (bench) using data sets; clinical trials conducted within a health facility; and combined clinical trials. All scenarios are illustrated with flowcharts (Figure 1).

The standard also includes test options for assessing AI system resistance to errors in input data and testing using synthetic and combined data. The new GOST K standard allows the testing of AI systems that are compatible with various data types and presentation formats. The following can be used for AI system testing in clinical physiology:

- Measured physiological parameter values (blood pressure, heart rate, and saturation level)
- Digitized biological signals (electrocardiogram and vessel pressure indicator)
- Induced and returned signals (neuromyogram, rheogram, Doppler curve, and ultrasound M-scan)
- Dynamic images (cine loops, for example, in an ultrasound examination mode and motion video recordings)
- Complex data containing data of several types listed above (synchronized and in-phase)

The data can represent the results of single measurements (patient studies), or they can be chosen to systematically represent the development of pathological processes (a time series of homogeneous measurements), or they can reflect changes upon presentation of graduated stimuli, or they can reflect changes in parameters depending on external

⁶ GOST R 59921.9-2022. National Standard of the Russian Federation. Artificial intelligence systems in clinical medicine. Algorithms for data analysis in clinical physiology. Testing methods. General requirements. Available at <https://docs.cntd.ru/document/1200193730>.

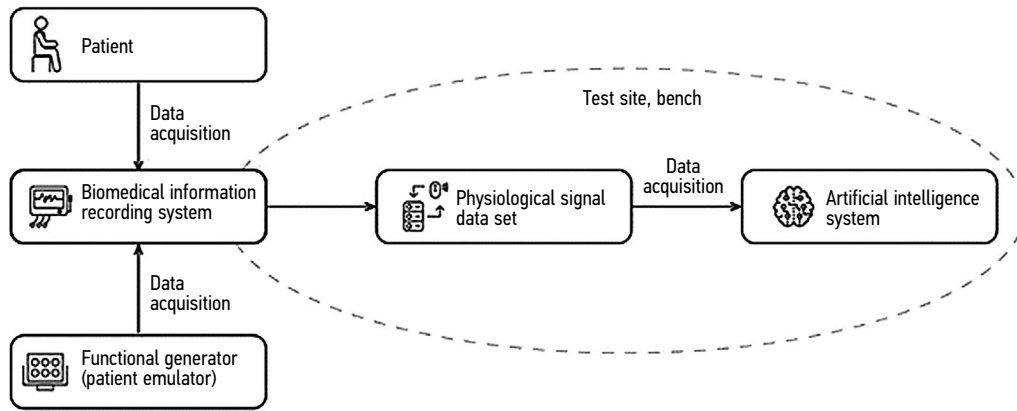


Figure 1. Flowchart for conducting clinical trials with data sets (one implementation option)

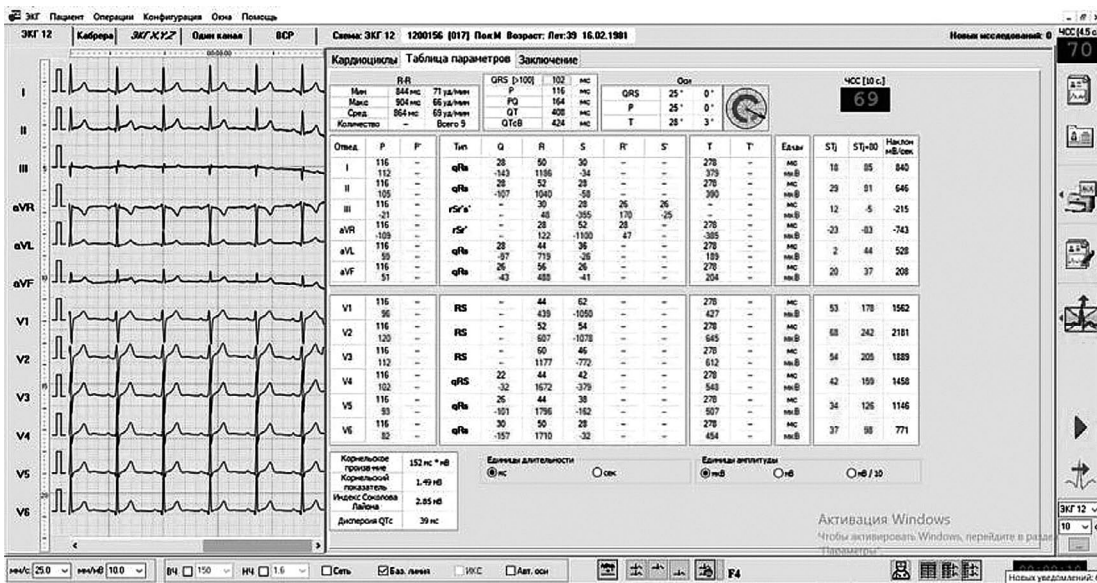


Figure 2. An example file from the demo data set of GOST R 59921.9-2022, Artificial Intelligence Systems in Clinical Medicine. Algorithms for data analysis in clinical physiology. Testing methods

conditions (during sleep, at rest, during physical or mental stress, distress, etc.).

The fact that the new standard is a quasimetric GOST R (i.e., it comes with a mandatory set of demo data) is also an important feature (Figure 2).

Russia was one of the world's first countries to develop quasimetric standards. In the field of artificial intelligence, 15 industrial standards will come into force in 2023, with two of them in medicine.^{7, 8}

CONCLUSION

Compliance with the aforementioned rules will allow for the acquisition of a data set for AI system training in such a way that all three phases of clinical trials are potentially

passed, namely, (a) testing to ensure the accuracy of the input data (recognition of signals received with a violation of the study technology, as well as those containing artifacts and noise); (b) testing to ensure the accuracy of the recognition of syndromes, phenomena, clinical equivalents, and/or the formation of a conclusion (annotation) according to an agreed thesaurus or glossary; and (c) testing on synthetic and combined data (recognition of a synthetic stimulus signal that initiates or amplifies natural signals and evaluation of stimulation efficiency or inefficiency).

ADDITIONAL INFORMATION

Funding source. This article was not supported by any external sources of funding.

⁷ GOST R 59921.7-2022. National Standard of the Russian Federation. Artificial intelligence systems in clinical medicine. Algorithms of medical images analysis. Testing methods. General requirements. Available at <https://docs.cntd.ru/document/1200193728>.

⁸ GOST R 59921.9-2022. National Standard of the Russian Federation. Artificial intelligence systems in clinical medicine. Algorithms for data analysis in clinical physiology. Testing methods. General requirements. Available at <https://docs.cntd.ru/document/1200193730>.

Competing interests. The authors declare that they have no competing interests.

Authors' contribution. All authors made a substantial contribution to the conception of the work, acquisition, analysis, interpretation of data for the work, drafting and revising the work, final approval of the version to be published and agree to be accountable for all

aspects of the work. D.V. Shutov, D.V. Drozdov — work concept and design, editing and approval of the final version of the manuscript, advisory support; D.E. Sharova — work concept and design, data analysis, writing the text of the article, editing and approval the final version of the manuscript; L.R. Abuladze — writing the text of the article, editing.

REFERENCES

1. Kurzanov AN. Clinical physiology: formation, goals, tasks, limits of competence, place in the system of higher professional medical education. *International journal of experimental education*. 2012;(4):128–130. (In Russ).
2. Gusev AV, Vladzimirsky AV, Sharova DE, et al. Development of research and development in the field of artificial intelligence technologies for healthcare in the Russian Federation: results of 2021. *Digital Diagnostics*. 2022;3(3):178–194. (In Russ). doi: 10.17816/DD107367
3. Al-Mousily MF, Baker GH, Jackson L, et al. The use of a traditional nonlooping event monitor versus a loan-based program with a smartphone ECG device in the pediatric cardiology clinic. *Cardiovasc Digit Heal J*. 2021;2(1):71–75. doi: 10.1016/j.cvdhj.2020.11.008
4. Ding EY, Pathirivasan CH, Schramm E, et al. Design, deployment, and usability of a mobile system for cardiovascular health monitoring within the electronic Framingham Heart Study. *Cardiovasc Digit Heal J*. 2021;2(3):171–178. doi: 10.1016/j.cvdhj.2021.04.001
5. Bashar SK, Hossain MB, Lázaro J, et al. Feasibility of atrial fibrillation detection from a novel wearable armband device. *Cardiovasc Digit Heal J*. 2021;2(3):179–191. doi: 10.1016/j.cvdhj.2021.05.004
6. Goodwin AJ, Eytan D, Greer RW, et al. A practical approach to storage and retrieval of high-frequency physiological signals. *Physiol Meas*. 2020;41(3):035008. doi: 10.1088/1361-6579/ab7cb5
7. Bartlett VL, Ross JS, Shah ND, et al. Physical activity, patient-reported symptoms, and clinical events: Insights into postprocedural recovery from personal digital devices. *Cardiovasc Digit Heal J*. 2021;2(4):212–221. doi: 10.1016/j.cvdhj.2021.06.002
8. Mishra S, Khatwani G, Patil R, et al. ECG paper record digitization and diagnosis using deep learning. *J Med Biol Eng*. 2021;41(4):422–432. doi: 10.1007/s40846-021-00632-0
9. Kashou AH, Mulpuru SK, Deshmukh AJ, et al. An artificial intelligence-enabled ECG algorithm for comprehensive ECG interpretation: Can it pass the ‘Turing test’? *Cardiovasc Digit Heal J*. 2021;2(3):164–170. doi: 10.1016/j.cvdhj.2021.04.002
10. Wagner P, Strodthoff N, Bousselet RD, et al. PTB-XL, a large publicly available electrocardiography dataset. *Sci Data*. 2020;7(1):154. doi: 10.1038/s41597-020-0495-6
11. Zheng J, Zhang J, Danioko S, et al. A 12-lead electrocardiogram database for arrhythmia research covering more than 10,000 patients. *Sci Data*. 2020;7(1):48. doi: 10.1038/s41597-020-0386-x
12. М 80 Regulations for the preparation of data sets with a description of approaches to the formation of a representative sample of data. Part 1. Methodological recommendations. Ed by S.P. Morozov, A.V. Vladzimirsky, A.E. Andreichenko, et al. Moscow, 2022. 40 p. (The series “Best practices of radiation and instrumental diagnostics”). (In Russ).

СПИСОК ЛИТЕРАТУРЫ

1. Курзанов А.Н. Клиническая физиология: становление, цели, задачи, пределы компетентности, место в системе высшего профессионального медицинского образования // Международный журнал экспериментального образования. 2012. № 4–2. С. 128–130.
2. Гусев А.В., Владзмирский А.В., Шарова Д.Е., и др. Развитие исследований и разработок в сфере технологий искусственного интеллекта для здравоохранения в Российской Федерации: итоги 2021 года // Digital Diagnostics. 2022. Т. 3, № 3. С. 178–194. doi: 10.17816/DD107367
3. Al-Mousily M.F., Baker G.H., Jackson L., et al. The use of a traditional nonlooping event monitor versus a loan-based program with a smartphone ECG device in the pediatric cardiology clinic // *Cardiovasc Digit Heal J*. 2021. Vol. 2, N 1. P. 71–75. doi: 10.1016/j.cvdhj.2020.11.008
4. Ding E.Y., Pathirivasan C.H., Schramm E., et al. Design, deployment, and usability of a mobile system for cardiovascular health monitoring within the electronic Framingham Heart Study // *Cardiovasc Digit Heal J*. 2021. Vol. 2, N 3. P. 171–178. doi: 10.1016/j.cvdhj.2021.04.001
5. Bashar S.K., Hossain M.B., Lázaro J., et al. Feasibility of atrial fibrillation detection from a novel wearable armband device // *Cardiovasc Digit Heal J*. 2021. Vol. 2, N 3. P. 179–191. doi: 10.1016/j.cvdhj.2021.05.004
6. Goodwin A.J., Eytan D., Greer R.W., et al. A practical approach to storage and retrieval of high-frequency physiological signals // *Physiol Meas*. 2020. Vol. 41, N 3. P. 035008. doi: 10.1088/1361-6579/ab7cb5
7. Bartlett V.L., Ross J.S., Shah N.D., et al. Physical activity, patient-reported symptoms, and clinical events: Insights into postprocedural recovery from personal digital devices // *Cardiovasc Digit Heal J*. 2021. Vol. 2, N 4. P. 212–221. doi: 10.1016/j.cvdhj.2021.06.002
8. Mishra S., Khatwani G., Patil R., et al. ECG paper record digitization and diagnosis using deep learning // *J Med Biol Eng*. 2021. Vol. 41, N 4. P. 422–432. doi: 10.1007/s40846-021-00632-0
9. Kashou A.H., Mulpuru S.K., Deshmukh A.J., et al. An artificial intelligence-enabled ECG algorithm for comprehensive ECG interpretation: Can it pass the ‘Turing test’? // *Cardiovasc Digit Heal J*. 2021. Vol. 2, N 3. P. 164–170. doi: 10.1016/j.cvdhj.2021.04.002
10. Wagner P., Strodthoff N., Bousselet R.D., et al. PTB-XL, a large publicly available electrocardiography dataset // *Sci Data*. 2020. Vol. 7, N 1. P. 154. doi: 10.1038/s41597-020-0495-6
11. Zheng J., Zhang J., Danioko S., et al. A 12-lead electrocardiogram database for arrhythmia research covering more than 10,000 patients // *Sci Data*. 2020. Vol. 7, N 1. P. 48. doi: 10.1038/s41597-020-0386-x
12. М 80 Регламент подготовки наборов данных с описанием подходов к формированию репрезентативной выборки данных. Часть 1. Методические рекомендации / под ред. С.П. Морозова, А.В. Владзмирского, А.Е. Андрейченко, и др. Москва, 2022. 40 с. (Серия: Лучшие практики лучевой и инструментальной диагностики).

AUTHORS' INFO

*** Dmitry V. Shutov**, MD, Dr. Sci. (Med.);
address: 24/1 Petrovka street, 127051 Moscow, Russia;
ORCID: <https://orcid.org/0000-0003-1836-3689>;
eLibrary SPIN: 9381-2456; e-mail: ShutovDV@zdrav.mos.ru

Dariya E. Sharova;
ORCID: <https://orcid.org/0000-0001-5792-3912>;
eLibrary SPIN: 1811-7595

Liya R. Abuladze, Junior Research Associate;
ORCID: <https://orcid.org/0000-0001-6745-1672>;
eLibrary SPIN: 8640-9989; e-mail: AbuladzeLR@zdrav.mos.ru

Dmitrii V. Drozdov, MD, Cand. Sci. (Med.);
ORCID: <https://orcid.org/0000-0001-7374-3604>;
eLibrary SPIN: 2279-9657; e-mail: cardioexp@gmail.com

ОБ АВТОРАХ

*** Шутов Дмитрий Валериевич**, д.м.н.;
адрес: Россия, 127051, Москва, ул. Петровка, д. 24, стр. 1;
ORCID: <https://orcid.org/0000-0003-1836-3689>;
eLibrary SPIN: 9381-2456; e-mail: ShutovDV@zdrav.mos.ru

Шарова Дарья Евгеньевна;
ORCID: <https://orcid.org/0000-0001-5792-3912>;
eLibrary SPIN: 1811-7595

Абуладзе Лия Руслановна, м.н.с.;
ORCID: <https://orcid.org/0000-0001-6745-1672>;
eLibrary SPIN: 8640-9989; e-mail: AbuladzeLR@zdrav.mos.ru

Дроздов Дмитрий Владимирович, к.м.н.;
ORCID: <https://orcid.org/0000-0001-7374-3604>;
eLibrary SPIN: 2279-9657; e-mail: cardioexp@gmail.com

* Corresponding author / Автор, ответственный за переписку